Reproducing Glaucoma-like Elevated SRTs

By Desensitizing a Healthy Human Retina using Half-field and Localized Photobleaching

Thesis Report

Mayukh Sarkar

Delft University of Technology

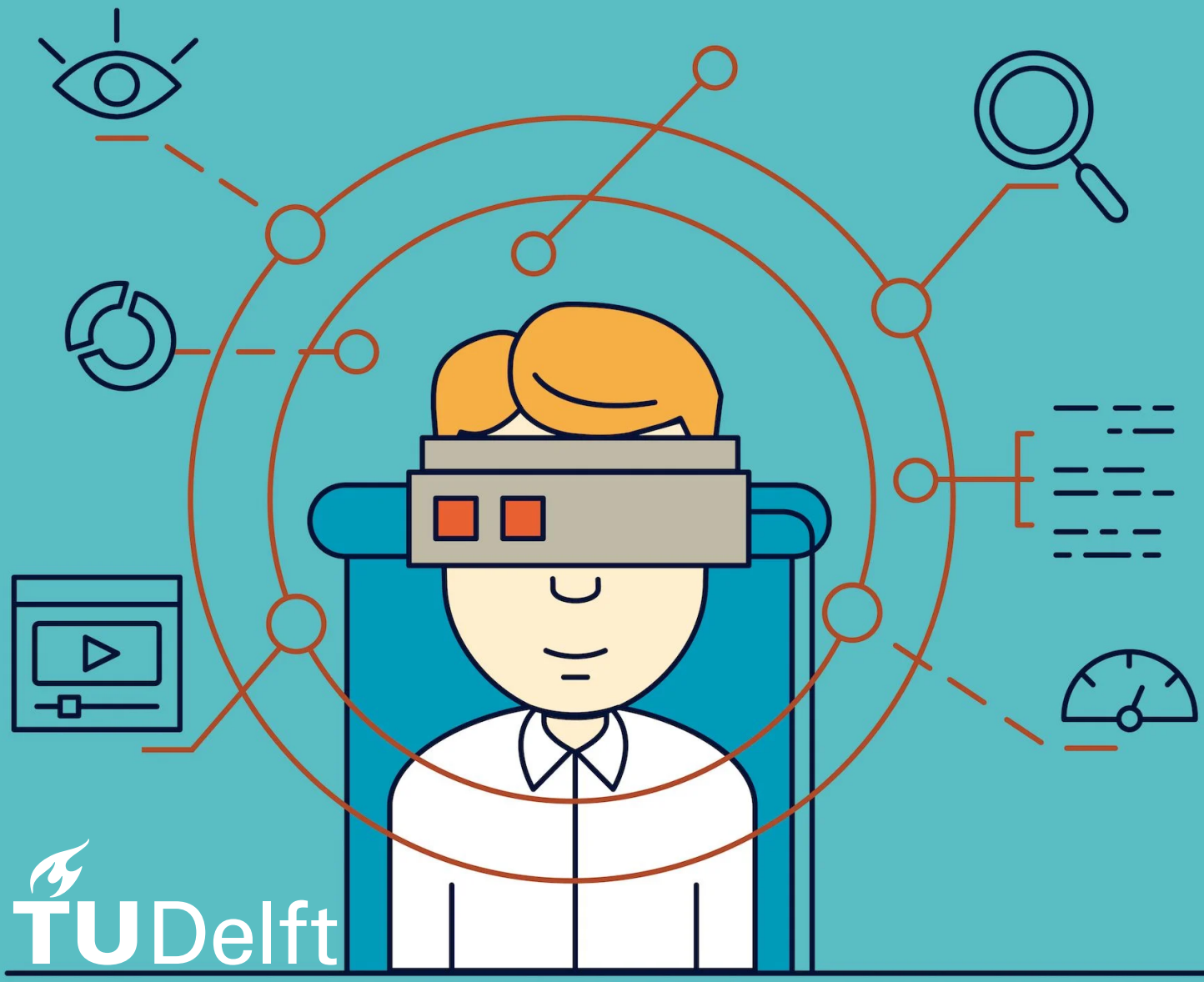

TU Delft

Reproducing Glaucoma-like Elevated SRTs

By Desensitizing a Healthy Human Retina using Half-field and Localized Photobleaching

Thesis report

by

Mayukh Sarkar

to obtain the degree of Master of Science
at the Delft University of Technology
to be defended publicly on April 19, 2023 at 13:00

Thesis committee:	
Chair:	Dr.ir. M.M van Passen[1]
Supervisors:	Dr.ir. Daan M. Pool[1]
	Dr. Peter Bremen[2]
	Dr.ir. Johan Pel[2]
External examiner:	Dr.ir. Yasemin Vardar[3]
Place:	Faculty of Aerospace Engineering, Delft
Project Duration:	March, 2022 - April, 2023
Student number:	5219507
Affiliations:	[1]Department of Control & Simulation, Aerospace Engineering , TU Delft
	[2]Department of Neuroscience, Erasmus MC
	[3]Cognitive Robotics, 3mE, TU Delft

An electronic version of this thesis is available at `http://repository.tudelft.nl/`.

Faculty of Aerospace Engineering · Delft University of Technology

Cover: Glaucoma foundation Research(glaucoma.org) (Modified)

TU Delft

Preface

This document was written in partial fulfillment of the title Master of Science in Aerospace Engineering. As I write this, I am reminded of the long hours spent researching, drafting, and editing that has gone into producing this work. It has been a challenging and rewarding experience, and I am thrilled to share it with readers finally. There are not enough words to thank all those around me for their kindness and patience throughout my studies.

Firstly, I want to thank Dr. ir. Daan Pool, who was my daily supervisor at TU Delft during the entirety of this thesis. I feel fortunate enough to have had the opportunity to work under his caring and excellent guidance. Daan made an everlasting impression on me and instilled an interest in working on human-in-loop studies when I took a Human-machine system course under him in 2020. Since then, I have looked forward to him as my thesis supervisor. Thanks to my constant asking him for thesis topics since the first year of my master's, I could finally do a thesis of my choice under him. I also want to thank Dr. Peter Bremen, my supervisor at Erasmus MC, for his diligent guidance during the entire thesis phase. He taught me a lot about programming, systematic thinking, and troubleshooting. While working with him, I found my passion in contributing to health and society. I also want to thank Dr. ir. Johan Pel also supervised me during this time. He was the person who motivated me by patiently providing out-of-the-box solutions every time I went with a problem.

Next, I want to thank Alex, who constantly helped me test my experiment setup and code. He has done close to 100 runs which is incredible. I also want to thank my close friend, Flori, who has patiently listened to my stories, be it good or bad. She played a big part in my master's journey at TU Delft and supported me selflessly in the last 3 years. Lastly, I want to mention my mentee and friend Ioana, who constantly supported me throughout my thesis through her positive and wise words.

I want to take this special moment to mention my family, without whom my dream and passion of being an engineer would never have been fulfilled. My supportive father, Mr. Ramendra Nath Sarkar, never stopped believing in my abilities and supported me throughout the journey. My mother, Mrs. Sovana Sarkar, who always cared for me and my needs since my childhood, even though being far away from me. I also want to thank my sister Swohinee Sarkar who never failed to cheer me up during my sad days.

I want to extend my sincerest appreciation to my beloved girlfriend, Ishita, whose unwavering support and motivation have been instrumental throughout my thesis journey. Her unconditional love and presence in my life have been a constant source of inspiration, and I am incredibly grateful to have her by my side. Ishita's dedication and encouragement have driven my academic success, and I am deeply grateful for her strong belief in me despite my vulnerable side. Thank you, Ishita, for being the beautiful light in my life and always bringing out the best in me.

Mayukh Sarkar
Delft, April 2022

Summary

The report is divided into two parts. Part I focuses on the scientific article which is the outcome of this thesis project. The findings in the article can be summarised as follows:

"Glaucoma impacts vision by affecting visual processing at the retinal ganglion cell level. Photobleaching has been proposed to reversibly and temporarily induce glaucoma-like saccadic reaction time to recreate its impact on visual processing. It has been established that photobleaching elevates the threshold detection levels of visual stimuli in a healthy retina. This study investigated the potential implementation of photobleaching to recreate glaucoma-like SRTs. Results from the study show that photobleaching increased the SRT and reduced the ability to detect targets within the photobleaching zone of the visual field. The elevated SRTs from the study indicate that photobleaching is a valid method for obtaining mild glaucoma-like SRTs. Furthermore, the effects of photobleaching were found to be highly localized, with the impact primarily observed within the bleaching zone. Attempts to replicate the localized effects of glaucoma using discrete photobleaching were inconclusive, with elevated SRTs observed in some cases. Still, the effect is directly related to the total area bleached. These findings provide the relationship between photobleaching, saccadic response, and their potential implications for artificially recreating glaucoma-like elevated SRTs."

Part II focuses on the background literature study and the development work done before the commencement of experimentation for the thesis. The various components of the eye tracking algorithms are described in the appendix, along with the individual results from each subject who had taken part in the study. The appendix also contains some excess results from the experiment, mainly the influence of photobleaching on saccade gain and results from the main sequence equation. The results from saccade gains show that targets in the bleached area were undershot during photobleaching trials. Still, the undershot was primarily because of lower target detections in those areas and higher positioning errors. The main sequence equations' findings show that the saccade's dynamic properties, like saccade velocity and duration, remain uninfluenced by photobleaching. The appendix lastly contains the necessary ethics, experiment briefing, data management, and questionnaires filed and used during the thesis phase.

Contents

List of Figures

List of Tables

Abbreviations

CRT Cathode Ray Tube 40, 50

EMP Eye Movement Perimetry 25, 32, 33, 34, 41, 57

FDT Field Doubling Perimetry 31, 32, 34

HFA Humphrey Field Analyser 31, 32, 41

IOP Intra-Ocular Pressure 29, 30

LDT Lexical Decision Task 40

MDI Mean Deviation Index 34

RGC Retinal Ganglion cell 27, 28, 29, 30, 41, 42
RTT Roundtrip time 68

SAP Standard Automated Perimetry 25, 31, 32, 33, 34
SITA Swedish Interactive Testing Algorithm 32, 34
SRT Saccadic Reaction Time x, 25, 33, 34, 35, 41, 42, 43, 70

VFI Visual Field Index 32, 33, 34

List of Symbols

c Constant parameter for saccade velocity

n Constant power parameter for saccade duration

Constants

K Weber Contrast

k Constant

Greek Symbols

α Minimum subtended angle

β Power

ω Angular velocity

ϕ Total vertical viewing angle

ϕ_{deg} Vorizontal viewing angle of the subject converted from pixels

τ Decay constant

θ Total horizontal viewing angle

θ_{deg} Horizontal viewing angle of the subject converted from pixels

Units

c/deg Cycles per degree

cdm^{-2} candelas per meter square, light luminance per meter square

min Minutes

ms milli seconds

nm namo-meter , used as a measurement of wavelength of light in the text

Td Trolands - unit of retinal luminance

Variables

δI Difference of light intensity of target stimuli and background

ΔT Time of recovery post photobleaching

a Angle of rotation of eye

a_0 Amplitude of saccade

C	Contrast of stimuli
C_0	Contrast threshold
d	diameter of pupil
I	Intensity of light source
L	Luminance of light source
R	Reaction time in ms
r	percentage of photoreceptors bleached
R_{min}	Minimum reaction time in ms
S	Search time in ms
S_{min}	Minimum search time in ms
T	Duration of saccade in ms
t	exposure time in minutes - when used for photobleaching in chapter 4
v	Linear velocity
X	Eye movement in horizontal direction used in chapter 3
x	Change in bleaching percentage
Y	Eye movement in vertical direction used in chapter 3
Δt	Time period used for velocity calculation
A	Saccade amplitude
D	Saccade duration
D_1	Duration of saccade with 1 ° amplitude
V	Peak saccade velocity
v	Euclidean saccade velocity
V_{max}	Asymptotic peak saccade velocity

Part I

Master thesis scientific article

Reproducing Glaucoma-like Elevated SRTs by Desensitizing a Healthy Human Retina using Half-field and Localized Photobleaching

Mayukh Sarkar (Msc student)*
Supervisors: Dr. Ir. D.M. Pool*, Dr.Ir. J.J.M. Pel† and Dr. P. Bremen†
*Dept. of Control & Simulation, Faculty of Aerospace Engineering, Delft University of Technology, Delft, Netherlands
†Dept. of Neuroscience, Erasmus MC, Rotterdam, Netherlands

***Abstract*—Glaucoma impacts vision by affecting visual processing at the retinal ganglion cell level. To recreate its impact on visual processing, photobleaching has been proposed to reversibly and temporarily induce glaucoma-like saccadic reaction time. It has been established that photobleaching elevates the threshold detection levels of visual stimuli in a healthy retina. This study investigated the potential implementation of photobleaching to recreate glaucoma-like SRTs. Results from the study show that photobleaching increased the SRT and reduced the ability to detect targets within the photobleaching zone of the visual field. The elevated SRTs obtained from the study indicate that photobleaching is a valid method for obtaining mild glaucoma-like SRTs. Furthermore, the effects of photobleaching were found to be highly localized, with the impact primarily observed within the bleaching zone. Attempts to replicate the localized effects of glaucoma using discrete photobleaching were inconclusive, with elevated SRTs observed in some cases, but the effect is directly related to the total area bleached. These findings provide the relationship between photobleaching, saccadic response, and their potential implications for artificially recreating glaucoma-like elevated SRTs.**

***Index Terms*—Photobleaching, Dark adaptation, glaucoma, saccadic reaction time, target detection.**

NOMENCLATURE

Δt	Time period used for velocity calculation
A	Saccade amplitude
C	Contrast
c	Constant parameter for saccade velocity
C_0	Contrast threshold
D	Saccade duration
d	Diameter of pupil
D_1	Duration of saccade with 1° amplitude
I	Luminance
K	Weber constant
k	Constant
L	Luminance of source
n	Constant power parameter for saccade duration
P	Percentage of stimulus area within the bleaching zone
R	Saccadic reaction time
r	Percentage of bleached photoreceptors
R_{min}	Minimum saccadic reaction time
t	Time of bleaching
V	Peak saccade velocity
v	Euclidean saccade velocity
V_{max}	Asymptotic peak saccade velocity
x_i, y_i	Position of the saccade at i^{th} point

I. INTRODUCTION

Numerous neurodegenerative diseases can negatively impact our visual system's ability to process input from the eyes. Glaucoma is such a disease. It is the world's leading cause of irreversible blindness caused by retinal ganglion cell (RGC) death, which leads to decreased visual sensitivity [1]. According to predictions, approximately 111.8 million individuals risk losing their vision due to glaucoma by 2040 [2]. Glaucoma progressively affects the visual field; the onset can be initially peripheral or localized and progresses to other areas of the retina [3]. One of the known causes of glaucoma is axonal degeneration of the RGC, leading to the death of the RGC and thus impairing the visual field [4].

Axonal degeneration also affects the flow of electrical signals through the neurons, preventing visual information flow to the brain, thus impacting sensory information processing. The degeneration process is non-selective and is triggered by injuries to the RGCs, or due to increased intraocular pressure (IOP) [5]. The IOP, regulated by the balance of aqueous humor secretion and drainage, is the only risk factor that can be managed to delay the onset of severe glaucoma [6]. The onset of glaucoma during its early stage often goes unnoticed, making it the "silent thief of sight" [7]. Early-stage glaucoma goes unnoticed due to the brain's ability to fill in missing information with minimal damage to the visual field and overlapping visual fields where the unaffected eye can compensate for missing information in the affected eye [8]. In its advanced stage, the disease leads to a complete loss of the visual field, resulting in tunnel vision. Figure 1 shows two common visual field deficit patterns observed in glaucoma patients, adapted from the study of Mazumdar [7]. Any damage to the visual field is known to impact activities requiring eye-hand coordination [9]. Pursuit eye motion in glaucoma is also affected due to the damaged visual system and neural undersampling. Saccades are also affected due to glaucoma [10]. Patients suffering from

glaucoma exhibit higher saccadic reaction times. Saccadic reaction time (SRT) is the delay between target onset and goal-directed or target-directed eye movement initiation.

A. Glaucoma in flying

Glaucoma affects visual processing, motion detection, spatial orientation, and visual search, thereby affecting tasks like driving, flying, etc. [11]. The fitness to fly is a crucial aspect of a pilot's job in modern-day aviation, and the safety risks associated with glaucoma in pilots must be addressed. However, minimal attention has been given to this disease by aviation regulators, which mainly focus on IOP and visual field degradation due to glaucoma based on threshold detection tests [12]. The different glaucoma detection techniques are explained later in Section I-B. Saccade properties like SRT are also affected by glaucoma due to errors induced in visual processing [11], [13]. Additionally, glaucoma influences the visual field, which can impact pilots' ability to scan the environment [14]. Aviation regulators such as the FAA, DGCA, and ICAO only prohibit applicants with severe glaucoma from flying. The FAA guidelines consider applicants with secondary open-angle glaucoma and $23\,\mathrm{mm}$ of Hg IOP fit for flying [15]. Secondary open-angle glaucoma can be caused by other eye diseases that trigger glaucoma. The DGCA considers a pilot fit to fly even when mild glaucoma is detected [16]. However, all evaluating tests are based on threshold detection automated perimetry [16]. Neglecting delayed SRT and anomalies in performance-based tasks in pilots suffering from glaucoma can cause severe safety issues. It is crucial to incorporate additional measures in evaluating pilots with glaucoma to ensure their safety and the safety of their passengers. Including tests that assess visual reaction time, motion detection, spatial orientation, and visual search can provide a more comprehensive evaluation of the impact of glaucoma on pilots' performance. Moreover, considering the effects of glaucoma on saccade properties like SRT can help regulators identify potential risks and make informed decisions about a pilot's fitness to fly. In conclusion, glaucoma can significantly affect pilots' performance and impact performance-based tasks like flying and monitoring.

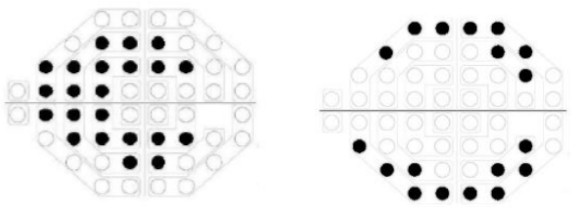

(a) Arucate sparing periphery (b) Peripherical defects

Fig. 1: Two common visual field deficits observed in glaucoma. Adapted from the study of Mazumdar [7].

B. Glaucoma diagnosis techniques

Clinical detection of visual field impairment is primarily based on functional evaluation, with Humphrey's Field Analyzer (HFA) as the protocol [17], [18]. HFA defines the test protocol to be adapted for various locations of the visual field correlated with the severity of the disease. Standard Automated Perimetry (SAP), the most commonly used algorithm, measures the minimum detection threshold of light sensitivity at various locations within the visual field [19]. However, SAP is limited by several factors, including patient discomfort, fatigue, false results, and the troxler's fading effect. This effect occurs when the patient must maintain a central fixation for an extended period, causing peripheral targets to fade and leading to inaccurate results [20]. Moreover, patients are often required to suppress natural reflexive eye movements, resulting in further discomfort, fatigue, and potential false outcomes.

It is essential to highlight that the limitations of SAP are primarily associated with its lengthy evaluation period. Various alternatives have been developed to address this challenge to reduce the time taken for evaluation. One such method is Field Doubling Perimetry (FDT) which utilizes contrast sensitivity to diagnose glaucoma. However, it does not track the disease's progression [21]. The Swedish Interactive Testing Algorithm (SITA) and its variants are more efficient regarding evaluation duration. SITA employs a staircase approach, where the stimulus threshold is increased after a missed detection to determine the minimum threshold of detection [22]. Additionally, SITA reduces the number of locations evaluated in the visual field, compensating for the evaluation time. A later version of SITA, SITA Faster, further decreased the evaluation period by eliminating the calculation of false negatives, retesting, and improving the staircase model. SITA Faster is currently the fastest evaluation algorithm, taking approximately 2 minutes to perform a visual field test. Eye Movement Perimetry (EMP) is another algorithm considering the SRT as an evaluation parameter. EMP addresses the issue of suppressing reflexive eye movements in SAP by supporting natural eye movements [10]. However, while addressing a more extended evaluation period of SAP, all these alternatives have disadvantages. For example, FDT cannot monitor the progression of glaucoma, and SITA risks an increase in false negatives and is unreliable for retesting. EMP also has reported calibration issues which can consume extra time. EMP utilizes fewer locations and only one repetition per location to expedite the evaluation process. However, this approach lacks sufficient samples for the SRT distribution, leading to inaccurate results [10]. Table I gives an overview of the different evaluation techniques and used parameters with the evaluation duration.

Since most techniques described above have flaws, developing new techniques is crucial. Timely detection and diagnosis of glaucoma are necessary to prevent its progression, emphasizing the need to develop effective techniques. To develop and test new techniques, we need glaucoma subjects.

TABLE I: Different techniques used to evaluate glaucoma with their evaluation parameter and duration.

Technique	Evaluation Parameter	Duration (min)
SAP [19]	Threshold detection	15
FDT [21]	contrast sensitivity	4-5
SITA [22]	Threshold detection	6
SITA faster [22]	Threshold detection	2
EMP [10]	SRT	6-12

However, incorporating patients in the development and testing is time-consuming. Patients are vulnerable and are not always readily available. Incorporating healthy subjects in the testing and development process is a potential solution if it is possible to induce glaucoma-like eye movement properties in healthy subjects temporarily. This paper investigated such an experimental protocol that can alter the properties of saccades in a healthy person for a brief duration by photobleaching, limited to a few seconds, without compromising the person's health. We hypothesized that the detection and performance of saccades would be affected under photobleached conditions that can successfully replicate the delayed SRTs and detection deficits observed in glaucoma. Furthermore, the study will act as a precursor to evaluate the effect of delayed SRT on performance-based tasks like flying or driving. The scenarios simulated here can be adapted to a glare-like environmental condition and can further assist in understanding the impact elevated SRTs have under glare vision.

II. Understanding and reproducing the effects of glaucoma

A. General effects of glaucoma

Attempts have been made to evaluate the effects of glaucoma on eye movements by analyzing scan paths during a free-uncontrolled television viewing by Crabb *et al.* [14]. The protocol used *"eye movement"* signatures to detect a neurodegenerative condition in subjects. Eye movement signature is an amalgamation of scan paths consisting of saccades and fixation points. The study successfully demonstrated that a group of patients with a neurodegenerative disease could be segregated from their healthy peers by considering eye signatures alone. Gorge *et al.* have shown that evaluating saccades can reliably measure the effects of a neuro-degenerative disease [23].

1) Effects on reading: Eye movements are connected to the process of reading. It is denoted by perceptual span - the amount of information captured and stored by the visual system at any time. So it is reasonable to suspect that people with visual field loss have compromised perceptual span, thereby influencing their reading capabilities. Individuals with glaucoma demonstrate slower reading speeds concerning perceptual spans, which is also evident due to the restricted visual field [24]. Another study by Cerulli *et al.* [25] on reading patterns of glaucoma patients reported no comprehensive relationship between reading speed and accuracy. However, it was discovered that individuals with glaucoma often overshot the presented target stimuli, followed by significant corrections. An error in visual processing during the identification process can lead to significant corrections in saccadic eye movements and thus cause a more substantial number of fixations [26].

2) Effects on performance-based tasks: Glaucoma is known to affect several visual functions alongside peripheral vision loss. Performance tasks are affected due to neural under-sampling as an outcome of RGC death or impairment. Glaucoma patients suffer from deficits in contrast sensitivity, color, and shape detection, often leading to reduced task performance [11]. Glaucoma also affects visual processing speeds, motion detection, spatial orientation, and visual search, affecting performance-based tasks like biking, driving, or daily activities. Again these are caused by dysfunctional RGC. Although the effect of glaucoma on performance-based tasks is evident, the relationship with the size and shape of the visual field or structural damage is still unknown. However, visual performance can be linked to the saccadic reaction time exhibited by glaucoma patients. Mazumdar *et al.* [13] demonstrated that individuals affected with glaucoma have higher saccadic reaction time than healthy individuals. These reaction times can sometimes be 50% more at locations with large eccentricity in the visual field. Besides elevated SRT, glaucoma patients also demonstrate increased contrast detection threshold and reduced percentage of seen scores in an EMP test [10].

B. Methods of elevating detection threshold and SRT

The human visual system can adapt to a wide range of light intensities, covering $10\log_{10}$ units [27].Two classes of photoreceptors mediate this ability; the rods and cones [28]. Cones mediate vision in light conditions (daylight), and rods mediate vision in dark conditions (moonless night sky) as shown in Fig. 2 [29]. The visual system adapts rapidly to gradually changing light conditions. However, this rapid adaptation is compromised in certain conditions. Two changes occur in the photoreceptors when the retina enters a bright environment from a dark environment. Firstly, the rods that were functional in the dark are hypersensitive to light, and when exposed to sudden bright light, the rods lose their structure and functionalities. The eye loses its retinal sensitivity for a small duration. Secondly, the cones, which are functional in bright conditions, become active on exposure to light. It takes close to $5\,\mathrm{min}$ for the cones to become fully active and the eye to regain retinal sensitivity and visual acuity to see in bright conditions. This rapid process of the retina adapting to bright conditions is called "light adaptation". When the eye enters a completely dark environment from a bright environment, the cones lose their functionality. The rod cells activate in the dark environment. However, the rods take a larger period to regain full functionality. As the rod cells activate, the rods produce the rhodopsin protein necessary for rod-mediated vision. It takes 20 - $30\,\mathrm{min}$ to fully generate the rhodopsins. Once the rhodopsins are generated, the rods become fully

functional, and visual acuity and retinal sensitivity are gained to function in a dark environment. This prolonged process of adapting to a dark environment is known as "dark adaptation" [27]. The rod system immediately bleaches when the retina is dark-adapted and exposed to a bright light source. The rods get bleached, and this process of losing retinal sensitivity when exposed to a bright light source in dark conditions is called "photobleaching". Since the rods facilitate vision in low light or dark conditions, the loss of retinal sensitivity due to bleached rods affects visual processing, thus hampering the ability to see or detect objects in photobleached condition [30]. The important thing to note is that the bleaching of cone photopigment has a smaller effect on cones. The effect of photobleaching on the rod and cone system is shown in Fig. 3. It can be observed in Fig. 3b for a 0.5 proportion of rods bleached, the detection threshold raised by $8\log$ units, whereas for the same proportion of cones bleached, the threshold increases by only $1\log$ units. Rods also take a higher time to recover from bleaching; for 0.5 proportion rods bleached, the recovery time is almost $10\,\mathrm{min}$ as shown in Fig. 3a.

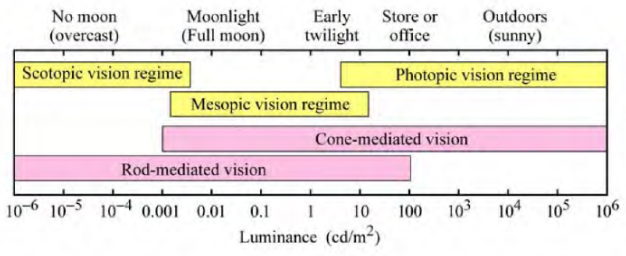

Fig. 2: Functional luminance range of rod and cones. Rods remain active in dark conditions, shown in the figure as a scotopic vision regime. The cones facilitate vision in bright conditions, shown as a photopic vision regime. Both rods and cone cells remain active in the mesopic vision regime of dim light conditions [29].

Stiles *et al.* [31] found that $30\,\mathrm{min}$ of dark adaptation can elevate the threshold of detection. The stimuli contrast is given by $K = \frac{\delta I}{I}$, where δI is the difference between the intensity of the target stimulus and I intensity of the background. It is also crucial to understand how long the effect of dark adaptation lasts. Hecht *et al.* [32] found that after a subject is dark-adapted and photo-bleached, it takes around $40\,\mathrm{mins}$ for the subject to return to its original threshold detection level under normal conditions. Equation (1) represents the percentage of photoreceptors bleached for a certain luminance over a period [33]. The Eq. (1) is valid when the bleaching period (t) is less than $120\,\mathrm{s}$, r is the percentage of photoreceptors bleached, I is the luminance of the light source in trolands, and t is the exposure time in minutes. Trolands is the unit of retinal luminance, $Td = L \times d$; L = Luminance of source, d = pupil diameter. $1\,\mathrm{cdm}^{-2}$ is equivalent to $\frac{4}{\pi d^2}$Td [34].

$$\log_{10}(1-r) = -\frac{It}{2\times 10^7} \tag{1}$$

Alongside elevated detection threshold, dark-adapted and photobleached subjects also showcase higher reaction times than normal subjects [35]. The reaction time can also be expressed as a function of the background luminance of the test screen or display, keeping the stimuli parameters fixed [36]. It is noted that the reaction time is inversely proportional to the background luminance. A rise in background luminance results in lower reaction times and vice-versa [36]. The relationship can be formulated by Eq. (2), where R is the reaction time, R_{min} is the minimum reaction time, C is the contrast, C_0 is the contrast threshold, and k is a constant. Cao *et al.* [37] also pointed out that the SRTs of the rods and cones increase when a subject is dark-adapted and photobleached.

$$R = R_{min} + \frac{k}{C - C_0} \tag{2}$$

To achieve elevated SRTs, photobleaching, and dark adaptation will be used simultaneously to hinder the visual processing of photoreceptors.

III. Methodology

A. Identifyable parameters and algorithm

In Section II-A, it was found that evaluating saccades can lead to a better understanding of eye movements in glaucoma. SRT is used as a parameter for EMP. The algorithm measured the reaction time to certain targets when presented in the visual field and compares normative SRT values of age-matched control groups with normal vision to detect glaucoma. All the alternative algorithms to SAP prioritize reduction in evaluation time while also focusing on accuracy. Short trial durations will also help to avoid any possible fatigue of the subject and the Troxler effect, thus eliminating the possibility of bad data quality.

B. Eye movement selection

It has been noted that the mechanism of saccades is affected by glaucoma due to damaged sensory processing and RGC. These saccades are characterized by higher reaction time and are often accompanied by multiple correction saccades. The most observed parametric changes in saccades are the SRTs. Selection of valid saccades was done using a 8° region of interest around the target stimulus. The selection procedure is shown in Section IV-A. If the endpoint of the primary saccade lies within that area, then the saccade is considered valid. Additionally, saccades below $180\,\mathrm{ms}$ were regarded as anticipatory saccades and thus disregarded. Also, SRTs above $700\,\mathrm{ms}$ were disregarded as they were considered very late responses to a target. 30% of the total saccades were removed during the analysis after implementing the above criteria.

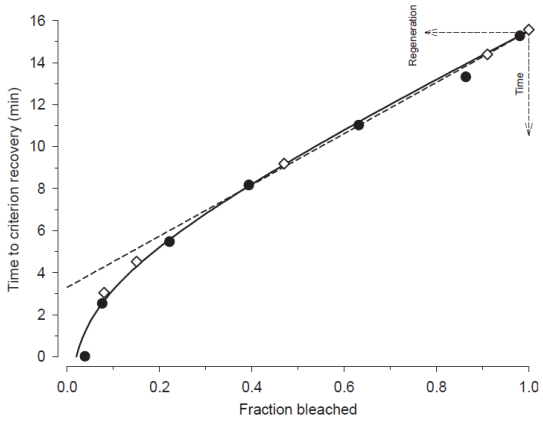

(a) Time of recovery for fraction of photoreceptors(rods) bleached [27].

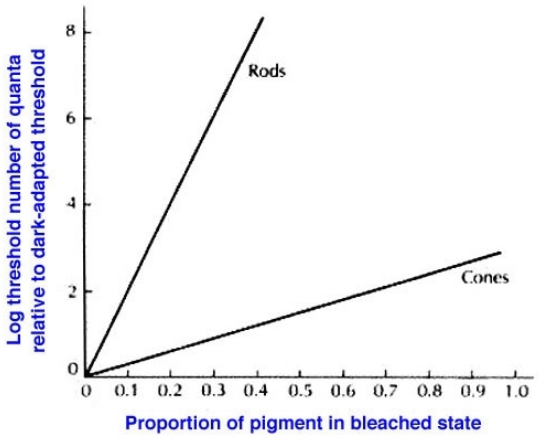

(b) The effect of bleaching on the threshold of stimuli detection of rods and cones [30].

Fig. 3: Figure 3a shows the time taken for a certain fraction of bleached photoreceptors(rod cells) to recover. In Fig. 3b, it can be observed that the rod system is hugely affected by bleaching than cones. A 0.5 proportion of bleached rods raises the minimum detection threshold by 8 log units, whereas for a fully bleached cone system, 2 log units only raise the detection threshold.

C. Methods of stimulation

The effect of photobleaching is instantaneous when the eye is in a dark-adapted state or a dark environment. Dark adaptation activates the rod system, which is highly sensitive to light, making the retina susceptible to a sudden bright light source. This simplifies bleaching the visual system as a less intense light source is needed for a shorter duration. Also, this process has less chance of permanently damaged to the eye as the effect lasts for a limited period only.

D. Eye tracking

The used binocular eye tracker is based on infrared tracking of the pupil reflection where the eye tracker samples the movement of the pupil at $120\,\mathrm{Hz}$. This section focuses on various aspects of the eye-tracking methods used during the study and the saccade detections performed. The section is divided into three subsections: calibration, gaze estimation, and saccade detection.

1) Eye tracker calibration: The eye tracker software must adapt according to the subject to accurately estimate the gaze points and direction. This adaptation and adjustment are achieved by calibrating when the user tracks a set of points on the active display area. A 9-point calibration procedure was used where the subject had to track points presented randomly to calibrate the eye tracker. In this case, the active display area is the screen display where the user looks [38].

2) Saccade detection: Saccades are high-velocity eye movements measured in hundredths of a second performed by directing the sensitive region of the retina towards a point of interest in the visual field. Salvucci and Goldberg provided an overview of several saccade-detection algorithms based on different criteria [39]. Velocity-based detections are a robust and fast way of detecting saccades which have been used during this study.

For velocity-based saccade detection, Velocity-Threshold Identification (VTI) is preferred. VTI takes only one input parameter, i.e., the minimum detectable velocity. It differentiates points based on their velocity; the algorithm calculates the distance between two points and the time to determine the velocity. A simplified form of VTI can be described by Eq. (3) is implemented in the thesis, and the detection is shown in Fig. 4. When a saccade is performed, a higher threshold of $100\,^{\circ}\mathrm{s}^{-1}$ is implemented first to obtain a region of interest. For more accurate detection, a second criterion is implemented with a lower threshold of $50\,^{\circ}\mathrm{s}^{-1}$ to obtain the start and end of the saccade accurately.

$$v = \frac{\sqrt{(x_i - x_{i-1})^2 + (y_i - y_{i-1})^2}}{\Delta t} \tag{3}$$

E. Experiment design

1) Lower Hemifield bleaching Pattern (LHB): The lower hemifield bleaching pattern is used to understand the effects of photobleaching on saccades when only the lower hemifield of the visual field is bleached. This pattern aims to bleach the photoreceptors in the eye's lower half. The target stimuli are shown as circles in Fig. 5. The pattern is adapted from the grid used by Pel *et al.* [10]. The time course of each trial is shown in Fig. 6. The first interval lasts for a duration of $4\,\mathrm{s}$, including the bleaching pattern if it is a bleaching trial or a blank frame for a non-bleaching trial. It is followed by a $0.4\,\mathrm{s}$ fixation interval and then by a $0.1\,\mathrm{s}$ blank interval. In the 4^{th} frame shown in Fig. 6, a random target is displayed for $0.2\,\mathrm{s}$, followed by a $1\,\mathrm{s}$ post blank interval.

A second variation of this pattern is used where the duration of the 1^{st} and 4^{th} frames shown in Fig. 6 is changed to $1.5\,\mathrm{s}$ and $1.2\,\mathrm{s}$. This adapted pattern version will be

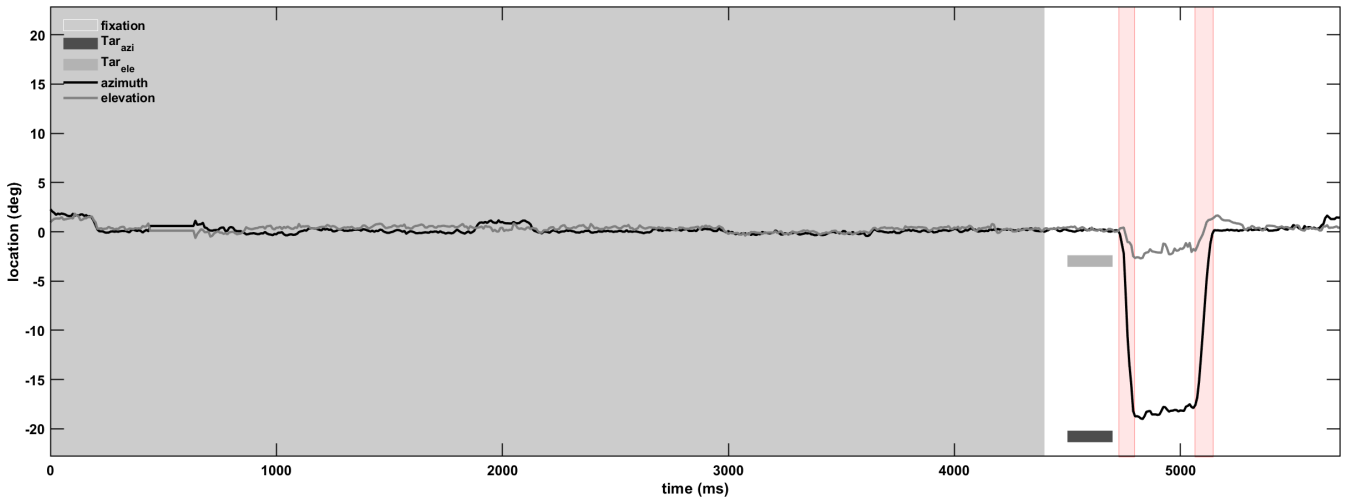

(a) Example of two saccades performed in response to a certain target by a subject during experimentation.

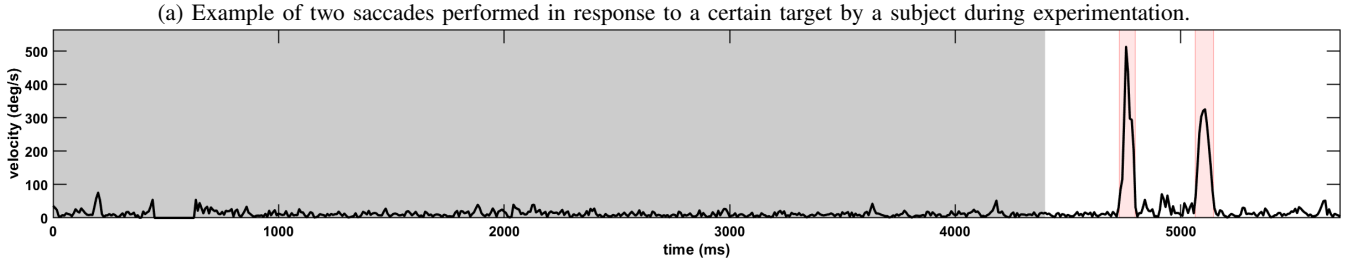

(b) Two velocity peaks detected by the algorithm corresponding to the saccades shown above.

Fig. 4: An example of a saccade detected using the velocity threshold algorithm. The area of interest marked by a red patch is determined if the saccade velocity is above $100\,^{\circ}\mathrm{s}^{-1}$. Then for the detected saccade, a lower threshold of $50\,^{\circ}\mathrm{s}^{-1}$ is implemented to detect the start and end of the saccade further accurately. The gray patch represents the fixation duration. The azimuth and elevation of the targets are represented by the two small black and gray boxes, respectively.

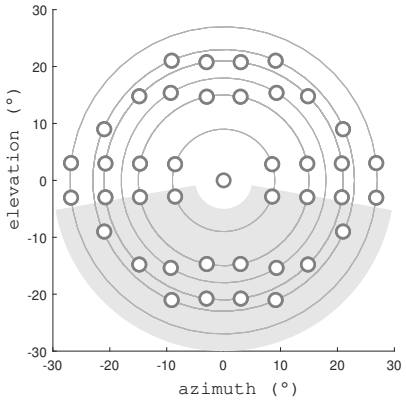

Fig. 5: 40-point stimuli grid pattern used for LHB. The circle in the center is the CoF visible in the 2nd frame in Fig. 6. During the bleaching trials, the grey-shaded area on the lower half is shown in the 1st frame shown in Fig. 6. For non-bleaching trials, this grey area is absent, and the 1st frame in Fig. 6 is replaced by a blank frame.

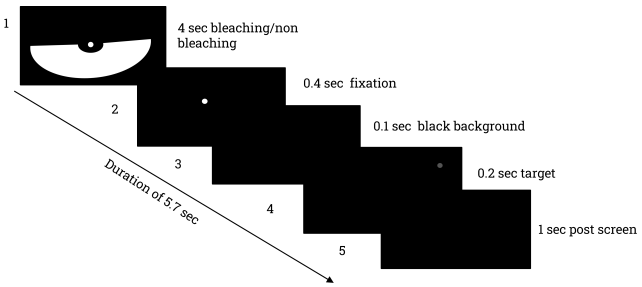

Fig. 6: Representation of the different frames shown sequentially in a trial within a set for the experiment LHB

denoted as LHB_V_2. This variation was used to observe if a short bleaching period and longer target presentation duration would result in more targets seen and elevated SRTs.

Hypothesis I : The SRTs and the total number of targets detected are only expected to be affected by photobleaching. The obtained SRTs will mimic the SRTs obtained in glaucoma with a lower number of targets detected.

2) Bleaching overlap effect (BO): This experiment was conducted to observe the effect of the percentage overlap of the target with the bleaching area. A box-shaped central patch is taken as the bleaching area, and the targets lie on the left and right sides of the patch as shown in Fig. 7. The targets shift horizontally along their diameter of $0.5\,^{\circ}$. The stimulus area within the bleaching zone was based on the area of the

sector of the stimulus circle within the bleaching zone. A 0% overlap means the target is entirely outside the bleaching area, and a 100% overlap implies the target is inside the bleaching area. The targets were gradually shifted from 0 to 100 % overlap. The overlaps used are 0%, 10%, 50%, 90% and 100% of the stimulus area within the bleaching zone. The supporting hypothesis for this experiment is as follows:

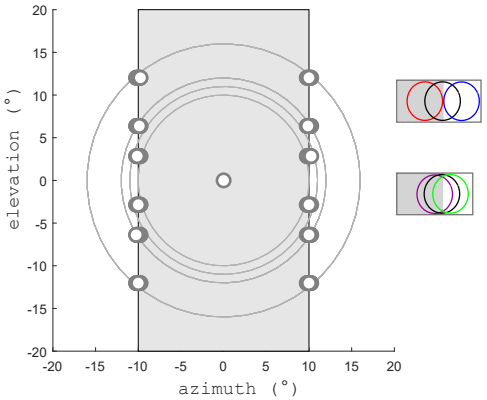

Fig. 7: Figure showing the BO pattern. Each target has a diameter of $0.5\,°$, and they shift along their diameter. The red circle (○) represents the target fully outside the bleaching zone, and the blue one (○) is when the target is fully inside the bleaching zone. The 50% overlap is shown by the black circle (○). The green (○) and purple(○) represents the 10% and 90% overlaps respectively.

Hypothesis II : The amount of target area overlapped by the bleaching zone is directly proportional to the increase in SRT. With the linear increase of the area overlap, the SRT is expected to increase linearly. The effect of photobleaching will be localized only to the areas bleached.

3) Localized Glaucoma Patterns (LGP): The localized glaucoma patterns that are being reproduced are arcuate sparing periphery (ASP), peripheral defects (PD), and early superior paracentral defects (ESP). These patterns attempt to reproduce the standard localized effects of glaucoma in the visual field. The effects of glaucoma are seen in the early and moderate stages. The patterns are adapted from the thesis work of Mazumdar [7]. The ASP, PD, and ESP patterns are shown in Fig. 8. Figure 8a and Figure 8b show the ASP and PD bleaching pattern, which are 40-point grid patterns. The ESP bleaching pattern, shown in Figure 8c, is a 24-point grid. All these bleaching patterns attempt to demonstrate the localized effect of photobleaching. The supporting hypothesis for the local bleaching effects is given by:

Hypothesis III : Bleaching discrete areas of the visual field can elevate the SRTs obtained at those locations equivalent to the SRTs obtained in glaucoma patients.

F. Experiment variables

The term "trial" means a chain of frames shown to the target at different intervals to represent one stimulus. For example,

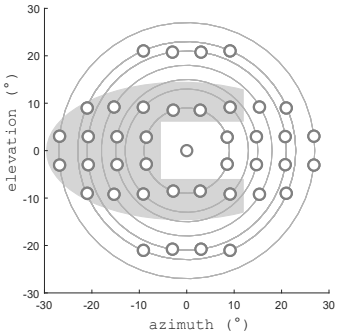

(a) ASP bleaching pattern

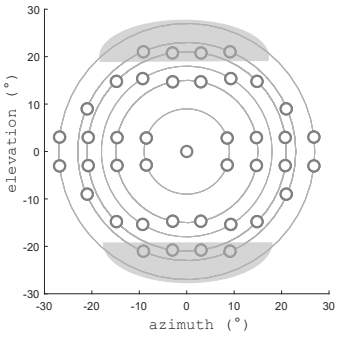

(b) PD bleaching pattern

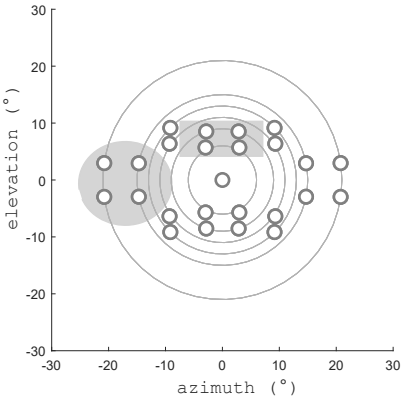

(c) ESP bleaching pattern

Fig. 8: Localized bleaching patterns used for experimentation, adapted from the thesis of Mazumdar [7]. The areas shaded in grey represent the bleaching zones.

the frames shown at different intervals for a specific target in Fig. 6 is one trial. One "repetition" consists of a *N* number of trials.

1) Control variables: These variables or factors are fixed to prevent bias and ensure fair evaluation during the experimental phase. Three sets of control variables were considered for the study.

(i) *Experiment setup:* The monitor display (iiyama monitor), where the stimulus was presented and the eye tracker used for the experimentation, is kept constant. The luminance is modulated to two levels; $350\,\mathrm{cdm}^{-2}$ and $262\,\mathrm{cdm}^{-2}$. Fixing the luminance also controls

TABLE II: Overview of the different subjects who participated in the study.

Subject No.	Gender	Age	History
2	Female	22	Myopia
3	Male	23	
4	Female	20	
5	Female	24	
6	Male	23	Mild myopia
7	Male	39	Night blindness
8	Male	42	Myopia
9	Male	51	

the number of photoreceptors bleaching during the photobleaching process. The bleaching duration and the stimulus duration were kept constant within each variation of the experiments conducted for the study. The non-bleaching condition was used as a control with the same duration as bleaching. Figure 6 shows the events within a trial. In the first frame, the white semicircle is absent if the trial is a non-bleaching trial. Instead, it displays a black background with the center of fixation (CoF) for $4\,\mathrm{s}$. The distance to the monitor was kept constant at $60\,\mathrm{cm}$. No hardware or software changes were made during the experimentation phase.

(ii) *Stimulus:* The second control variable here is the characteristics of the stimulus presented. A circular stimulus with diameter $0.5\,^{\circ}$ was given for all the experiments. The color of the stimulus was fixed at the RGB value of [0.05 0.05 0.05]. The background also remained fixed at RGB values of [0 0 0], while the bleaching patterns used had an RGB value of [1 1 1].

(iii) *Task:* The subject has to react to a stimulus presented on the screen at a pseudo-randomized location after both bleaching and non-bleaching trials by initiating eye movements. For the task, the subjects had to stabilize their head and chin against a head-chin rest to prevent involuntary head rotations while reacting to a particular target. Also, each subject was exposed to a $30\,\mathrm{s}$ pre-adaptation bleaching period before the start of each repetition. This pre-adaptation was done to get the photoreceptors' state in each subject's retina to a similar starting level. The subjects also had to perform a calibration trial to calibrate the eye tracker.

2) Independent variables: : The independent variables are the bleaching patterns and the bleaching (BL) or non-bleaching (NBL) trials performed within a set.

3) Dependent variables: The dependent variable for this study is the SRTs obtained from the subjects. Also, the ability to detect targets is taken as a dependent variable.

G. Subjects and experiment matrix

For the experiment total of 8 subjects were recruited, three female subjects and five male subjects. Table II shows a chart of different subjects with gender, age, and eye disease history.

The total experiment time was four hours for each subject and was divided over two days of two hours each. All the subjects had to perform ten repetitions of experiments LHB and BO each. 10 repetitions were considered sufficient to collect a larger sample from each participant. Next, they were given one pattern from the localized bleaching experiment in which they had to perform five repetitions. Inside each repetition, the stimulus was shown in random patterns to negate the effect of the stimulus prediction. Table III shows how the repetitions were distributed over two days for each participant. The LGP mentioned in Table III denotes one pattern from the localized bleaching patterns the subject performed. It has to be noted that each subject performs only one of the said variations. The subjects were dark adapted before the experiments for $10\,\mathrm{mins}$. A small gap of $2\,\mathrm{min}$ was given between two repetitions while being dark-adapted, and the break mentioned in Table III was for $15\,\mathrm{min}$ in a bright environment. No dark adaptation was performed after the breaks. Subjects 2 and 9 also performed 10 repetitions of the LHB_V_2 variation separately. The background luminance level for this variant was set to $262\,\mathrm{cdm}^{-2}$. For subject 7, it was not possible to reliably extract saccade parameters from the data. Accordingly, we excluded all data from this subject.

IV. Results

A. LHB results

The data has been pooled across all subjects to analyze saccade properties based on the finding of Hopf *et. al* [40].

1) Effect on SRT: It is observed that the bleaching affected the SRTs in both the hemifields as shown in Figure 9. In the upper hemifield region, the median SRTs recorded during the bleaching trials increased minimally from the median SRTs in non-bleaching trials, as shown in Fig. 9a. The difference between the median SRTs observed from the bleaching and non-bleaching trials for the upper hemifield varies between 20 - $40\,\mathrm{ms}$. The results Kolmogorov-Smirnov test performed for the SRTs at each eccentricity, as shown in Table V, accept the similarity condition across all eccentricities n the upper hemifield except $15\,^{\circ}$ and $23\,^{\circ}$. However, as can be seen, Fig. 9a, the difference of the median SRTs at that two eccentricities is very small, in the order of 20 - $40\,\mathrm{ms}$. The SRTs increase almost monotonically till $23\,^{\circ}$ and then drop at $27\,^{\circ}$. This sudden decrease in trend is also evident in the lower hemifield, as shown in Fig. 9b. This sudden decrease of SRTs at higher eccentricity can be caused due to the participants predicting the target locations. Only two targets were present at $27\,^{\circ}$. Because the fixation shifts to accommodate higher eccentricities during the experiment, it is possible that the participants could predict the locations of stimuli. It can be observed from Fig. 9b that there is a significant difference between the median SRTs of the bleaching and non-bleaching trials at each eccentricity of the lower hemifield. A Kolmogorov-Smirnov test rejects the similarity condition for the SRT distributions at all eccentricities between the bleaching and non-bleaching trials in the lower hemifield as shown in Table V. The mean difference is roughly around

TABLE III: Distribution of experiments over two days for each subject.

Day 1	LHB	BO	LGP	LHB	LHB	BO	Break	BO	LHB	LGP	BO	LHB	BO	
Day 2	LHB	BO	LGP	LHB	LHB	BO	Break	BO	LHB	LGP	BO	LHB	BO	LGP

100 ms. A larger spread in the SRTs from bleaching trials in the lower hemifield can also be observed in Fig. 9b. This larger spread is primarily due to the variability of the SRTs inside the bleaching zone. As shown in Table IV, the median inter-quartile range (IQR) of the SRTs in the lower hemifield is $180.8\,\mathrm{ms}$, which is significantly higher than the non-bleaching condition. The higher IQR denotes higher variability because of the fewer detections in the lower hemifield during the bleaching trials and the higher SRTs in those trials.

TABLE IV: Inter-quartile range (IQR) values for non-bleaching and bleaching conditions in both hemifields. Units in [ms].

Conditions	NBL IQR (ms)	BL IQR (ms)
Upper hemifield	78.4	97.1
Lower hemifield	73.8	180.8

TABLE V: Kolmogorov-Smirnov test to check for the similarity between SRT distribution at each eccentricity in the two hemifields between the bleaching and non-bleaching condition. H = 0 and P $>$ 0.05 denotes the similarity between the two distributions. H = 1, and P $<$ 0.05 rejects the similarity condition.

Hemifield	Upper Hemifield		Lower Hemifield	
Statistics	H	P	H	P
9°	0	0.17	1	0
15°	1	0.02	1	0
18°	0	0.92	1	0
21°	0	0.06	1	0
23°	1	0.02	1	0.02
27°	0	0.1	1	0

2) Accuracy of saccades: This study investigates the effect of partial visual field bleaching on saccades, emphasizing the lower hemifield bleaching, as illustrated in Fig. 5. The accuracy is investigated here to identify filtration criteria for selecting valid saccades for the study. It has been observed that the euclidean distance error increases with eccentricity for both the hemifields in Fig. 10. The positional accuracy of saccades in the upper hemifield, shown in Fig. 10a for both the conditions, are similar, and the accuracy decreases with an increase in eccentricity. A Mann-Whitney U test (H = 0, P = 0.56) accepts the similarity condition. The similarity in distribution is not found in the lower hemifield where the bleaching zone was present. A Mann-Whitney U test (H = 1, P = 0.04) rejects the null hypothesis. The non-similarity shown in Fig. 10a is primarily because of the lower number of detection during the bleaching trials. Only 29.4% of stimuli were detected in the lower hemifield during bleaching trials, whereas 82% of total stimuli were successfully detected in the lower hemifield during non-bleaching trials. The detections in the upper hemifield were also lower during bleaching trials by 6%. However, the difference is insignificant. An overview of the total number of detections is given in Table VI. Also, since photobleaching impacts the stimuli processing capabilities of the photoreceptors, the subjects could not identify a stimulus and its position, resulting in fewer detections and lower accuracy. The maximum median error is found to $8\,^\circ$ in Fig. 10b for the bleaching criteria and is used as the selection criteria for saccades. Also, saccades with SRT below $180\,\mathrm{ms}$ were not considered as they might be anticipatory.

TABLE VI: Total percentage of stimuli detected in each hemifield during non-bleaching and bleaching trials.

Conditions	NBL	BL
Upper hemifield	77.8%	71.6%
Lower hemifield	82%	29.4%

3) LHB_V_2 SRTs: A modified version of LHB was also studied to increase the number of targets seen in LHB and to achieve similar SRTs. Only subjects 2 and 9 participated in the LHB_V_2 experiment; thus, only their data from the original LHB experiment is used for comparison. It was expected that lowering the bleaching period from $4\,\mathrm{s}$ to $1.5\,\mathrm{s}$ would decrease the intensity of bleaching and thereby enabling the subject to detect more stimuli. More detections can reduce the variability in the recorded SRTs. The luminance of the display was set to $262\,\mathrm{cdm}^{-2}$ for this experimentation. The SRTs for both the participants from LHB and LHB_V_2 are shown in Fig. 11. As shown in Fig. 11d, the SRTs from the bleaching trials are higher than the non-bleaching trials in the lower hemisphere. Also, the number of stimuli detected during the bleaching trials is significantly lower. Table VII shows the percentage of stimuli detected by the subjects in both experiments. For the non-bleaching condition, the same number of stimuli were detected in both the hemifields for both experiments. However, for the bleaching trials in LHB_V_2, 10% more stimuli were detected than LHB in the upper hemifield. The number of stimuli detected in the lower hemifield for both experiments during the bleaching trials was approximately the same. Also, the expected result of lower variability was not observed. The IQR shown in Table VIII for both the hemifields during the non-bleaching trials of the experiments varies between 3 - $9\,\mathrm{ms}$, implying that the variability is almost identical in both cases. The same can also be noticed for the bleaching trials in the upper hemifield. However, $100\,\mathrm{ms}$ difference in IQR can be noticed between the bleaching trials of the experiments in the lower hemifield. This increased variability can depend on the difference in SRTs between the two subjects. However, it can be concluded that the LHB_V_2 experiment successfully elevates the SRT; a lower bleaching period can be used in the future to achieve elevated SRT. However, since results were obtained from only two participants, the values shown in Fig. 11 can be biased,

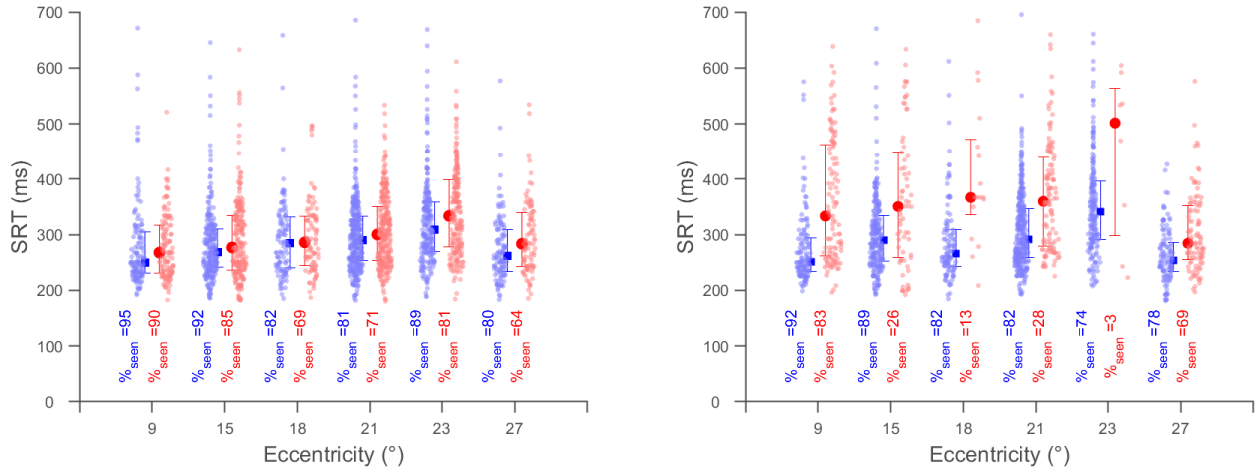

(a) Upper hemifield SRT comparison

(b) Lower hemifield SRT comparison

Fig. 9: SRT distribution of non-bleaching and bleaching conditions for upper and lower hemifield, respectively, pooled across all subjects. The small light blue dots (●) and light red dots (●) are the SRTs for non-bleaching and bleaching conditions. The blue square (■) and red circle (●) represent the median values of SRTs in both hemifields' non-bleaching and bleaching conditions. The 25^{th} and 75^{th} percentile of SRTs are given by the blue (–) and red (–) error bars for each condition in each hemifield. $\%_{\text{seen}}$ signifies the percentage of detections at each eccentricity for each condition.

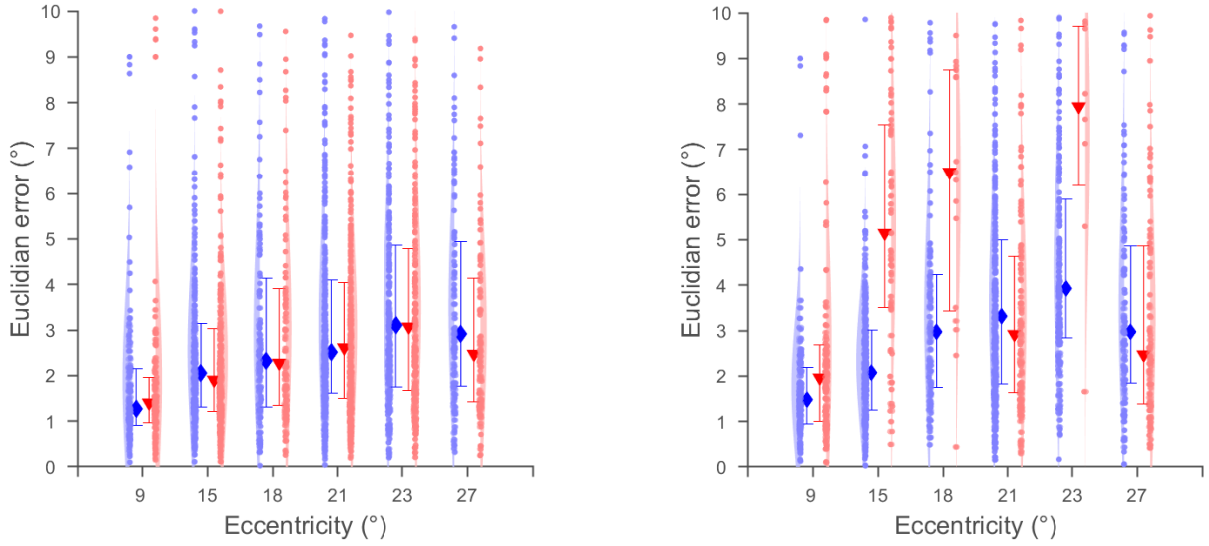

(a) Positional accuracy of saccades in upper hemifield

(b) Positional accuracy of saccades in lower hemifield

Fig. 10: distribution of positional accuracy of saccades during both hemifields' non-bleaching and bleaching trials pooled across all subjects. The small blue dots (●) and red dots (●) are the euclidean errors for non-bleaching and bleaching conditions. The blue diamond (◆) and red triangle (▼) represent the median values of euclidean errors in both hemifields' non-bleaching and bleaching conditions. The 25^{th} and 75^{th} percentile of error values are given by the blue (–) and red (–) error bars for each condition in each hemifield.

and more data is needed to reach a definitive conclusion.

It can be concluded from the results of LHB that higher errors and elevated SRTs were primarily obtained from the participant's inability to detect stimuli in the lower hemifield during the bleaching trials. Even when a stimulus was detected, the detection was slower, resulting in higher SRT, and the subject could not reach the location where the stimulus was displayed. Furthermore, fewer detections in the lower hemifield increased the variability observed in the errors and SRT. Thus, photobleaching primarily affected the ability to identify and distinguish a stimulus, resulting in delayed reactions increasing the SRTs.

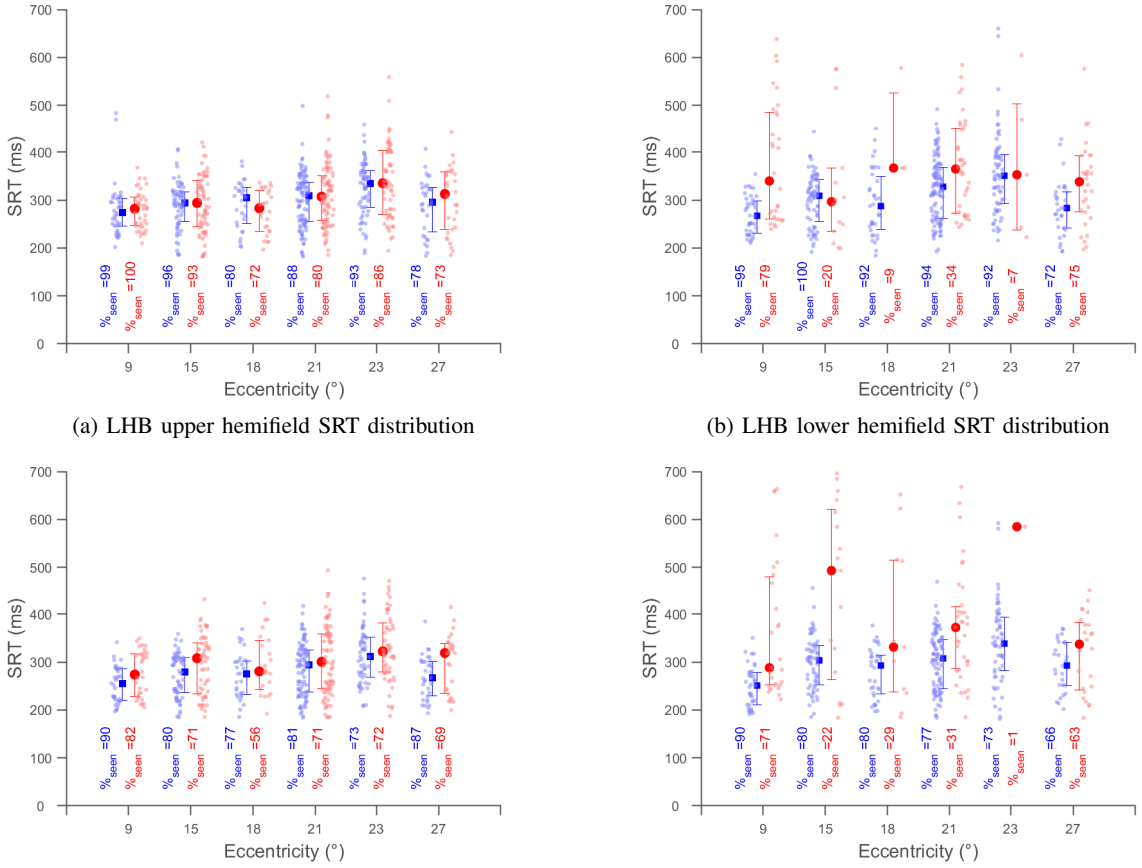

(a) LHB upper hemifield SRT distribution

(b) LHB lower hemifield SRT distribution

(c) LHB_V_2 upper hemifield SRT distribution

(d) LHB_V_2 lower hemifield SRT distribution

Fig. 11: SRT distribution of non-bleaching and bleaching conditions for upper and lower hemifields pooled from subjects 2 and 9. The results from LHB and LHB_V_2 are shown here. The small light blue dots (●) and light red dots (●) are the SRTs for non-bleaching and bleaching conditions. The blue square (■) and red circle (●) represent the median values of SRTs in both hemifields' non-bleaching and bleaching conditions. The 25^{th} and 75^{th} percentile of SRTs are given by the blue (−) and red (−) error bars for each condition in each hemifield. N signifies the percentage of detections at each eccentricity for each condition.

TABLE VII: Total percentage of stimuli detected in each hemifield during non-bleaching and bleaching trials in LHB and LHB_V_2 pooled from subjects 2 and 9.

Conditions	NBL		BL	
Experiment	LHB	LHB_V_2	LHB	LHB_V_2
Upper Hemifield	83%	76.5%	68%	78%
Lower Hemifield	83%	76.5%	30%	28.75%

TABLE VIII: LHB and LHB_V_2 IQR values for non-bleaching and bleaching conditions in both hemifields pooled from subjects 2 and 9 . Units in [ms].

Conditions	NBL IQR (ms)		BL IQR (ms)	
Experiment	LHB	LHB_V_2	LHB	LHB_V_2
Upper hemifield	75.6	72.1	94.9	103.35
Lower hemifield	94.36	85.9	202.08	301.29

B. BO results

The results obtained in this experiment are based on the reaction times recorded at each elevation separately based on the bleaching pattern shown in Fig. 8. The results are derived from 6 participants who took part in this experiment. The recorded elevations were $\pm 12.2\,^{\circ}$, $\pm 6.4\,^{\circ}$ and $\pm 2.8\,^{\circ}$. A linear equation given by Eq. (4) was fitted to SRT distribution at each elevation to visualize if a linear trend exists. R_{fit} is the fitted SRT curve, c is a constant, m is the slope of the fitted line, and P is the percentage of stimuli area overlap. Fig. 12 gives the overview of the fitted equation at all elevations.

$$R_{fit} = c + m.P \tag{4}$$

In all the subplots shown in Fig. 12, a significant difference of almost $100\,\text{ms}$ can be noticed between the median SRTs at 0% and 100% overlap. It can be noticed that the number of detected stimuli decreases with the increase in elevation in both directions as shown in Table IX. The same can be noticed in Fig. 12. Lower R^2-values and larger confidence intervals were expected since the fitted curve considered the larger spread and variability of the recorded SRTs. Fitting the

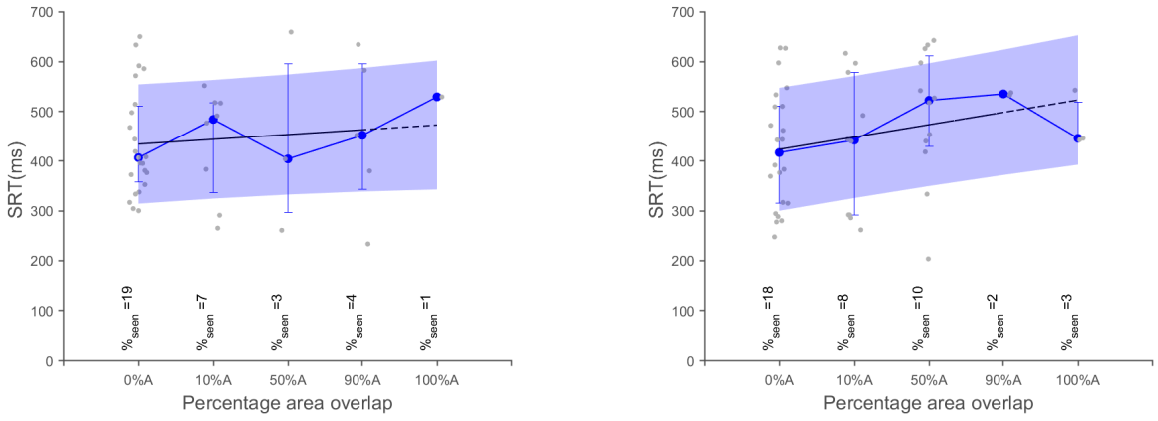

(a) SRTs at for +12.2° R^2 = 0.09 N_{total}% = 5.7

(b) SRTs at for -12.2° R^2 = 0.09 N_{total}% = 9.8

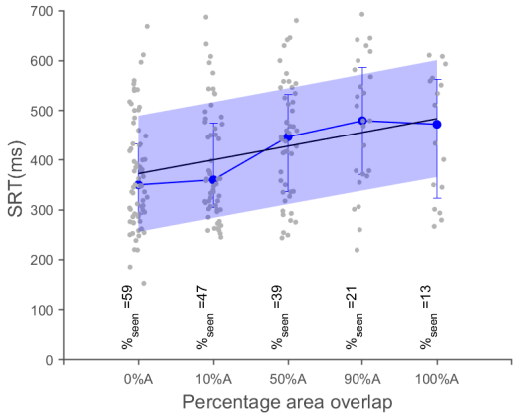

(c) SRTs at +6.4° R^2 = 0.25 N_{total}% = 30.7

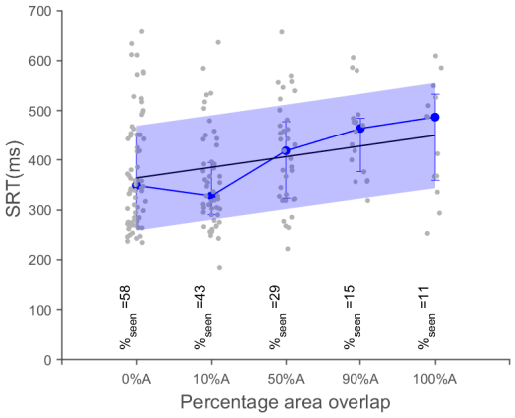

(d) SRTs at for -6.4° R^2 = 0.24 N_{total}% = 26.7

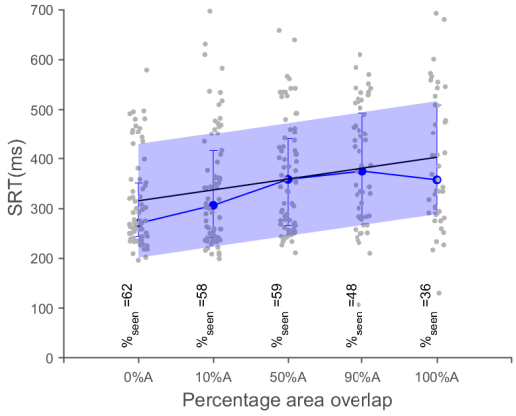

(e) SRTs at +2.8° R^2 = 0.3 N_{total}% = 45

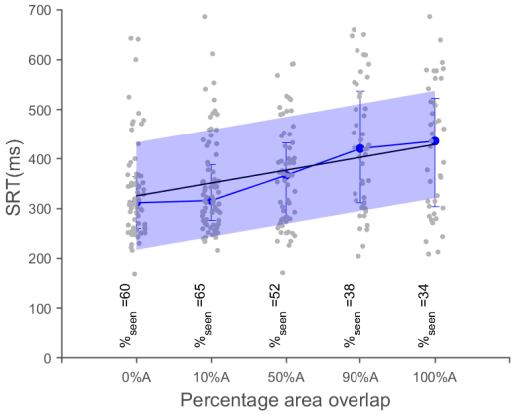

(f) SRTs at for -2.8° R^2 = 0.32 N_{total}% = 42.6

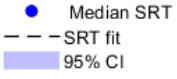

(g) Figure Legend

Fig. 12: A linear equation fit to SRT distributions across 6 elevations from experiment BO pooled across all subjects. The dark blue(●) circle indicates the median values of the SRTs. Gray dots show individual SRTs (◉). The blue error bars represent the 25^{th} and 75^{th} percentile of SRTs. The black shows a linear fit dashed lines (−). N represents the percentage of targets detected at a specific elevation. Each elevation had a total of 600 targets. Each overlap has 120 targets

TABLE IX: Percentage of stimuli detected at each elevation

Elevation	$2.8\,^\circ$	$6.4\,^\circ$	$12.2\,^\circ$
Upper hemifield (+)	45%	30.7%	5.7 %
Lower hemifield (-)	42.6%	26.7%	9.8%

curve through the median values would have resulted in a smaller confidence interval and higher R^2-values as shown in Fig. A.I. In Fig. A.I, elevations $\pm 6.4\,^\circ$ and $\pm 2.8\,^\circ$ give a higher R-value close to 1. The higher correlation coefficient value denotes a strong correlation between the median SRTs obtained at those elevations and the stimulus area overlap. However, a stronger correlation cannot be established for the elevations $\pm 12.2\,^\circ$. Also, it can be noticed in Fig. 12 that the number of detections also decreases along with the increased area overlap. Thus, targets are less visible when the stimulus is fully inside the bleaching zone. From the results, it can be concluded that the increase in the SRT is directly proportional and linearly related to the increase in the amount of stimulus area overlapped by the bleaching zone. This linearity also signifies that the effect of photobleaching on the visual field is localized in nature.

C. Local Bleaching effect results

1) ASP results: The experiment results from only one participant (Subject 4) are presented in Fig. 13. Figure 13a shows the median SRTs for individual target locations at different eccentricities obtained during the non-bleaching trials. Each location had 5 targets, and the lower percentage of detections implies that the subject had difficulty identifying targets under non-bleached conditions. In Fig. 13b, the subject fails to detect a larger proportion of targets inside the bleaching zone during the bleaching trials, which were detected in the non-bleaching trials. Also, it can be noticed that most of the detected targets inside the bleaching area exhibited higher SRTs. However, the bleaching effect can also be seen outside the bleaching area in Fig. 13b as the subject fails to detect a large proportion of targets outside the bleaching zone during the bleaching trials. This failure in detection can be caused by the leakage of the bleaching effect to other areas of the visual field because of the prolonged experiment period. Also, this specific subject can be more reactive to photobleaching. Due to the lack of data and the hyper-reactive nature of the subject to photobleaching, no conclusion can be reached.

2) PD results: For this experiment, the results obtained from two subjects (Subjects 2 and 8) are shown in Fig. 14 and Fig. 15. For subject 2 in Fig. 14, the differences between the SRTs and the detected targets were observed between the non-bleaching and bleaching trails outside the bleaching zone were in the order of 20 - 50 ms. However, it can be noticed in Fig. 14b that 20% of targets were detected inside the bleaching area during the bleaching trials, significantly lower than the detections made at those areas during the non-bleaching trials. Also, the subject fails to detect some targets completely during the bleaching trials. Thus the effect of local photobleaching on subject 2 was only observed in terms of failed detections, not in elevated SRTs. For subject 4, a change in median SRTs (in the order of 20-50 ms) was observed between targets outside the bleaching zone during the non-bleaching and bleaching trials, as shown in Fig. 15. The number of targets detected within the bleaching zone during the bleaching trials is 0 compared to the 72% detected targets at the same area during non-bleaching trials, as shown in Fig. 15b. The lower detections within both subjects during the bleaching trials can result from the photobleaching effect coupled with the extreme position of the targets. In conclusion, it can be said that local photobleaching successfully mimicked the peripheral defects observed in glaucoma but was also influenced by the vertical peripheral locations of the targets.

3) ESP results: The results for this experiment were obtained from subjects 3, 6, and 8. The bleached eccentricities are $6\,^\circ$ and $9\,^\circ$ shown by the rectangular gray patch; and $15\,^\circ$ and $21\,^\circ$ shown by a circular patch in Fig. 8c. The results from subject 3, as shown in Fig. 16, show abnormalities regarding the median SRTs obtained and detected targets. Median SRTs from the non-bleaching condition from subject 3 have a value of approximately 355 ms at most target locations, with some locations having median SRTs of 230 ms as shown in Fig. 16a. This higher variation of median SRTs is unusual for the non-bleached condition. The median SRTs obtained during the bleaching trials for this subject is shown in Fig. 16b. It can be observed that the SRTs inside the circular bleaching zone remain unaffected. There is an increase of the median SRTs inside the rectangular bleaching zone at the $9\,^\circ$ eccentricity from 355 ms to 480 ms. The detected targets within the bleaching zone remain approximately equal to those in the same region during the non-bleaching trials. However, strangely 0 targets were detected at the $21\,^\circ$ eccentricity outside the bleaching zone, and 50% fewer targets were detected for the $15\,^\circ$ eccentricity outside the bleaching zone.

For subject 6, the median SRTs are uniform at all locations during the non-bleaching trials. As shown in Fig. 17a the median SRTs obtained are 230 ms to 265 ms at all eccentricities lower than $15\,^\circ$. At 3 locations on the $21\,^\circ$ 300 ms, median SRT is obtained during the non-bleaching trials. However not much difference in median SRTs can be seen for the targets within the bleaching zone located at $15\,^\circ$ and $21\,^\circ$. The SRTs and the number of detection at this region during the bleaching trials remain the same as the non-bleaching trials denoting bleaching had no effect. Only small changes can be noticed in the eccentricities $6\,^\circ$ and $9\,^\circ$ during the bleaching trials. Strangely, as observed in subject 3, subject 6 also failed to identify stimuli located outside the bleaching zone at $15\,^\circ$ and $21\,^\circ$ during the bleaching trials. This erratic behavior can be the effects of bleaching leaking from other experiments or over-saturation of the visual system due to bleaching.

The data from subject 8 was used to verify the results obtained from the other two subjects. The results obtained from subject 8 shown in Fig. 18 exhibit similar SRTs for both the bleaching and non-bleaching conditions across all eccentricities, implying the bleaching effect was minimal

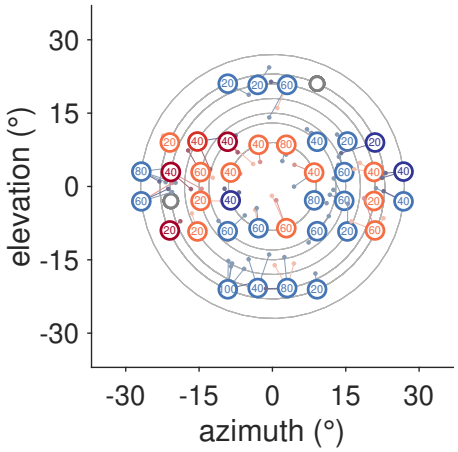

(a) SRT distribution of subject 4 from non-bleaching trials

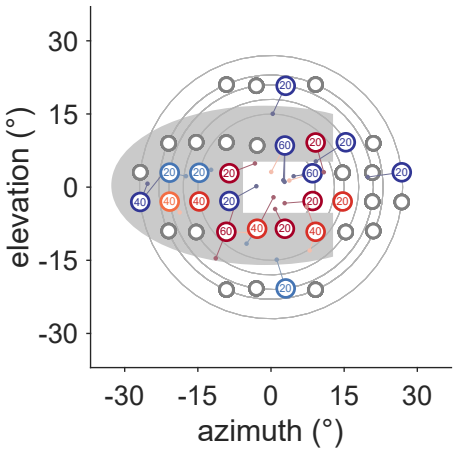

(b) SRT distribution of subject 4 from bleaching trials

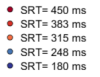

(c) Legend

Fig. 13: SRT distributions obtained in experiment ASP for subject 4. The small circles in both the subplots represent the target locations, also shown in Fig. 8a. The number within each circle signifies the percentage of targets detected by the subject at that location. The color of the circles denotes the median SRT of the targets at that location; the associated median SRT to each color is shown in the legend in Fig. 13c. The undetected targets are the open gray circles (○). The colored lines emerging from each circle connect the endpoints of the saccades made for a specific target to the target. The gray patched area in Fig. 13b represents the bleaching zone.

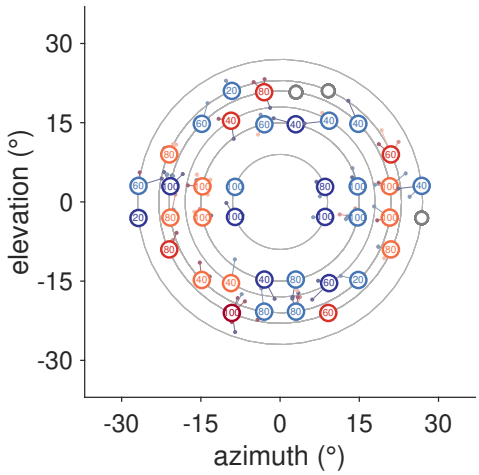

(a) SRT distribution of subject 2 from non-bleaching trials

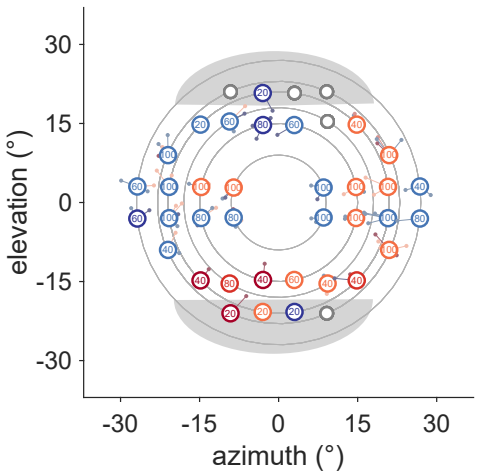

(b) SRT distribution of subject 2 from bleaching trials

(c) Legend

Fig. 14: SRT distributions obtained in experiment PD for subject 2. The small circles in both the subplots represent the target locations, also shown in Fig. 8b. The number within each circle signifies the percentage of targets detected by the subject at that location. The color of the circles denotes the median SRT of the targets at that location; the associated median SRT to each color is shown in the legend in Fig. 14c. The undetected targets are the open gray circles (○). The colored lines emerging from each circle connect the endpoints of the saccades made for a specific target to the target.The gray patched area in Fig. 14b represents the bleaching zone.

for this subject. The results from this experiment showcased mixed outcomes. For subjects 3 and 6, the cause can be fatigue and leakage of the bleaching effect from other experiments. Prolonged exposure to bleaching can also be a reason. However, noticing subject 8's results, the total area of the bleaching zone can also influence the SRTs. The bleaching area in this experiment was significantly smaller than in previous experiments, and the smaller area had a very minimal effect and bleached a smaller number of photoreceptors.

The lack of data is one of the reasons for the inconclusiveness of the local bleaching experiments. Furthermore, fatigue and leakage of the bleaching effect are due to prolonged

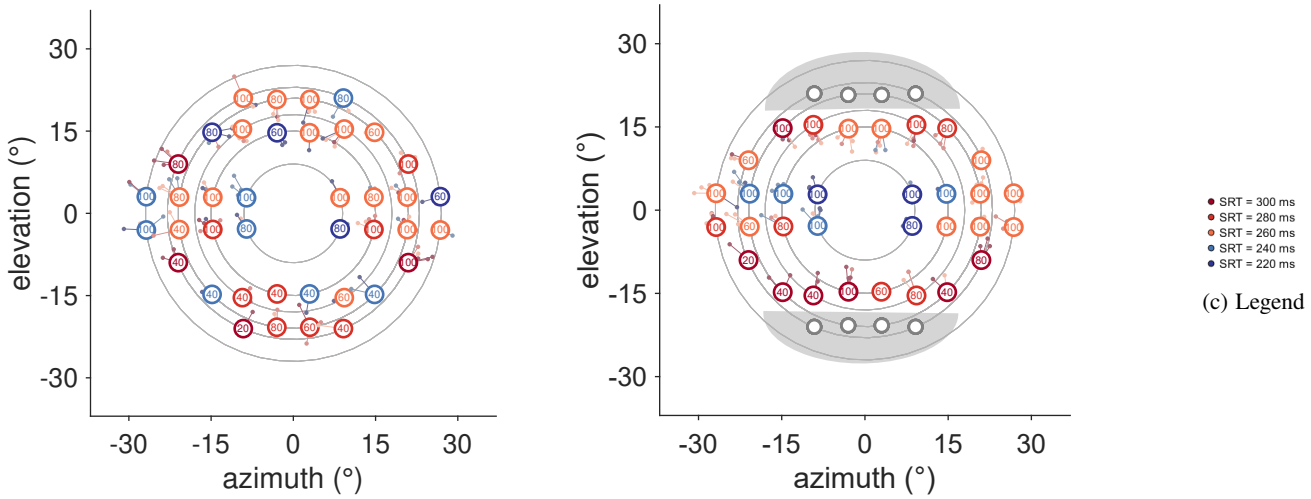

(a) SRT distribution of subject 8 from non-bleaching trials (b) SRT distribution of subject 8 from bleaching trials (c) Legend

Fig. 15: SRT distributions obtained in experiment PD for subject 8. The small circles in both the subplots represent the target locations, also shown in Fig. 8b. The number within each circle signifies the percentage of targets detected by the subject at that location. The color of the circles denotes the median SRT of the targets at that location; the associated median SRT to each color is shown in the legend in Fig. 15c. The undetected targets are the open gray circles (○). The colored lines emerging from each circle connect the endpoints of the saccades made for a specific target to the target.The gray patched area in Fig. 15b represents the bleaching zone.

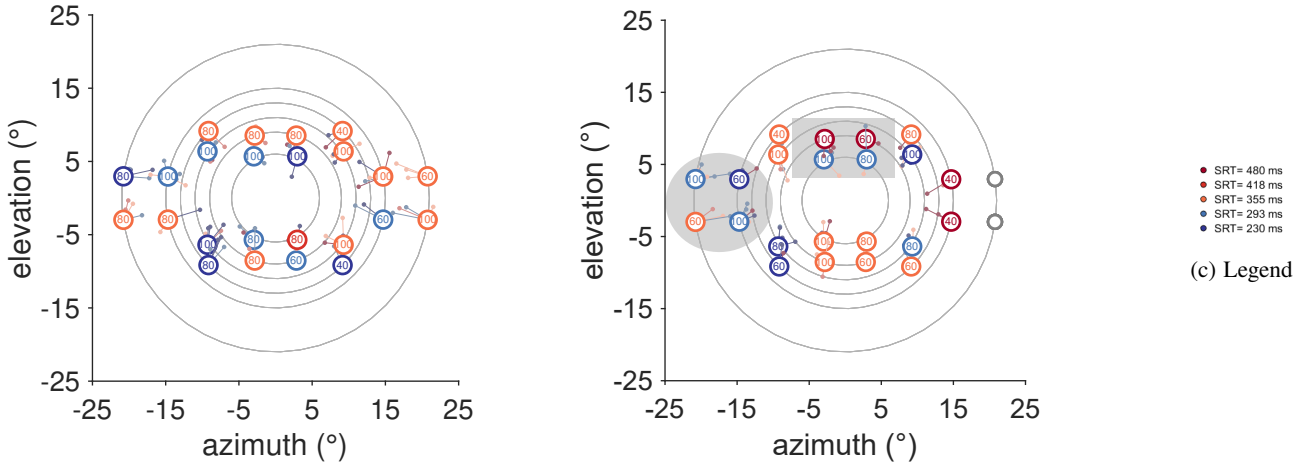

(a) SRT distribution of subject 3 from non-bleaching trials (b) SRT distribution of subject 3 from bleaching trials (c) Legend

Fig. 16: SRT distributions obtained in experiment ESP for subject 3. The small circles in both the subplots represent the target locations, also shown in Fig. 8c. The number within each circle signifies the percentage of targets detected by the subject at that location. The color of the circles denotes the median SRT of the targets at that location; the associated median SRT to each color is shown in the legend in Fig. 16c. The undetected targets are the open gray circles (○). The colored lines emerging from each circle connect the endpoints of the saccades made for a specific target to the target.The gray patched area in Fig. 16b represents the bleaching zone.

experimentation, and photobleaching also contributed to inconclusive results.

V. Discussion

This paper aims to reproduce glaucoma-like elevated SRTs by desensitizing a healthy retina using photobleaching. The paper analyzes the variation in SRT and target detection in a bleached retina. Furthermore, it attempts to relate the effect of bleaching on the SRTs and target detection by correlating the area of the stimulus present within the bleaching zone. Lastly, the effect of localized bleaching on the visual field to obtain higher SRTs is also studied.

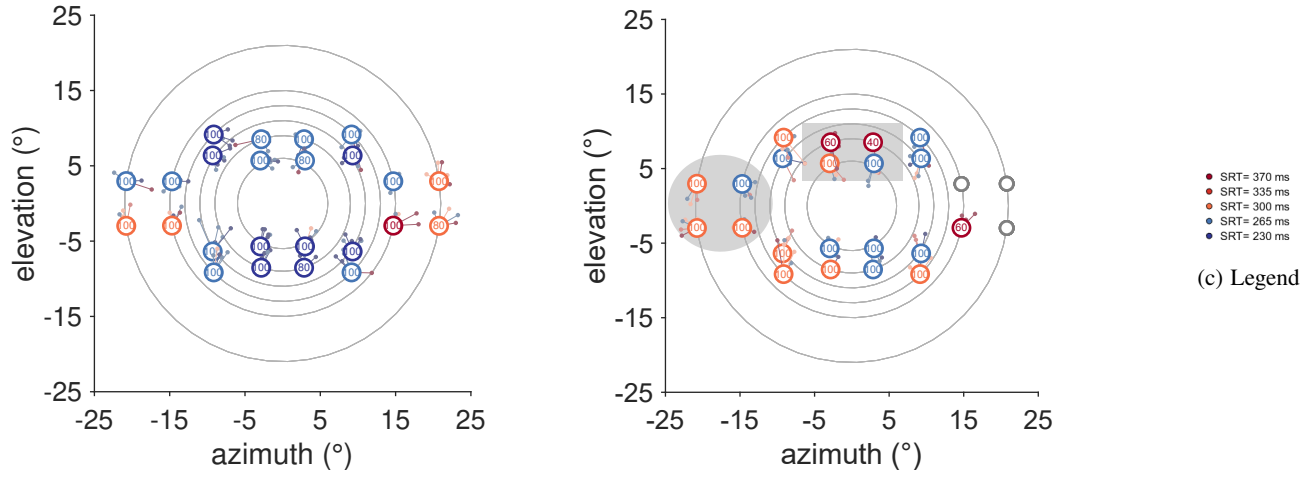

(a) SRT distribution of subject 6 from non-bleaching trials (b) SRT distribution of subject 6 from bleaching trials (c) Legend

Fig. 17: SRT distributions obtained in experiment ESP for subject 6. The small circles in both the subplots represent the target locations, also shown in Fig. 8c. The number within each circle signifies the percentage of targets detected by the subject at that location. The color of the circles denotes the median SRT of the targets at that location; the associated median SRT to each color is shown in the legend in Fig. 17c. The undetected targets are the open gray circles (○). The colored lines emerging from each circle connect the endpoints of the saccades made for a specific target to the target.The gray patched area in Fig. 17b represents the bleaching zone.

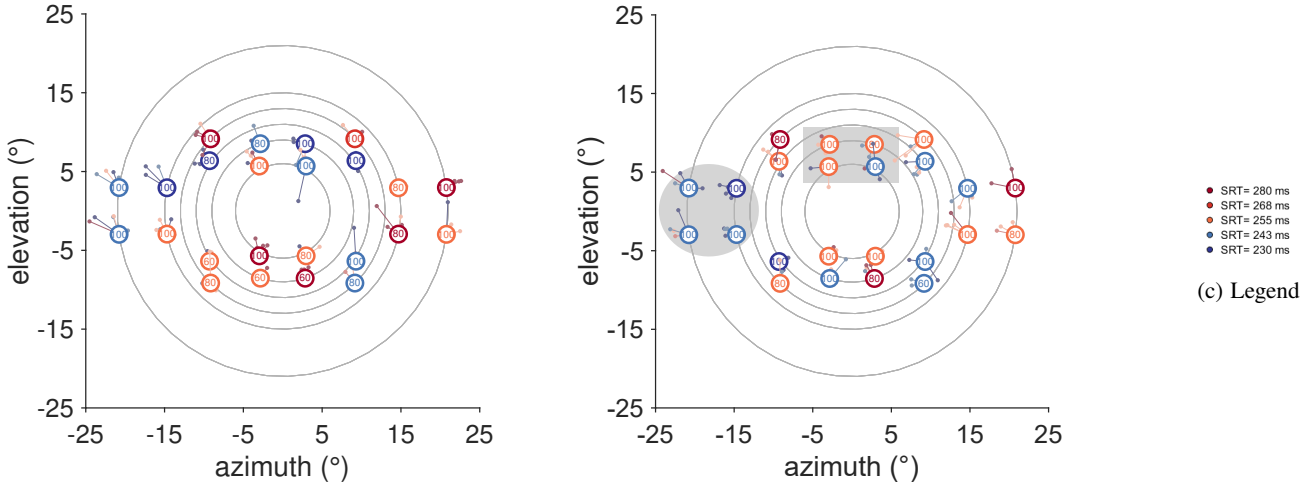

(a) SRT distribution of subject 8 from non-bleaching trials (b) SRT distribution of subject 8 from bleaching trials (c) Legend

Fig. 18: SRT distributions obtained in experiment ESP for subject 8. The small circles in both the subplots represent the target locations, also shown in Fig. 8c. The number within each circle signifies the percentage of targets detected by the subject at that location. The color of the circles denotes the median SRT of the targets at that location; the associated median SRT to each color is shown in the legend in Fig. 18c. The undetected targets are the open gray circles (○). The colored lines emerging from each circle connect the endpoints of the saccades made for a specific target to the target.The gray patched area in Fig. 18b represents the bleaching zone.

Hypothesis I predicted that photobleaching and dark adaptation would affect a subject's SRT and target detection ability. Based on the results from Section IV-A, it was found that the bleaching trials resulted in a significantly lower number of detections in the lower hemifield than the non-bleaching trials. During the bleaching trials, the detection was less by 50% inside the lower hemifield bleaching zone. According to the results obtained in Section IV-B, the ability to detect stimuli was affected in the eccentricities 15°, 18°, 21°, 23° but the eccentricities 9° and 27° seemed to be unaffected. For targets located at 9°, the distance between the fixation and the targets was the least. Due to their location almost at the edge of the bleaching zone,

identifying the targets was easier. Thus the targets at 9° only demonstrate elevated SRTs. SRTs should monotonically increase with eccentricity [41]. However, the trend only exists till 23°. The sudden drop in SRT for both the bleaching and non-bleaching condition at 27°, along with the approximately equal number of stimuli detected, point towards a prediction of the targets happening at that location during both bleaching and non-bleaching trials. To accommodate the targets at 27°, the fixation point is shifted to the left or right based on the side the stimulus is known. If the target appears on the left, the fixation is shifted toward the right. This unique shift only happens for 27°. Since there are only 4 targets assigned to that eccentricity, the subject could predict the target's location after a few sets of experiments. Also, an unexpectedly higher accuracy is observed at the location, implying a target location prediction. The fewer detections at 15°, 18°, 21°, 23° resulted from the inability to detect targets when bleached combined with the larger distance from the fixation. The inability to detect is because of the desensitized photoreceptors in the area of the visual field that is photobleached. As photobleaching temporarily desensitizes or depletes the photoreceptors, no visual signal is processed at that location, thus hindering the detecting and distinguishing targets. Higher SRTs were observed at all eccentricities except 27°.

The differences observed in accuracy and saccade gains are primarily due to the fewer detections in the bleaching trials. Results from LHB_V_2 are also similar. A lower number of detections are observed during the bleaching trials in the lower hemifield at all locations except 9° and 27°. The overall targets detected by subjects 2 and 9 remain the same for both experiments. However, during the bleaching trials, 10% more has been detected at the upper hemifield in the LHB_V_2 experiment. Apart from that, LHB_V_2 also results in higher SRTs. The results from both experiments show that the bleaching period can be further reduced to $1.5\,\mathrm{s}$ to obtain elevated SRTs.

Based on the findings from the results of LHB, hypothesis I can be accepted. Photobleaching resulted in elevated SRTs and fewer detections but affected the signal-processing capabilities of the bleached photoreceptors. Also, a substantial amount of error has been introduced in the visual processing, leading to less detection, as expected in glaucoma [10]. However, the LHB variant's grid can be altered for future studies. A prediction pattern was noticed across all subjects for the stimuli located at eccentricity 27°. Thus the eccentricity does not supply any valuable information and can be omitted. Instead, the grid can be limited up to eccentricity of maximum 23°. For a better analysis of intermediate and lower eccentricities, eccentricities of 3°, 6°, and 12° can be added. Visual responses are asymmetric when the upper and lower hemifields are compared. Instead, left or right-half bleaching could be used to obtain symmetrical comparison results.

Hypothesis II attempted to prove that the bleaching effect is highly localized and is directly proportional to the amount of stimulus area within the bleaching zone. The results show that the increase in SRT can be expressed by a linear line fitted through the distributions. Due to the high variability in the obtained SRTs, the R^2 values are lower. Better R^2 values can be obtained when the linear equation is fitted through the median SRTs, which removes the variability. The linearity can be observed in all the fits shown in Section IV-B. When a specific portion of the visual field is exposed to any intense light source (bleaching), the photoreceptors' ability to process images in that visual field area is compromised. Based on the results, hypothesis II is accepted, establishing a direct relationship between SRT and the stimulus area within the bleaching zone. It also indicates that the bleaching process is localized, and the effect is mainly limited to the bleached area of the visual field. However, it was often found as a complaint by the participants that the bleaching pattern with a central strip was overwhelming. Repeating the $4\,\mathrm{s}$ bleaching for 60 trials caused the participants discomfort. An alternative can be found by implementing $1.5\,\mathrm{s}$ bleaching, as found in the LHB_V_2's results, to reduce the level of discomfort caused and detect more targets with elevated SRTs. Additionally, the duration of the blank frame after the stimulus frame can be increased by 2-3 s. To reduce the leaking effect of the bleaching to the next trial and also to give the retina optimum time to return to its original state. Additionally, the 12° elevation can be removed, and a 9° elevation can be added.

Hypothesis III expected that bleaching discrete areas of the visual field would yield a slower reaction time in the discrete bleached areas, similar to those found in the other two hypotheses. The results from the ASP localized glaucoma pattern experiment showed that the bleaching zone raised the SRTs across all eccentricities. It is also noticed from the results that the number of detection in the bleaching condition also reduces. Higher SRTs and lower target detection were also observed for stimuli outside the bleaching zone during the trials. However, since there was only one participant in the experiment, the results cannot be accepted as they are a single event, and no comparison exists to verify or validate the results. Thus no solid conclusion can be reached due to a lack of data.

For the PD experiment, the expected effects of bleaching were observed. The SRT increased for the locations where bleaching was performed, and the number of stimuli detected was low. However, the higher vertical position of the stimuli meant that the subject had to make vertical eye movements and cover a larger distance to reach the target, which added more difficulty in performing the task [7]. So the higher SRTs and lower detections were also influenced by the vertical peripheral location of the stimulus. Thus, in this case, discrete bleaching gave the expected result but was influenced by another factor, the location.

The ESP experiment also showed mixed results. The bleach seemed to affect subjects 3 and 6. No trend in increased SRTs and the number of detections in both trials were

identified. Subject 8 showed no identifiable change between the bleaching and non-bleaching condition. If we look at subject 8's data, the bleaching had no effect. The reason can be the amount of area bleached. If the experiment LHB and BO were observed, almost close to 50% and 33% of the area were bleached. The ASP variant had close to 50% of the total visual field area bleached. For the PD pattern, the results were influenced by the extreme location of the stimuli along with the bleaching. However, the total area bleached for the ESP pattern was smaller than in the other experiments. The smaller area can be the reason for the non-effectiveness of bleaching on subject 8.

Hypothesis III is rejected here as most of the results were inconclusive. The lack of data in the ASP experiment makes the results unreliable. PD experiments were successful however were influenced by the location of the targets. The results of the ESP experiment were also inconclusive and needed further investigation. However, there can be a relation between the effect of bleaching on the photoreceptors and the total area bleached. It can be concluded that hypothesis III can be true if larger areas are bleached. Smaller bleaching zones have minimal effect on the visual field. The recommendation here is to collect more data to conduct a proper analysis. It was suspected that the bleaching effect often leaked from one experiment to another. A higher time gap between two experiments and trials could negate this effect.

Apart from that, the methodology used for this study can be used to study eye movement behavior in glare conditions. The photobleaching process closely resembles the phenomenon of glare. It can be used to assess the effects of elevated SRTs due to glare on performance-based tasks like driving, flying, or simple tracking tasks. Furthermore, as mentioned in Section I, little attention is given to the effectiveness of pilots with glaucoma. The study can be used to understand the performance of pilots under bleached conditions and the effect of delayed SRTs on flying and monitoring.

VI. Conclusion

The study investigated the effect of photobleaching and dark adaptation on SRTs. It was found that photobleaching successfully increased the SRT for the stimuli present within the bleaching zone. It was further discovered that the ability to detect targets within the bleached area was hampered when photobleached. The elevated SRTs obtained from the study also match the SRTs obtained by Mazumdar in mild glaucoma cases [13]. Thus, it can be concluded that photobleaching and dark adaptation are valid for obtaining glaucoma-like SRT. The results also conclude that the SRTs are related to the area of stimulus present within a bleaching zone. SRTs and detections are only influenced by the bleaching process when the targets are present within the bleaching zone. It proves that photobleaching is a localized phenomenon, and the effects of bleaching are only observed inside the bleaching zone. Attempts to recreate the localized impact of glaucoma using discrete bleaching were unsuccessful. Leakage of the bleaching effect during prolonged experimentation was one of the causes of inconclusive results. Furthermore, the lack of reliable data made it difficult to reach conclusions. Also, it was determined that discrete bleaching could deliver elevated SRTs, but it is area dependent.

References

[1] R. N. Weinreb, T. Aung, and F. A. Medeiros, "The pathophysiology and treatment of glaucoma: a review," *Jama*, vol. 311, no. 18, pp. 1901–1911, 2014.

[2] K. Allison, D. Patel, and O. Alabi, "Epidemiology of Glaucoma: The Past, Present, and Predictions for the Future," *Cureus*, 11 2020.

[3] C. X. Hu, C. Zangalli, M. Hsieh, L. Gupta, A. L. Williams, J. Richman, and G. L. Spaeth, "What do patients with glaucoma see? visual symptoms reported by patients with glaucoma," *The American journal of the medical sciences*, vol. 348, no. 5, pp. 403–409, 2014.

[4] E. C. Johnson, Y. Guo, W. O. Cepurna, and J. C. Morrison, "Neurotrophin roles in retinal ganglion cell survival: lessons from rat glaucoma models," *Experimental eye research*, vol. 88, no. 4, pp. 808–815, 2009.

[5] Y. Budak and M. Akdogan, "Retinal ganglion cell death," *Glaucoma: Basic and Clinical Concepts. Croatia: InTech*, pp. 33–56, 2011.

[6] A. Sommer, *Intraocular pressure and glaucoma*. American Journal of Ophthalmology, 2 1989, vol. 107, pp. 186–188.

[7] D. Mazumdar, "Visual field responsiveness in glaucoma: An eye tracking approach," *Final PhD defence report*, 2021.

[8] R. George, R. S. Ve, and L. Vijaya, "Glaucoma in India: Estimated burden of disease," *Journal of Glaucoma*, vol. 19, no. 6, pp. 391–397, 8 2010.

[9] M. L. Popescu, H. Boisjoly, H. Schmaltz, M.-J. Kergoat, J. Rousseau, S. Moghadaszadeh, F. Djafari, and E. E. Freeman, "Explaining the relationship between three eye diseases and depressive symptoms in older adults," *Investigative ophthalmology & visual science*, vol. 53, no. 4, pp. 2308–2313, 2012.

[10] J. J. M. Pel, M. C. M. van Beijsterveld, G. Thepass, and J. van der Steen, "Validity and Repeatability of Saccadic Response Times Across the Visual Field in Eye Movement Perimetry," *Translational Vision Science & Technology*, vol. 2, no. 7, p. 3, 11 2013.

[11] F. A. Medeiros, R. N. Weinreb, E. Boer, and P. N. Rosen, "Driving simulation as a performance-based test of visual impairment in glaucoma," *Journal of glaucoma*, vol. 21, no. 4, p. 221, 2012.

[12] R. Schwartz, C. Stern, M. Klemm, J. Draeger, and R. Winter, "Glaucoma and aircraft pilot fitness," *Der Ophthalmologe: Zeitschrift der Deutschen Ophthalmologischen Gesellschaft*, vol. 93, no. 1, pp. 76–79, 1996.

[13] D. Mazumdar, J. J. Pel, M. Panday, R. Asokan, L. Vijaya, B. Shantha, R. George, and J. Van Der Steen, "Comparison of saccadic reaction time between normal and glaucoma using an eye movement perimeter," in *Indian Journal of Ophthalmology*, vol. 62, 1 2014, pp. 55–59.

[14] D. P. Crabb, N. D. Smith, and H. Zhu, "What's on TV? Detecting age-related neurodegenerative eye disease using eye movement scanpaths," *Frontiers in Aging Neuroscience*, vol. 6, no. NOV, 2014.

[15] "Guide for aviation medical examiners," https://www.faa.gov/about/office_org/headquarters_offices /avs/offices/aam/ame/guide/app_process/exam_tech/item32/amd/, accessed: 2022.

[16] "Glaucoma and flying fitness," http://dgcamedical.in/Glaucoma.htm, accessed: 2008.

[17] J. Landers, A. Sharma, I. Goldberg, and S. L. Graham, "Comparison of visual field sensitivities between the Medmont automated perimeter and the Humphrey field analyser," *Clinical and Experimental Ophthalmology*, vol. 38, no. 3, pp. 273–276, 4 2010.

[18] C. A. Johnson, M. Wall, and H. S. Thompson, "A History of Perimetry and Visual Field Testing," Tech. Rep., 2011. [Online]. Available: www.optvissci.com.

[19] A. Heijl, "The Effect of Perimetric Experience in Normal Subjects," *Archives of Ophthalmology*, vol. 107, no. 1, p. 81, 1 1989.

[20] A. Toepfer, E. Kasten, T. Guenther, and B. A. Sabel, "Perimetry while moving the eyes: implications for the variability of visual field defects," *Journal of Neuro-Ophthalmology*, vol. 28, no. 4, pp. 308–319, 2008.

[21] A. J. Anderson and C. A. Johnson, "Frequency-doubling technology perimetry." *Ophthalmology Clinics of North America*, vol. 16, no. 2, pp. 213–225, 2003.

[22] A. Heijl, V. M. Patella, L. X. Chong, A. Iwase, C. K. Leung, A. Tuulonen, G. C. Lee, T. Callan, and B. Bengtsson, "A New SITA Perimetric Threshold Testing Algorithm: Construction and a Multicenter Clinical Study," *American Journal of Ophthalmology*, vol. 198, pp. 154–165, 2 2019.
[23] M. Gorges, E. H. Pinkhardt, and J. Kassubek, "Alterations of eye movement control in neurodegenerative movement disorders," 2014.
[24] M. A. Bullimore and I. L. Bailey, "Reading and eye movements in age-related maculopathy." *Optometry and vision science: official publication of the American Academy of Optometry*, vol. 72, no. 2, pp. 125–138, 1995.
[25] A. Cerulli, M. Cesareo, E. Ciuffoletti, M. L. Montanaro, R. Mancino, C. Mirisola, R. Sorge, C. Cedrone, C. Nucci, and L. Cerulli, "Evaluation of eye movements pattern during reading process in patients with glaucoma: A microperimeter study," *European Journal of Ophthalmology*, vol. 24, no. 3, pp. 358–363, 2014.
[26] J. Stein and J. Talcott, "Impaired neuronal timing in developmental dyslexia—the magnocellular hypothesis," *Dyslexia*, vol. 5, no. 2, pp. 59–77, 1999.
[27] T. D. Lamb and E. N. Pugh, "Dark adaptation and the retinoid cycle of vision," pp. 307–380, 5 2004.
[28] H. Kolb, E. Fernandez, and R. Nelson, "Webvision: the organization of the retina and visual system [internet]," 1995.
[29] M. Perz, "Flicker perception in the periphery," *Eindhoven: TU Eindhoven*, 2010.
[30] M. Kalloniatis and C. Luu, "Visual acuity," *Webvision: The Organization of the Retina and Visual System [Internet]*, 2007.
[31] M. Aguilar and W. S. Stiles, "Saturation of the rod mechanism of the retina at high levels of stimulation," *Optica Acta: International Journal of Optics*, vol. 1, no. 1, pp. 59–65, 1 1954.
[32] S. Hecht, C. Haig, and A. M. Chase, "The influence of light adaptation on subsequent dark adaptation of the eye," *The Journal of general physiology*, vol. 20, no. 6, pp. 831–850, 1937.
[33] H. B. Barlow, D. Jameson, and L. M. Hurvich, *Dark and Light Adaptation: Psychophysics*. Berlin, Heidelberg: Springer Berlin Heidelberg, 1972, pp. 1–28.
[34] C. Q. Davis, O. Kraszewska, and C. Manning, "Constant luminance (cd· s/m 2) versus constant retinal illuminance (td· s) stimulation in flicker ergs," *Documenta Ophthalmologica*, vol. 134, pp. 75–87, 2017.
[35] J. L. Barbur, "Reaction-time determination of the latency between visual signals generated by rods and cones," *Ophthalmic and Physiological Optics*, vol. 2, no. 3, pp. 179–185, 1982.
[36] H. C. Walkey, J. A. Harlow, and J. L. Barbur, "Changes in reaction time and search time with background luminance in the mesopic range," *Ophthalmic and Physiological Optics*, vol. 26, no. 3, pp. 288–299, 2006.
[37] D. Cao, A. J. Zele, and J. Pokorny, "Linking impulse response functions to reaction time: Rod and cone reaction time data and a computational model," *Vision Research*, vol. 47, no. 8, pp. 1060–1074, 4 2007.
[38] Tobii, "Tobii analytics sdk developer's guide," *Tobii Analytics SDK Developer's Guide*, vol. 3, pp. 54–65, 2013.
[39] D. D. Salvucci and J. H. Goldberg, "Identifying fixations and saccades in eye-tracking protocols," in *Proceedings of the 2000 symposium on Eye tracking research & applications*, 2000, pp. 71–78.
[40] S. Hopf, M. Liesenfeld, I. Schmidtmann, S. Ashayer, and S. Pitz, "Age dependent normative data of vertical and horizontal reflexive saccades," *PloS one*, vol. 13, no. 9, p. e0204008, 2018.
[41] A. L. Yarbus, *Eye Movements and Vision*. Springer US, 1967.

APPENDIX

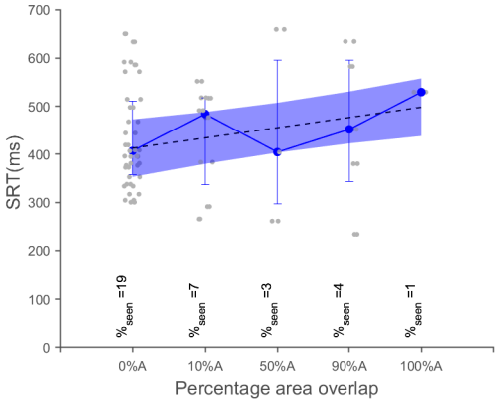

(a) SRTs at for +12.2° R^2 = 0.63 N_{total}% = 5.7

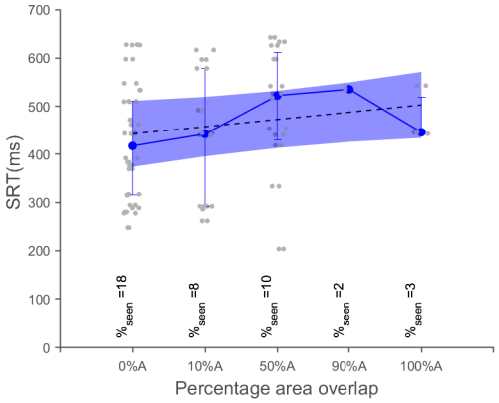

(b) SRTs at for -12.2° R^2 = 0.45 N_{total}% = 9.8

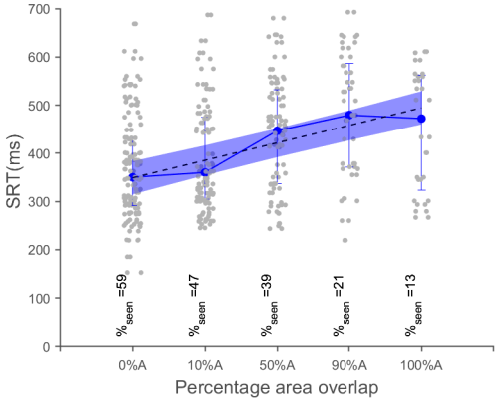

(c) SRTs at +6.4° R^2 = 0.93 N_{total}% = 30.7

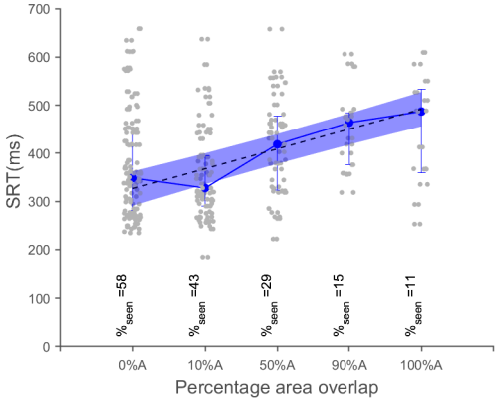

(d) SRTs at for -6.4° R^2 = 0.94 N_{total}% = 26.7

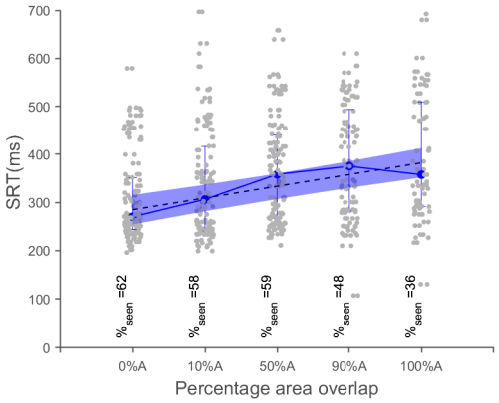

(e) SRTs at +2.8° R^2 = 0.88 N_{total}% = 45

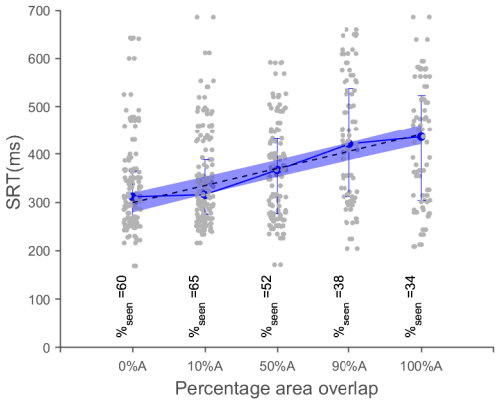

(f) SRTs at for -2.8° R^2 = 0.97 N_{total}% = 42.6

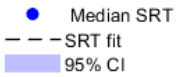

(g) Figure Legend

Fig. A.I: A linear equation fit to median SRTs across 6 elevations from experiment BO pooled across all subjects. The dark blue(●) circle indicates the median values of the SRTs. Gray dots show individual SRTs (●). The blue error bars represent the 25^{th} and 75^{th} percentile of SRTs. The black shows a linear fit dashed lines (–). Linearity and high correlation are proved in Fig. A.Ic to Fig. A.If. N represents the percentage targets detected at a specific elevation. Each elevation had a total of 600 targets. Each overlap has 120 targets

Part II

Preliminary Literature Study

*This part has been assessed for the course AE4020 Literature Study.

1 Introduction

Glaucoma, a neurodegenerative disease, is the world's leading cause of irreversible blindness. Early detection of the disease is complex, mainly because the patient does not feel any sudden difference in vision due to various factors discussed later in the report. The process of monitoring glaucoma progression relates to the percentage of visual field compromised. However, the visual field is much more complex spanning both vertically (135 °) and horizontally (155 °), and just denoting a percent loss of visual field does not necessarily inform about the intensity of the symptoms. The conventional diagnostic method, SAP, is based on evaluating the detection threshold of the presented stimulus. The approach is time-consuming, often causes false stimulus detection, and affects the results. To address the issues with the current method, alternatives are being developed, one of which is EMP. The thesis project will be based on the EMP, focusing on SRT.

Data is crucial in developing such diagnostic procedures. Data can be collected from glaucoma patients, but the bulk of data needed to create any diagnosis method or framework and validate the technique is difficult. Considering the amount of data required, collecting a sample of data from glaucoma patients is time-consuming and cost-intensive. But what if we can procure the required information about glaucoma without even considering an actual patient? A solution may be to artificially recreate the symptoms of the disease in a healthy subject without affecting the subject's anatomy. This thesis attempts to address the hypothesized solution by

Developing a human model of glaucoma by reversibly de-sensitizing areas of a healthy retina.

To move forward with mimicking glaucoma in healthy subjects, it is essential to understand the effect of glaucoma on the human visual system. The results are based on the characteristics of the longer SRTs found in glaucoma patients. The aim will be to reproduce the SRT characteristics of glaucoma patients in healthy subjects. To achieve the said goal of developing a human model, the following preliminary research question needs to be answered first:

What is a suitable method to develop a model for visual field deficit diseases such as glaucoma?

Since the thesis is focused on glaucoma, it is crucial to understand the disease and the current standards of diagnosis. In chapter 2, a brief overview of human vision and glaucoma is provided.

The chapter also focuses on the conventional method of detecting glaucoma and its issues. Alongside this, it gives an outlook on the possible diagnostic alternatives. Since the project is focused on eye movements in glaucoma patients, it is vital to acknowledge the eye movements performed by such patients. In chapter 3, outcomes of the previous research on eye movement of glaucoma patients are provided. Also, the different kinds of natural eye movements are studied based on the work of Yarbus. In chapter 4, the various methods that can be applied to simulate the symptoms of glaucoma are discussed. It mainly focuses on multiple means of elevating the visual thresholds of an individual to obtain longer saccadic reaction times based on either background luminance or stimuli luminance. It also touches upon the topic of photobleaching and its effects on vision. The report concludes with chapter 6 where the findings from the different chapters are provided. Lastly, an overview of the proposed plan for the project is delivered.

2

Human Vision & Glaucoma

Human vision is the ability to perceive objects in the visual field covered by our two eyes [1]. Vision is a dynamic and interactive process. The brain perceives and processes the visual information transmitted by the retina. Vision aids us in performing daily life activities like identifying obstacles and navigating around them, identifying a coffee mug on the counter, and making a goal-directed movement to grab the mug and drink from it. The process of vision, which includes perceiving and processing visual information, is directly associated with the retina's different neural networks and cells, which connect the eye with the different areas of the brain involved in visual processing [1]. For this project, we focus on the role of the human retina as glaucoma initially affects the neural structures in the retina [2], as discussed in the following sections. .

2.1. Human retina

The human retina is akin to the sensor of a camera. The retina is barely 0.5 mm thick cell layer that lines the back side of the eyeball. The tissue develops from the forebrain and thus constitutes a part of the brain [3].

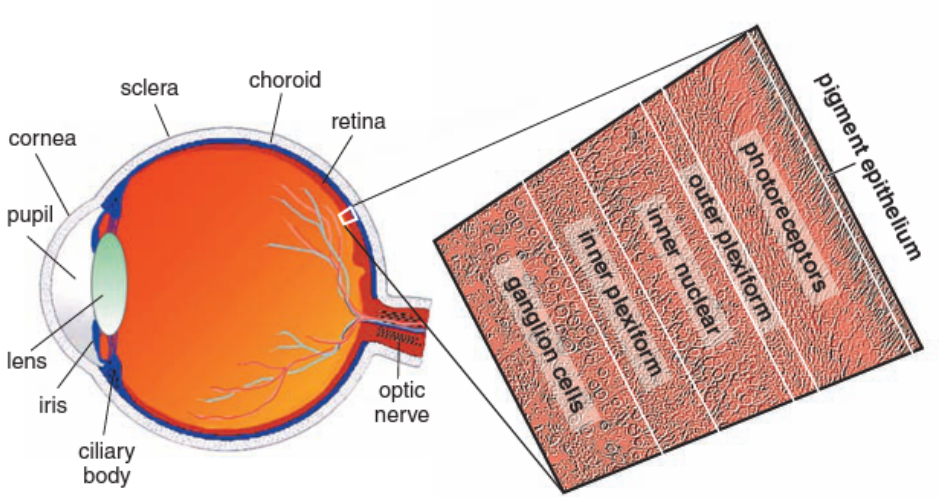

Figure 2.1: Schematic section of the human eye with retina [3].

RGC make up the optic nerve connects the eye with the brain. The RGCs lie innermost in the retina, close to the lens and front of the eye. The photoreceptors lie outermost in the retina. Light enters

the eye and travels through the retina, striking and activating the photo-pigments. The absorption of light by the photo-receptors triggers a biochemical process and then a subsequent electrical message concerning the photopic input. The retina performs visual information processing and the information is relayed to the brain via the RGC. RGCs have a bipolar appearance. A neuron consists of a dendrite and axons, which help them exchange information through electrical signals. The central part of the retina, which is close to the fovea, is thicker than the peripheral retina. The fovea is demarcated by a notch above the retina lining shown in fig. 2.1. The thickness is because of the densely packed photoreceptor and bipolar, and ganglion cells [3]. The central region of the retina near the fovea (foveal region) is concentrated with cone cells along with its connecting ganglion cells, and the peripheral retina (parafoveal region) is more dominated by the rod cells and its connecting neurons [3].

Photoreceptors

The retina comprises a variety of cell types of which the photoreceptors are sensitive to light of wavelengths in the range of 380 to 700 nm [4]. The cells use so-called opsin proteins that react to photons by changing their conformations [3]. Interestingly, the membrane potential of photoreceptors is slightly negative in the absence of light and becomes even more negative, i.e., hyper-polarized, upon stimulation with light [3]. The phenomenon is called “dark current". In the absence of a stimulus, Na^+ ions[1] flow through the membrane channels and photo-receptors remain depolarized [3]. The hyperpolarization process starts when a visual stimulus is presented, as shown in fig. 2.2a. A light stimulus of 550 nm wavelength, which humans perceive as green, is presented, and the cell membrane potential is measured. When the stimulus is on, the cell membrane potential drops rapidly and maintains the negative potential as long as the stimulus is active. The cell membrane potential returns to its original baseline after the stimulus offset.

(a) Polarisation of photoreceptor(cone cell) to a green flash

(b) Hyper polarisation of a cone cell

Figure 2.2: Drop in the potential of a photoreceptor when exposed to a green flash [3].

There are two types of photoreceptors in the retina: rods and cones, named for their characteristic shape [5]. As mentioned earlier, and in fig. 2.3a, rod cells are predominantly located in the peripheral region of the retina. Rods are generally responsible for vision under dim light conditions or scotopic vision. The rods consist of a single pigment type, rhodopsin, whose peak sensitivity is around 496 nm wavelength of light. The rod cells also exhibit high sensitivity, i.e., saturation in daylight and smaller dynamic range. They also have a slower response time than cones with low spatial resolution. Spatial resolution is the ability to resolve two points in space. Low spatial resolution is mainly because rod cells are absent in the foveal region. The cones are concentrated in the central retina, close to the fovea.

[1]Sodium ions

Cone cells are primarily for vision under light conditions or photopic vision. Based on the absorption spectrum of light wavelength, the cones are divided into blue cones – responding to a peak wavelength of 419 nm; the green cones with a peak at 531 nm wavelength of light and the red cones responding at 559 nm wavelength of light. The absorption spectrum of these pigments overlaps with each other. The rod cell's absorption spectrum only overlaps with the green and blue cones, as shown in fig. 2.3b. The cone cells saturate only in intense light and have a more extensive dynamic range. Also, the response time of cone cells is faster than the rods because of the shorter integration time. The fact that they are more densely packed (cells per m) at the central retina results in a higher spatial resolution [3].

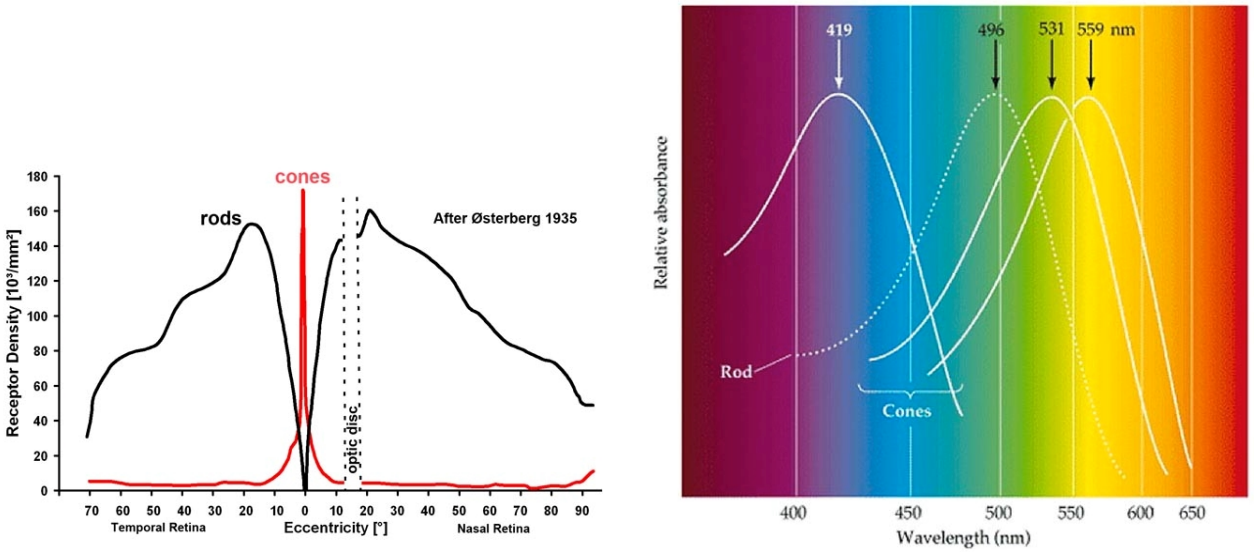

(a) Concentration of rods and cone cells relative to fovea in the human retina [6].

(b) Responding wavelengths of different types of rods and cone cells for human retina [4].

Figure 2.3: Distribution of photoreceptors across the retina and their response to different wavelengths of light.

2.2. Overview of glaucoma

Glaucoma, a group of optic neuropathies, is one of the leading causes of irreversible blindness in the the world next to cataracts [7]. It is predicted that by 2040, 111.8 million of the world's population will be affected by this disease [8], shown in fig. 2.4. Glaucoma progressively influences the visual field, starting from the periphery of the visual field [9]. This is primarily caused by the axonal degeneration of the RGCs, which also affects axonal transport. Axonal degeneration eventually leads to the death of RGC, thus impairing the visual field [10]. The process is nonselective and affects all RGCs, irrespective of the location. Axon death is usually caused by two processes [11]:

- **Wallerian degeneration:** Defined as the degeneration of the axon due to an injury, commonly found in severely damaged axons, and results in atrophy and rapid loss of structure throughout the entire length of the axon. Also, it leads to the disintegration of the insulating myelin sheath surrounding the axon.
- **Dieback:** Dieback is a slower process where the onset of glaucoma takes more time that Wallerian degeneration. It happens when the axon suffers a low to moderate injury, and the disintegration of the axon structure can take several months before the axon is fully damaged.

Glaucoma can also be triggered by increased IOP. IOP is regulated by a balance between aqueous humor secretion and drainage. Irregularity in the drainage or the secretion of the fluid can cause

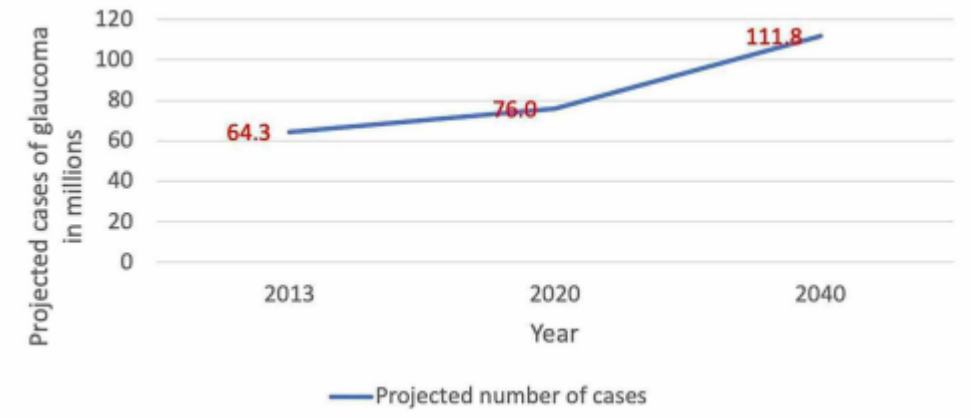

Figure 2.4: Glaucoma Projection by 2040 [8].

an increase in IOP, causing the death of the RGCs. However, IOP is the only risk factor that can be regulated to delay the onset of severe glaucoma [12].

The onset of the disease during its early phase often goes unnoticed [13]. Thus glaucoma is called the "silent thief of sight". Two factors are mainly responsible for this. The brain can fill the missing bits of information when minimal damage to the visual field. Another reason can be overlapping visual fields. If the defect is present in only one eye or asymmetric, the visual field of the other eye can complement the missing field on the affected eye. This can happen if the damage is restricted to the overlapping region of the visual field [14]. In its advanced phase, the disease is marked by a complete loss of visual field, creating tunnel vision. fig. 2.5 gives a general overview of some typical patterns observed in glaucoma patients [9]. Any form of damage to the visual field is known to impact activities requiring eye-hand coordination [15].

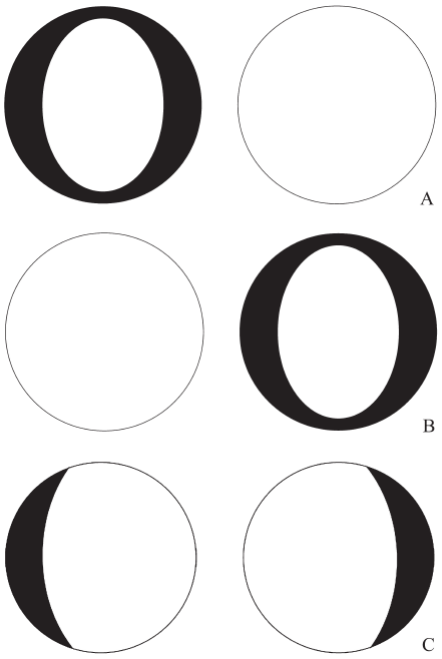

Figure 2.5: Variously affected visual fields in glaucoma patients: A) Left eye has advanced glaucoma, right eye normal; B) Right eye has advanced glaucoma, left eye normal; C) Peripheral visual field is effect for both eyes. [9].

2.3. Glaucoma diagonisis

Glaucoma diagnosis is dependent on the functional evaluation of the visual field. Currently, SAP is the most widely used method for evaluation of the visual field [16].

2.3.1. Standard automated perimetry

SAP uses differential light sensitivity to evaluate the visual field threshold at each test location [17]. It displays a series of achromatic light stimuli on a white background at various visual field locations and a center of fixation. SAP requires the subject to maintain a center of fixation with one eye. The apparatus is equipped with a response button. While the subject maintains the vision at the center of fixation, light stimuli are projected at different predefined areas of the field of vision. The subject has to press the response button whenever a stimulus is visible to them.

Humphrey field analyzer

SAP threshold tracking algorithm is based on the HFA. The HFA is a well-known tool to analyze the monocular visual field [18]. The HFA works on various testing protocols tailored to the extent of the disease.

- **10-2:** 10-2 is used to access glaucoma in the advanced stages. The protocol is used to identify glaucoma in the central area of the visual field within a radius of 10° from the center of fixation. The 10-2 pattern facilitates more detailed monitoring of the damage to the retina. It has a total of 68 points of measurement [19]
- **24-2:** The pattern is used to detect and monitor the early stages of glaucoma. It tests 24° temporally and 30° nasally and has a total of 54 points.
- **30-2:** This is an alternative to 24-2 and is used to determine the onset of glaucoma. It tests points presenting 30° temporally and nasally and has 76 test points. Severe defects occur centrally within 30° radius from the center of fixation [20].

Limitations of SAP

Troxler's fading effect due to neural adaption can be observed as the subject needs to maintain the center of fixation for the entire evaluation period with one eye [21]. This is experienced as the disappearing or fading of peripheral stimuli while fixating on the point of interest for more than 20 seconds [21]. This often leads to complaints like blurred vision, inattention, discomfort, and fatigue. A step forward will be to eliminate the primary cause of false results and discomfort, i.e., maintaining a constant center of fixation and suppressing reflexive eye movements. Suppressing reflexive eye movement to newly appearing stimuli necessitates a high concentration level and requires the active suppression of the innate, natural oculomotor reaction, i.e., orienting the eyes towards the stimulus [13].

2.3.2. Alternatives to SAP - FDT and SITA

FDT measures the contrast sensitivity to 0.25 c/deg vertical sine-wave gratings. The stimulus is counter-phased[2] flickered at 25 Hz and is displayed up to 720 ms. The setup uses a grid layout divided into four quadrants, each having 10 ° targets with an additional centered circular target. The

[2]the phase difference is 180 °

test protocols are C-20, testing 17 locations at 20 ° from the fixation point, and N-30, which tests 19 locations incorporating 2 additional points nasally [22]. FDT is also effective in detecting the early onset of glaucoma and monitoring visual field deficit progression that can not be detected by SAP [23]. The variability of results from FDT is independent of the severity of glaucoma and is more uniform [24]. However, no clear evidence has been found to support FDT for detecting the worsening of glaucoma.

Another alternative is SITA, a threshold testing algorithm class implemented in the HFA, taking 6 mins and is approximately 8 minsfaster than SAP. SITA follows a staircase pattern where the threshold is increased after each stimulus [25]. The current generations are SITA Fast and SITA Faster Perimetry which are faster than the SITA standard and provide accurate results. SITA standard reduces the number of stimuli explored by 25 to 30 % while delivering more accuracy than SAP. SITA Standard also reduces the testing time to 50% [25]. SITA Fast is another tested strategy based on the same algorithm as the SITA Standard with good reproducibility and rapid test time.

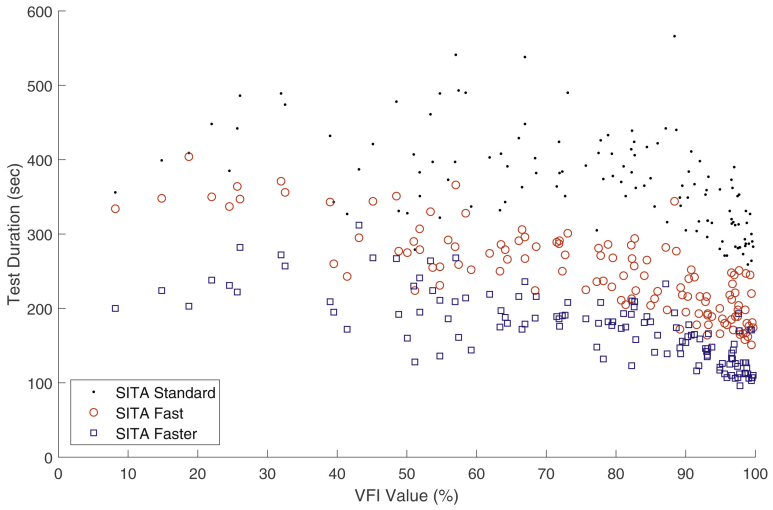

Figure 2.6: SITA, SITA Fast and SITA Faster test durations according to Visual Field Index value [26].

SITA Fast's rapid test time of 4 mins and flexibility in test parameters can mitigate the patient fatigue associated with SAP [27]. A later iteration is SITA Faster which incorporates minor changes in the algorithm by eliminating the calculation of false negatives, eliminating retesting, and replacing the 2-step staircase model from SITA. The test time was reduced by 30.4% while producing almost identical results as SITA Fast [26]. fig. 2.6 shows the comparison of test duration of the SITA variants based on VFI. It can be observed that the latest generation of SITA, SITA Faster, has a testing time of approximately 2 mins.

2.3.3. EMP as an alternative to SAP

New glaucoma testing methods primarily try to address the reliability issues caused by patient fatigue and false results, and duration drawbacks of SAP. These drawbacks prompted the development of Eye Movement Perimetry(EMP). EMP uses reflexive eye movements for glaucoma diagnosis. It relies on video eye-tracking to track the eye movements in response to the stimulus presented. The outcome measures are the percentage of stimulus seen and, notably, saccadic reaction time, i.e., the time difference between the appearance of the stimulus and the onset of eye movement [28]. At four levels of changing stimulus intensity, stimuli were plotted at 54 sites comparable to the 24-2

test coordinates of the Humphrey Field Analyser, shown in fig. 2.7. The gaze data was categorized as seen, unseen, or invalid using a judgment algorithm based on eye movement analysis. The eye movement responses were also measured as SRT for each of the seen stimuli [28].

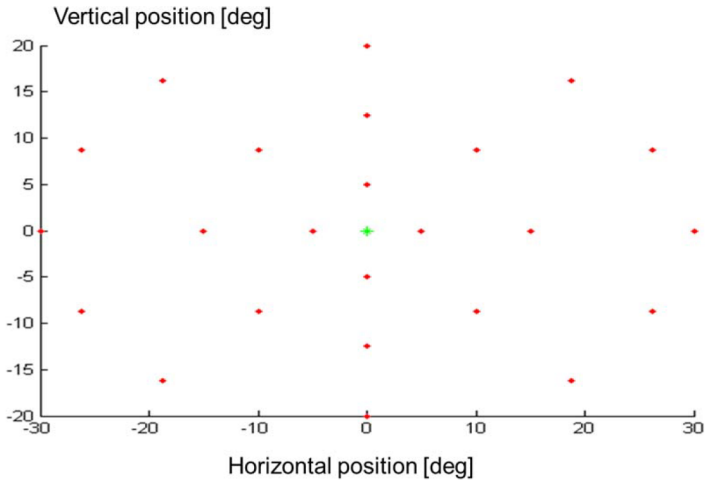

Figure 2.7: Schematic of 24-2 grid setup used in EMP [28].

The EMP algorithm incorporates major changes from the manually operated SAP [28]. These adjustments can be summarized as:

- Use of Contrast levels: EMP uses four contrast levels, 0.7, 0.8, 0.9, and 1.0 with brightness levels of 150 cd/m^2, 162 cd/m^2, 175 cd/m^2, and 190 cd/m^2.
- Saccadic Reaction time: In SAP, the subject has to press a button when stimuli are detected manually. EMP eliminates the manual detection by automatically detects the SRTs from the target-directed saccades.
- Categorised responses: EMP categorizes responses based on eye movements into seen, unseen and unknown. The events were classified as 'unseen' if no eye movement was made towards the direction of presented stimuli or if the saccade was not in the direction of the stimuli; 'unknown' for corrupted data due to blinking or reflexive eye movements or missed stimuli. 'Seen' was classified as a positive response to stimuli presented.
- Grid setup: EMP used a 54-point grid setup shown in fig. 2.7, where each grid location displays the three levels of contrast in varying order.

EMP successfully addresses the issue of suppressing natural eye movement by enabling the subject to perform reflexive eye moments. Like SAP, EMP also had an initial time period of 12 to 15 mins. However, the time can be reduced significantly by less repetition during tests. However, reducing repetitions depending on SRT variability may lead to wrong estimates of the underlying SRT distribution. Calibration, as stated, can affect the test, and the constant need for calibration will increase testing duration.

2.3.4. Progression monitoring - Visual Field Index

In clinical practice, the progression of glaucoma is monitored by analyzing the deviation of VFI from the mean baseline over time [29]. A linear regression model is used to estimate the change over time. Such a model fits the measurement taken over time, and the rate of progression can be provided with 95% confidence intervals [24]. Alternatively, models like exponential decay can also be used but are

not approved clinically. In linear models, the rate of change is expressed as decibels or percentage change. Such global indexes project the loss of visual field, the most common being the VFI. The index calculates the rate of progression by comparing the MDI. The deviation is calculated in percent as:

$$VFI = (1 - \frac{MDI_{meas}}{MDI_{min}}) \times 100, \tag{2.1}$$

where the MDI_{meas} was the measure MDI and MDI_{min} is the minimum MDI for a certain age [29].

2.4. Conclusion

The chapter gives an overview of human vision and its functionality. It helps to understand the relationship between human vision and glaucoma. The chapter aims to answer three basic questions: “What is glaucoma?"; “What are the measurable parameters and techniques for glaucoma detection?". The first question is answered in section 2.2, which gives an overview of glaucoma, describing the causes behind glaucoma and a general description of the effects on the visual field. The answer for the second question can be found in section 2.3. This section provides an overview of the standard diagnosis technique, SAP used for glaucoma detection and its associated demerits. SAP evaluates the threshold of detection of stimuli in a grid setup, other alternatives like FDT and SITA also does the same, describe in section 2.3.2. Another alternative is EMP described in section 2.3.3, evaluates the SRT to detect glaucoma and associates the duration of SRTs to each level of glaucoma. The findings from this chapter can be summarized below:

- **Reproducible parameters:** SRT and visual threshold of detection are the two parameters that help identify and monitor glaucoma’s progress. The thesis can aim to reproduce these two to develop the framework of inducing glaucoma in healthy subjects temporarily.

- **Algorithms :** If any of the above-said parameters are reproduced, the EMP algorithm will be suitable for performing the analysis. Furthermore, the design of EMP also automates the entire process since the patient or subject only has to perform the eye movements without indicating the seen or unseen stimuli.

- **Duration :** It will be ideal to keep the duration of each trial minimal and have breaks between trials. Small trial durations will also help to avoid any possible fatigue of the subject and the Troxler effect, described in section 2.3.1, thus eliminating the possibility of bad output data.

The finding above contributes to the experiment design procedure. Also, this chapter asks some questions like; “Why are the eye movements affected in glaucoma patients?" and “What are the effects of the eye movements in certain performance-based tasks, etc?". The next chapter aims to find the answer to these questions by exploring different studies performed on glaucoma.

3

Eye Movements

This chapter aims to search for answers to the question asked at the end of chapter 2. Neurodegenerative diseases can cause abnormalities in oculomotor control, causing changes to the neural pathways [30]. Eye movements involve an extensive cerebral network consisting of several elements of the central nervous system elements. Any damage to these areas, be it focal like glaucoma or widespread like dementia or Parkinson's, can alter the oculomotor functions. Evaluating saccades has proven to be a reliable method of understanding the effects of neurodegenerative diseases on the visual field [31]. However, to understand eye movements in glaucoma, the first step is to get a general overview of eye movements in healthy individuals.

3.1. General eye movements

It has been widely accepted that glaucoma patients exhibit a unique and distinguishable eye movement pattern [32]. Hence it is essential to understand these eye movements and the disease's dynamics, which can also assist in developing new diagnostic methods. Eye movement is a fundamental activity performed to perceive and understand the motion of objects in the field of vision and their related dynamics. However, for complex motion or tracking any object, alongside a rotation of eyes, movement of the head also takes place. Generally, three kinds of movements are performed; saccadic eye movement, pursuit eye movement, and a combination of both, including microsaccades.

3.1.1. Saccadic eye movements

A part of this thesis focuses on the saccadic eye movement of glaucoma patients since it has been found in chapter 2 that SRTs can be a reproducible parameter. Hence it is crucial to understand the mechanism of saccades. This section briefly touches upon the findings of Yarbus in terms of saccades and other eye movements in his book *Eye movement and Vision* [33]. As denoted by the author, saccadic eye movement has two main features; a) almost identical movements of both eyes and b) high velocity, measured in hundredths of a second [33]. Saccades function by changing the point of fixation by directing the sensitive region of the retina, the fovea, to the object of perception. The short duration due to the high velocity of saccades permits the eye to maintain a state of fixation for about 95% of the total time [33].

Duration of saccades

The saccades are mostly restricted to an amplitude of 20 °. If the amplitude exceeds 15 °, then eye movements can be composed of two or three saccades or even accompanied by a head rotation.

Normally the saccades are limited between 10 °-15 ° and seldom exceeds 15 ° [34]. However, the duration of the saccades is dependent on the amplitudes. For small saccadic movements, the duration is between 100 ms and 200 ms, whereas for saccades of 20 ° amplitude the duration may exceed 700 ms. Also, it should be noted that the duration is slightly dependent on the direction of the eye movement, specifically when the movement is relatively upwards, as seen in fig. 3.1. The duration of the saccades depends on the amplitude for all positions within the visual field except the periphery. Correction saccades are usually comprised of two or three regular saccades of smaller amplitude between the points of fixations. The saccadic eye movement also has small corrections to it. While transitioning from one point of fixation to the next, corrections follow the primary saccade [33]. It is also noted that blurred vision may occur during the saccade due to the high velocity of movements [33]. Under normal conditions, the duration, as discussed earlier, is linked to the angle of movement, and the relationship can be quantified by eq. (3.1) where T is the duration of the saccade, and a_0 is the angle through which the eye turns.

$$T = 0.021 a_0^{\frac{2}{5}} \tag{3.1}$$

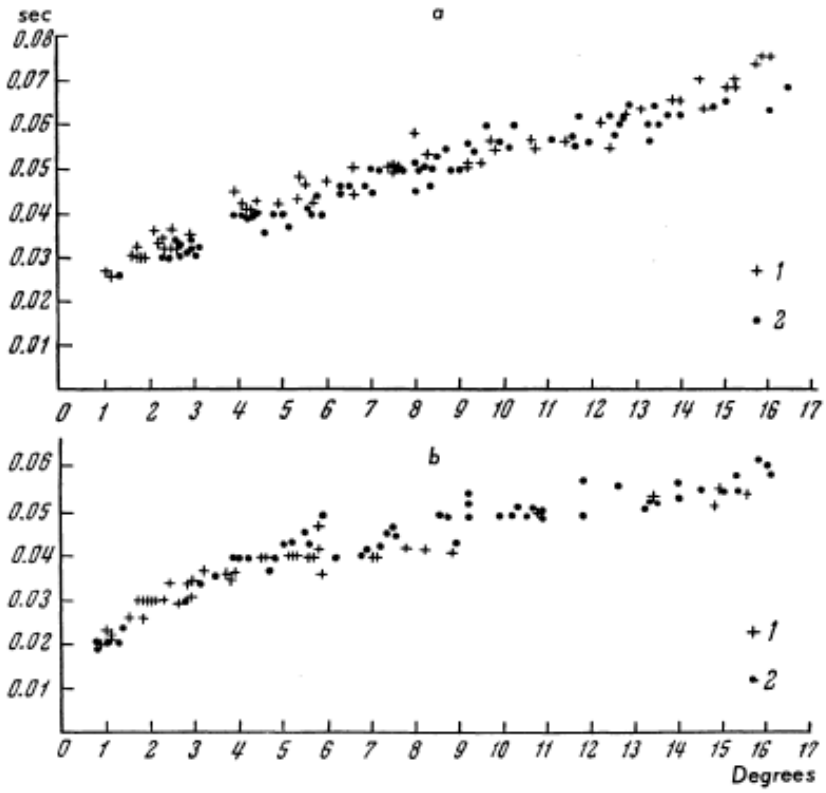

Figure 3.1: Duration of saccades as a function of angle with the eye at an angle of 45 ° relative to vertical a) Subject 1; b) Subject 2; 1)Readings derived when the subject's eyes moved upwards and to the right; 2) when the eye moves downwards to left [33].

Development of saccade

Yarbus [33] observed that vertical and horizontal saccades below 15 ° approximate a sinusoid. These saccades can be approximated by eq. (3.2) where t is the time in seconds,$(0 < t < T)$, a is the angle of rotation of the eye during the saccade in degrees,$(0 < a < a_0)$, T is the duration of the saccade in seconds, and a_0 is the amplitude of the saccade in degrees.

$$a = \frac{a_0}{2}\left(1 - \cos\frac{\pi}{T}t\right) \tag{3.2}$$

The angular velocity(ω) can be easily obtained from eq. (3.2) and can be related to the linear velocity(v) for saccades below 20 °. d is the diameter of the eyeball around 2.4 cm.

$$\omega = \frac{a_0 \pi t}{2T} \sin\frac{\pi}{T}t \tag{3.3}$$

$$v = \frac{d}{2}(\frac{\pi}{180})\omega = 0.021\omega \tag{3.4}$$

It is noted that the velocity of the saccade rises smoothly, reaches a maximum, and then falls to zero in the same pattern. For saccades below 15 °, the rise and fall of the saccades follow a smooth sine curve. Also, the maximum velocity depends on the saccade amplitude(a_0).

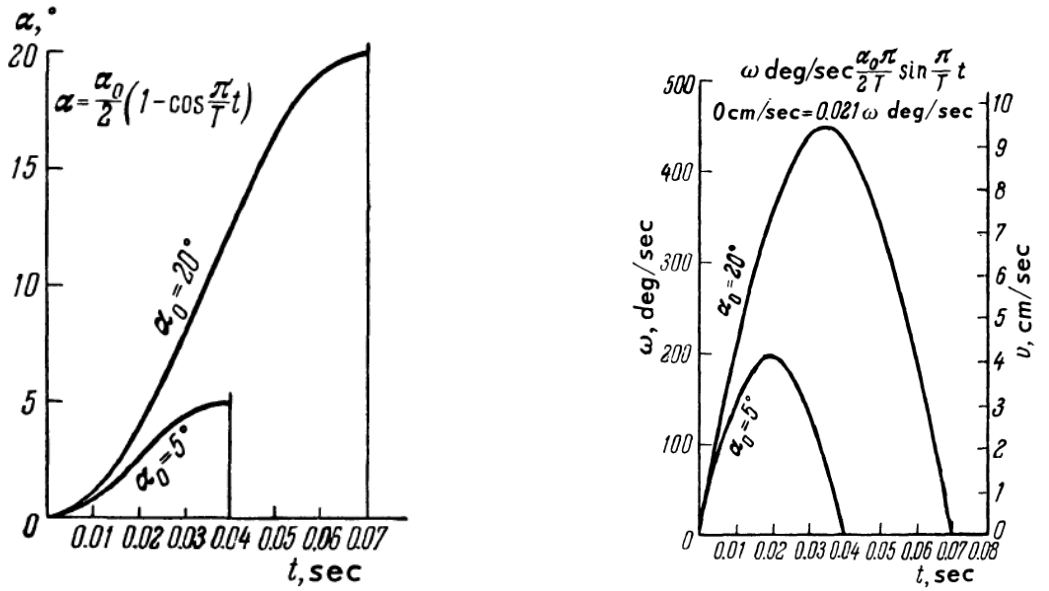

(a) Eye movement due to a saccade

(b) Variation of velocity of saccades with time

Figure 3.2: Amplitude and velocity variation based on the amplitude of saccades with respect to time [33]

The absolute magnitude of two accelerations[1] for small saccades are almost identical. Still, for saccades exceeding 15 °, the first acceleration is greater than the second. Maximum force calculated in ideal conditions for a saccade of 5 ° and 20 ° were 1 g and 1.5 g respectively. Later a model of a mass-spring-damper system representing the mechanism of saccadic eye movement was developed by Robinson [35]. The developed system closely resembles the spring-mass damper system used to represent the human arm movement [36].

3.1.2. Eye movement for shifting point of fixation

Switching from one object to another in the visual field is a natural phenomenon during everyday tasks. Suppose the fixation points are changed to various locations or distances in the visible area. In that case, the change is accompanied by two movements: a) convergence or divergence and b) a saccade. There is a considerable difference between the duration of saccades and convergence or divergence because saccade follows a predetermined program, whereas convergence and divergence

[1]first acceleration at the beginning of the saccade and the second when stopping the saccade

cannot be pre-programmed [37].

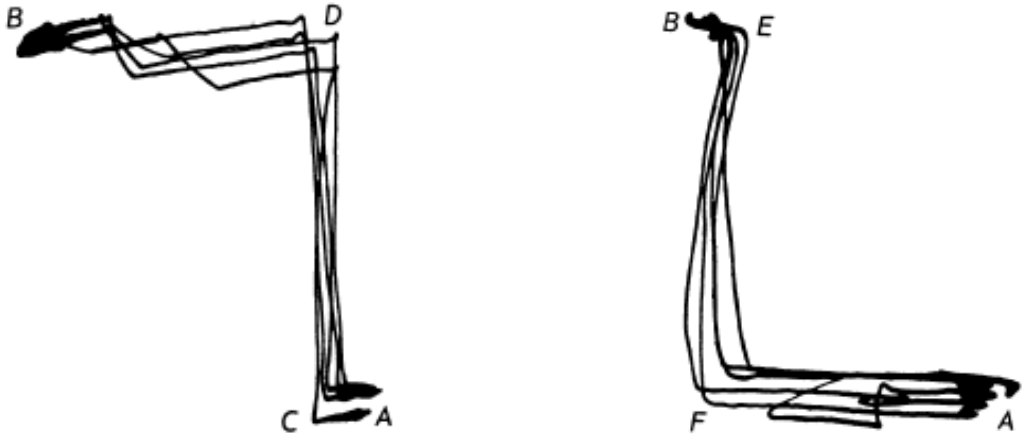

(a) Divergence movement of eye from point A to point B **(b)** Convergence movement of eye from point B back to point A

Figure 3.3: Convergence and Divergence motion of eye while transitioning from on point of fixation to another [37].

General divergence and convergence can be explained by the movements shown in fig. 3.3. Both the movements are composed of convergence or divergence of the optical axes and a primary saccade. More specifically, there is no need to rotate the eye for convergence or divergence. The divergence movement can be depicted by fig. 3.3a where the eye moves from a **A** to **B**. The eye makes a couple of divergences combined with a primary saccade. The eye makes a divergence towards **C**. After that, a saccadic eye movement is made towards **B** vertically upwards to reach the point **D** and then to make a second divergence movement to reach the target **B**. A similar set of movements are performed when the eye returns to the original point of fixation **A**. Here the eye performs a convergence movement towards **E** and then a primary saccade vertically down to reach the horizontal level of **A** followed by a convergence movement to fixate at **A**. It has to be noted from both the figures that the largest convergence or divergence occurs only after the saccade is performed. Sometimes the change in the fixation can be supplemented by small corrective saccades and minor corrective convergence or divergence. However, these corrective eye movements do not affect the primary movements required to change the point of fixations. Convergence or divergence is generally slower than saccades and may take up to tenths of seconds. The duration of convergence or divergence preceding a saccade is anywhere between 0.07 sec and 0.2 sec. However, the duration of the divergence is slightly longer than the duration of convergence, and they remain fairly fixed in subjects.

3.1.3. Eye movement for moving objects

Human beings perform smooth pursuit motion to track the movement of an object in the visual field [33]. According to Yarbus, the pursuit is primarily to make the retinal image of the moving object stationary relative to the retina [33]. Being stationary implies that the minute velocity of movement of the retinal image does not hamper the resolving power of the eye. However, pursuit is the general term, and pursuit eye movements involve a cluster of other eye movements. The eye tracks a moving object by combining pursuit movements, saccades changing points of fixation, corrective saccades, and convergence or divergence.

Pursuits are voluntary movements in terms of initiation and termination. If a moving object is present in the visual field, a subject can start and stop the pursuit at will. However, one cannot voluntarily interfere in the pursuit mechanism and alter the pursuit velocity. While pursuing an object at a low

angular velocity, smooth pursuit motion develops when the irregular drifts while pursuing transform into regular drifts in the direction of the motion. The experiments done by Yarbus [33] show that when the velocity reaches 5 minutes of arc per second, the smooth pursuit begins. Smooth pursuits are always accompanied by small correcting saccades, the dynamics of which are similar to normal saccades. Pursuit motion also develops for objects having high angular velocity. However, the ability to pursue them also depends on the continued presence of the object in the visual field. Other than the continuous presence of the object in the field of vision, pursuit motions also have a development period. Normally, the pursuit becomes infeasible if the object's period is less than 0.15 sec. Yarbus estimated this development time to be in between 0.15 sec and 0.2 sec. While tracking a moving object, the eye movements are also supported by the head's rotation in the object's direction [33].

A successful attempt to pursue an object can have two outcomes. If target stimulus follows a sinusoidal path, the observer must repeat the same sinusoid motion with the eyes. Sometimes a delay can be introduced here while the smooth pursuit happens, causing a phase shift. Irregularity can also occur in the amplitude caused by overshooting or undershooting the motion of the target stimulus. A more accurate version of pursuit will be one closely following the sinusoid motion of the target stimulus with high-velocity corrective saccades. Complex pursuit motions like tracking a sinusoid have two states - a state of fixation, which gives information about the orientation and angular velocity of the object; and a state of pursuit, which evaluates the difference in angular velocity of the object and the eye.

The mechanism of saccades and pursuit are tightly coupled during the target selection. Experiments performed by Erkelens show that saccades are prepared from the time that decision has been made to pursue an object [38]. In the study done by Erkelens, switching from one moving object to another was studied. The switching can follow a two-step process of preparation and execution. When switching moving targets in the field of vision, the preparation of saccading and pursuit change starts by engaging attention to the new target. The preparation phase terminates when the required parameters like magnitude and velocity are obtained. The execution phase begins by executing the saccade needed to switch targets and changing the saccade to a pursuit. This two-stage mechanism can explain the process of switching targets in a fast manner and then transforming them into a pursuit.

3.2. Eye movement in glaucoma

Attempts have been made to evaluate the effects of glaucoma on eye movement by analyzing scan paths during free-uncontrolled television viewing by Crabb *et al.* [32]. The experiment aimed to detect glaucoma by examining the pattern of eye movements when the subject naturally watches a movie. The protocol used *"eye movement"* signatures to detect a neurodegenerative condition in subjects. Eye movement signature is an amalgamation of scan paths consisting of saccades and fixation points [32]. Individuals with glaucoma were considered along with a control group to evaluate the hypothesis presented by Crabb *et al.* [32]. Participants were asked to watch movies with a viewing distance of 60 cm and chin rest unsupervised. The monocular vision was tested with the eye having the best quality of pupil detection and corneal reflection for tracking. Since neurological disorders affect eye movements, it is reasonable to expect that such conditions might alter eye movement patterns. The study successfully demonstrated that a group of patients with the neurodegenerative disease could be segregated from their healthy peers by considering eye signatures alone.

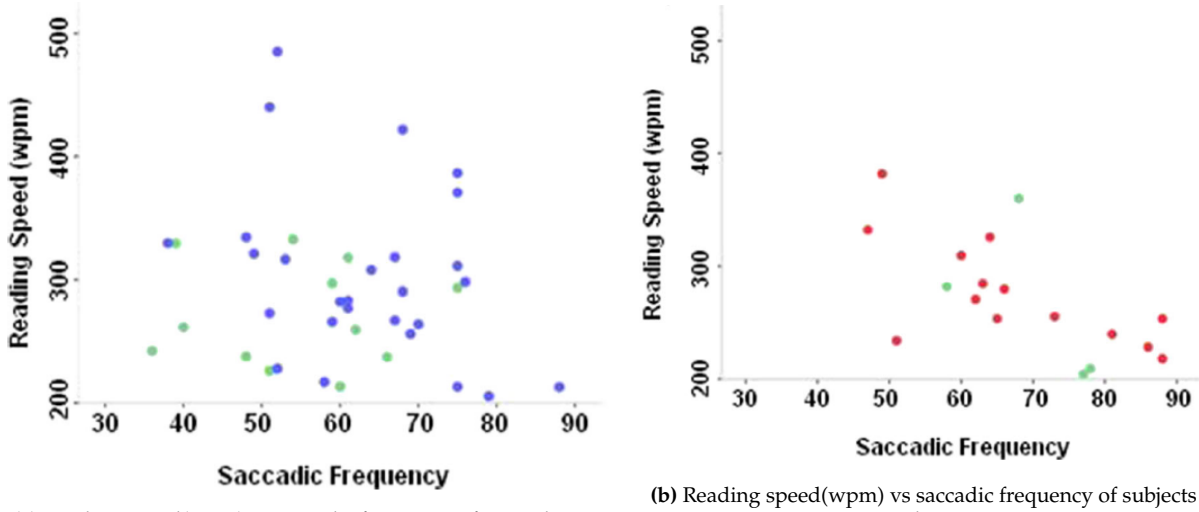

(a) Reading speed(wpm) vs saccadic frequency of control group

(b) Reading speed(wpm) vs saccadic frequency of subjects with glaucoma

Figure 3.4: Comparison of reading speed(word per minute) vs saccadic frequency of control group(blue) and glaucoma patients(red). Green dots denote if two or more errors are made [39].

3.2.1. Affects in reading

Eye movement is connected to the process of reading. It is partly denoted by perceptual span, i.e, the amount of information that can be captured and stored by the oculomotor system at any instance [39]. A study tried associating eye movement with reading speed in patients with advanced glaucomatous visual field loss [39]. So it is reasonable to suspect that people with visual field loss have compromised perceptual span, thereby influencing their reading capabilities. The study by Burton *et al.* consisted of two experiments evaluating reading speed vs. perceptual span and a LDT vs. saccadic frequency. LDT is used in many psychology and psycholinguistics experiments. The basic procedure involves measuring how quickly people classify stimuli as words or nonwords. For the first experiment, the subjects (control group and glaucoma patients) had to read eight paragraphs of text (68-79 wpm) on a CRT screen presented at 100 % contrast at a viewing distance of 60 cm. The texts had a font size of 48 subtending 38 pixels and height of 0.84°. The LDT involved the subject distinguishing two words, one false and true, with a font size of 14 and height of 1.4 °. The width was between 1.10 ° and 3.20 °. The eye movements for each trial for both experiments were recorded using an EyeLink device. Some patients demonstrated slower reading speeds concerning perceptual spans, which is also evident due to the restricted visual field [40]. The outcome from the LDT found that the patients had a higher saccadic frequency than the control group. A relationship between the reading speed in wpm and saccadic frequency is drawn up in fig. 3.4. It demonstrates that the patients made more saccadic eye movements for a specific word count. This can be because the patients with restricted visual fields exhibit additional or compensatory saccades impairing the reading speed.

Another study by Cerulli *et al.* on reading patterns of glaucoma patients reported no comprehensive relationship between reading speed and accuracy [41]. The eye movement patterns of glaucoma patients and control groups were accessed using a micro-perimeter. The evaluation parameters included reading speed and accuracy concerning eye movements along both axes using monocular vision. No significant difference was observed between the mean minimum amplitude of the eye movements made along the X and Y axis of the two groups [41]. However, it was found that the patients' X_{max} and Y_{max} values were significantly higher than the control group. This can be because defective motor neurons control saccadic eye movements [42]. An error in controlling eye movements during the identification process can lead to significant corrections in saccadic eye movement and

thus cause a more substantial number of fixations[42]. The result is compared to the works done in [39, 40, 41, 42] where the glaucoma patients were found to demonstrate a unique eye movement signature assisting in distinguishing glaucoma patients from healthy patients.

3.2.2. Tracking saccadic eye movements

In the EMP method SRTs of glaucoma patients are tracked based on eye-movement recordings made with a remote infra-red video camera.. A valid comparison between normal and glaucomatous vision based on SRT has been by Mazumder *et al.*[43]. The study included EMP tests across 54 locations resembling a 24 − 2 HFA program. The EMP setup included a laptop, a 17-inch display with an integrated eye-tracking device, and a 120Hz refresh rate (Tobii120, ELO Intellitouch system). The eye tracker worked on the principle of infrared corneal reflection tracking. The eye tracker software prompts 9 calibration points to perform the test and accurately obtain the gaze data that has been compared later. A nine-point blue stimulus was used that moves at 15 °angles up, down, left, and right from the center of the display. 8 zones were tested across all subjects having a normal and glaucomatous vision. Zone 1 has the lowest eccentricity, and zone 8 with the largest eccentricity for the test.

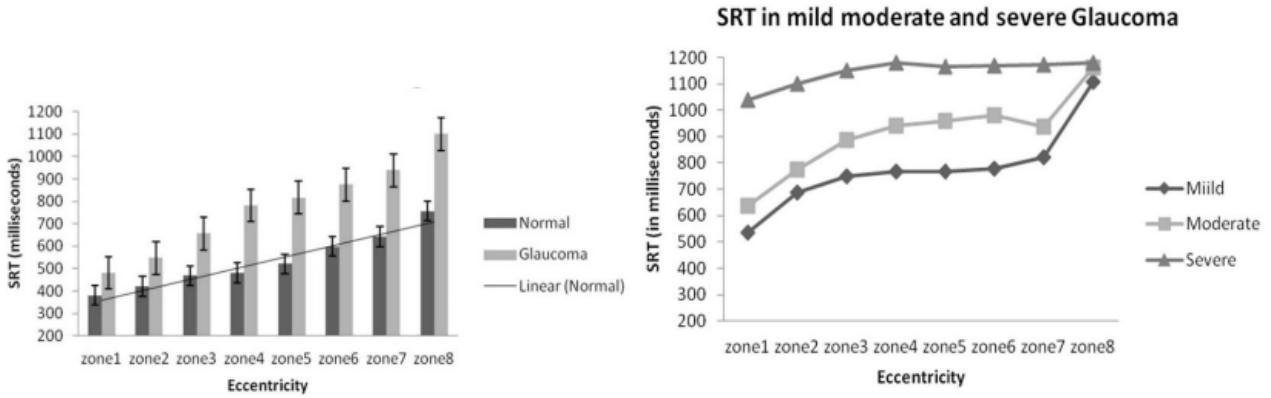

(a) SRT difference across all test zone between normal and glaucomatous visual field

(b) Variability of SRT across all test zones based on the progression of glaucoma .

Figure 3.5: Comparison of SRT of normal individuals and glaucoma patients [43].

The test results in fig. 3.5a depict the difference between a normal eye and a glaucomatous eye. It also confirms the constant variability of vision across the visual field, where the reaction time increases with the increase of the eccentricity. As glaucoma affects the visual field resulting in tunnel-like vision as it progresses, it is evident that the subjects with glaucoma will face difficulty in recognizing the stimuli. As the disease progresses, variability can also be observed across all stages of the disease. fig. 3.5b depicts how the reaction times vary according to the stages of the disease - mild, moderate, and severe. The zone 8 located peripherally has almost the same SRT because glaucoma affects peripheral vision first.

3.2.3. Effects on performance-based tasks

Glaucoma is known to affect several visual functions alongside peripheral vision loss. Performance tasks are affected due to the neural under-sampling as an outcome of RGC death or impairment. Even with good visual acuity, glaucoma patients suffer from deficits in contrast sensitivity, color, and shape detection can lead to reduced task performance [44]. Glaucoma also affects visual processing

speeds, motion detection, spatial orientation, and visual search, affecting performance-based tasks like biking, driving, or daily activities. Again these are caused by dysfunctional RGCs. For example, the study by Boer *et al.* [44] shows that individuals suffering from visual impairments like glaucoma, with less than 100 ° horizontal field of vision are twice as likely to have automobile accidents as those without deficits [44]. Although the effect of glaucoma on performance-based tasks is evident, the relationship with the size, shape of the visual field, or structural damage is still unknown.

3.3. Conclusion

This chapter briefly overviews different aspects of visual performance found in glaucoma patients. It shows that neurodegenerative diseases like glaucoma will produce unique eye movement patterns. Alongside it tries to answer the following questions "Why are the eye movements affected in glaucoma patients?" and "What are the effects of the eye movements in certain performance-based tasks, etc?". The abnormal eye movements made by glaucoma patients in terms of SRTs are linked to defective oculomotor neuron control. Impaired motor control can lead to a more significant number of corrections and also delayed reactions. Also, it is found in section 3.2.1 that the perceptual span is significantly reduced in glaucoma patients. The second question is also answered in section 3.2, where it is found that glaucoma patients perform more saccadic eye movement than their healthy counterparts. Also, it has been found that the amplitudes of the saccades made by glaucoma patients are significantly higher, which is also the case for the SRTs. The findings of this chapter can be summarized as follows:

- Glaucoma patients have a higher SRT than normal individuals, implying that the dynamics of the saccades made by glaucoma patients will differ. The dynamics of saccades formulated by Yarbus can be used to verify saccades' amplitude, velocity, and duration. The findings can also be compared to the SRTs of healthy and glaucoma patients for validation purposes.

- It is expected that after inducing glaucoma-like symptoms in healthy individuals, their eye movement patterns will also be similar to glaucoma patients. Smooth pursuits can be linked to continuous tracking tasks one performs daily, like driving, and biking, where people have to scan and track objects in their visual field constantly. The evaluated parameters will be errors in tracking either in terms of phase shift or amplitude, tracking pattern, and development of pursuit motion.

- A task combining for smooth pursuit task and discrete tracking task. Again it can be linked to the previous bullet point, where it is interesting to observe how people with glaucoma react to objects suddenly entering their visual field. Like, while driving a car, a person continuously scans the road and the traffic. If a pedestrian or another vehicle suddenly enters unexpectedly, how will a person with varied glaucoma react to it? What will be their eye movement pattern?

Now that the changes in vision-related tasks and the reasons behind them in glaucoma patients have been identified, the next step will be to search for appropriate methods that will assist in recreating the effects of glaucoma. The next chapter will try to answer the question: "How will the visual changes found in glaucoma be induced in a healthy individual without affecting the wellbeing?"

4

Simulating Glaucoma

In chapter 3, it has been found that the restricted visual field is the outcome of glaucoma. Glaucoma patients suffer from elevated SRT, increased contrast detection threshold, and reduced percentage seen scores [28][43]. A successful model of glaucoma needs to take the above effects into account. The goal is to create the above observations in healthy subjects to investigate glaucoma's dynamics. Earlier studies have shown that dark adaptation is suitable for obtaining increased contrast thresholds for healthy subjects.

4.1. Dark adaptation

The human visual system can adapt to a wide range of light intensities from the bright daylight to the starlit night sky that covers a range of more than $10 \log_{10}$ as shown in fig. 4.1 [45][46]. However, this rapid adaptation is compromised under certain conditions. Rods are several hundred times more sensitive than cones, but they saturate at much lower light levels, whereas cones have an extremely high photon saturation threshold. The process by which the eye recovers its sensitivity in the dark after exposure to bright lights is referred to as dark adaptation [47]. It is a biochemical process of regeneration of photoreceptors. When the eye enters a dark environment after prolonged exposure to an intense light source, many photoreceptors are bleached. It can take a much longer period for the eyes to regain their normal visual sensitivity, this slow recovery of visual sensitivity is coined as **'Dark Adaptation'**, distinguishing it from the light adaptation [45].

However, the term "adaptation" can have different meanings. For example, when the ambient illumination is altered, visual performance is affected, and the eye is said to adapt to the new luminance level. However, the change is not instant and can take several minutes. Adaptation can be due to the temporal changes in the detection threshold. Temporal changes can occur in the slow decline of the detection threshold during dark adaptation. In temporal adaptation, the changes in performance are studied as a function of time as the adapting level changes. The adaptation can be a steady-state one, where the visual system is given time to reach a certain level, and then the visual sensitivity is measured as a function of that level. Self-luminous objects appear dimmer when the ambient illumination is increased: a blazing fire appears to be extinguished by direct sunlight, and bright stars fade with the dawn. Other manifestations of the same basic phenomenon can be found. For example, the adjectives "black", "white", and "grey" refers to an object's reflectance rather than its luminance. This presumably confers a selective advantage because reflectance is the more constant attribute of an object and, thus, a more reliable aid to identification. However, the physiology behind it is that the eye responds primarily to contrast, not the absolute illumination level. The observer's ability to detect contrast is studied as the difference in the threshold, Weber's law, which states the ratio of the

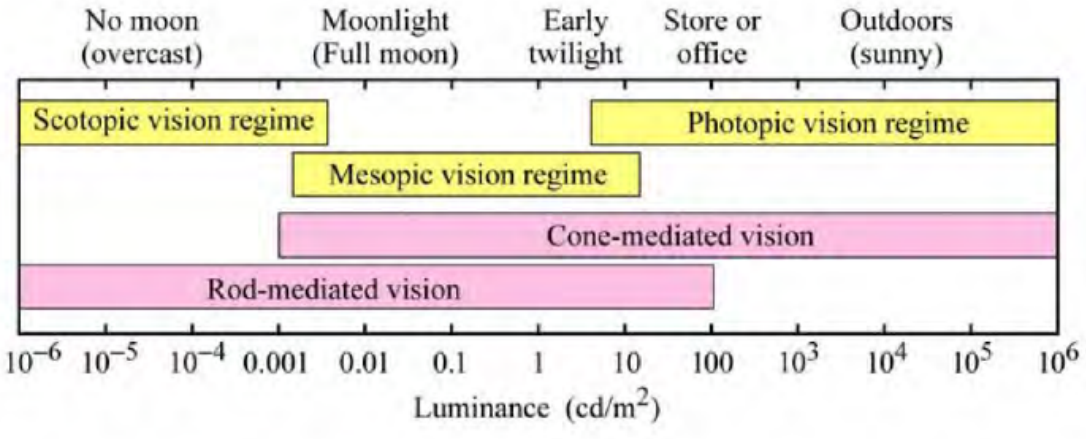

Figure 4.1: Luminance range of human visual system in cdm^2. In log scale the range will be from $-6\log_{10}10$ to $6\log_{10}10$ covering a range of $10\log_{10}10$ units [46].

increment threshold to background intensity is always constant. Here, we refer to the reduction in the ability to detect luminance increments at higher adaptation levels as "steady-state desensitization" [48].

4.2. Elevating detection threshold

The continuous change of visual detection threshold as a result of luminance and field intensity has been studied by Stiles et al. [49]. The study involved dark adapting a subject for 30 min. The measurement aimed to test the threshold of visibility of the stimulus. After each measurement, the field intensity was raised, and the subject had to look at the screen for 2-3 mins before a new stimulus appeared. The field brightness was measured under the same experimental conditions, expressed in trolands[1], and only the left eye was used for measurements. The approximate test duration was an hour for each subject. A test stimulus of 9 ° diameter, centered 9° from the fovea was exposed every 0.2 sec with an adapting field of 20°. The results obtained from the experiment for four subjects are shown in fig. 4.2.The curve under the areas (a), (b), (c) in fig. 4.2 is related to rod vision and area (d) to cone visions [49]. The line fits for all the curves are inline with the weber contrast, $K = \frac{\delta I}{I}$, where δI is the difference between the intensity of the target stimuli and background, and I intensity of the background. However, the outcome can also be used to distinguish how the visual sensitivity may be altered based on the change of background intensity levels after dark adaptation and bleaching.

The theory of “equivalent background brightness" studied by Stiles and Crawford can also be linked to fig. 4.2 [51]. It was found that the state of adaptation caused by a steady background light would produce equal desensitization. A subject who had 50% bleached rods was exposed to a small 0.833° and large 6° stimuli after being dark adapted. The increment of threshold and the background threshold change were plotted for both stimuli. The results were compared to a decrease in the detection threshold over time, as shown in fig. 4.3. The left half shows a dark-adapted curve log threshold plotted against time in dark adaptation following bleaching, and the right half shows the threshold curve for two stimuli. It can be noticed that the curves follow a similar trend. The highest detection threshold was around 7 log units for both the stimuli, with the initial difference of 3 log units. The drop of threshold after dark adaptation for both the stimuli from 7 log units takes about

[1] $Td = L \times d$; L = Luminance of source, d = diameter of the pupil. $1\,\text{cdm}^{-2}$ is equivalent to $\frac{4}{\pi d^2}$Td [50]

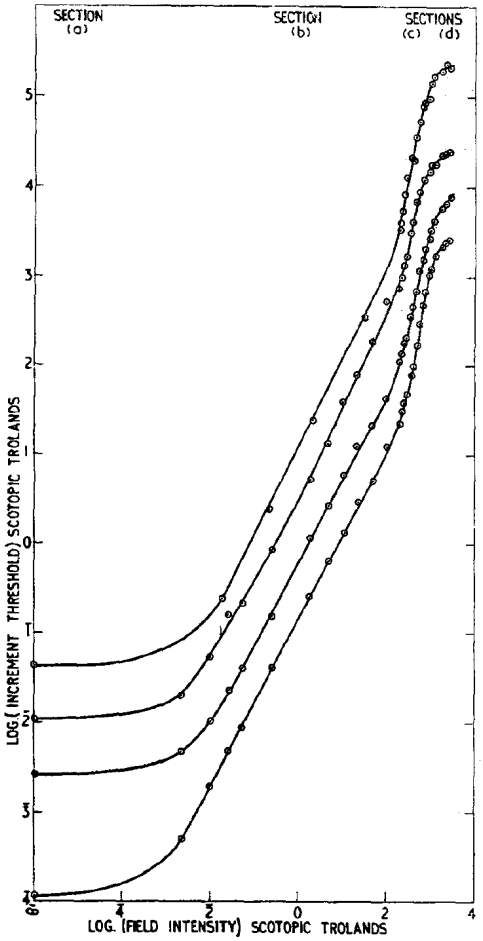

Figure 4.2: Variation of detection threshold against variation of background intensity with increment of 0.5, 1.0, 1.5 log units from the initial level [49].

40 mins which is also in line with the findings of Hecht *et al.* [52]. It is observed that the threshold for detecting the two stimuli returns to the original background luminance level covering a span of 6 log units in 40 mins. Also, the time taken was the same irrespective of the stimulus provided. Also, visual sensitivity due to background luminance is independent of the size of the test stimulus [53][54].

Another study made by H. Barlow [48] shows that the stimulus detection threshold is independent of the stimulus area and duration. For the experiment, a green stimulus was used on a red background. One larger stimulus was presented with a 55 min diameter and 1 sec duration; the other was with a shorter duration of 7 msec and 5.2 min of arc diameter. The intensities were separated by 1 log unit. It was observed that the curves tend to move towards each other and intersect, denoting in fig. 4.4 that the detection threshold is independent of the size and duration of the stimuli [54].

Peripheral threshold and eccentricity

Peripheral thresholds are typically measured while the eyes are held in a fixed position by gazing at a steady fixation point. Several visual functions are altered systematically as the eccentricity of the stimulated area increases [55]. The absolute detection threshold of the dark-adapted eye falls

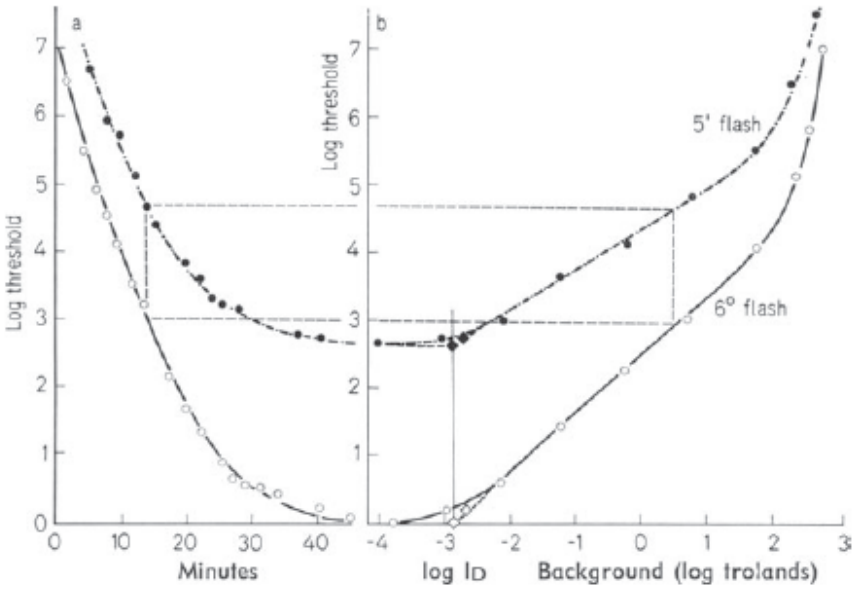

Figure 4.3: The comparison of the log threshold of detection of stimuli. The right-hand figure shows the threshold of detecting two stimuli with varying background intensity. The left-hand image is a mirror of the right one, showing the time taken after bleaching to return to the original level of detection threshold [51].

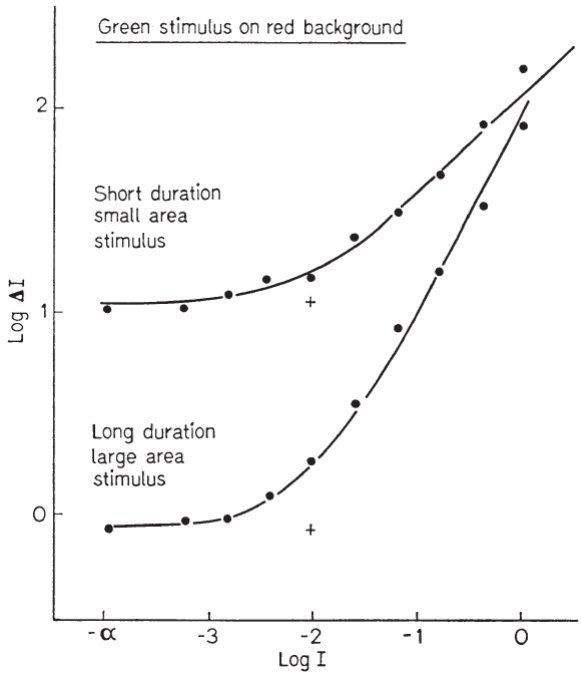

Figure 4.4: Comaprison made between the detection threshold of two different stimuli with varying background luminance levels [54].

as more peripheral regions are stimulated, reaching a minimum at about 18° before rising steadily [55].

Charles. N *et al.* [56] found that when there is a competition between foveally and peripherally presented stimuli, priority is given to the foveal stimulus. An experiment was conducted where dark-adapted subjects were asked to respond to a peripherally presented stimulus while maintaining

a center of fixation. The circular stimulus was 0.5 inches in diameter and was presented at 20°, 35°, 50°, 65°, 80°, and 90° on either side of the center of fixation, covering a 180° visual field and 70 cm away from the subject. If the subject missed a stimulus, feedback was given, and the luminance was increased. Two tests were run, where the fixation was interrupted 28 times per minute and 58 times per minute. The resulting log threshold luminance was plotted against the eccentricity of the stimulus presented. A total of five trials were conducted, and feedback was provided to all trials except the first trial. It was found that the threshold was the highest for the no-feedback session and steadily dropped for the feedback sessions, as shown in fig. 4.5. No changes were found for the slower interrupting task from the third and fourth sessions of the short interruption task. Nevertheless, for the faster interruption task, the detection threshold improved significantly peripherally, and post 65° is minimal. However, adaptability can be a confounding factor as subjects' experience in peripheral tasks can have a better visual understanding, denoted from visual acuity that increases with practice [57].

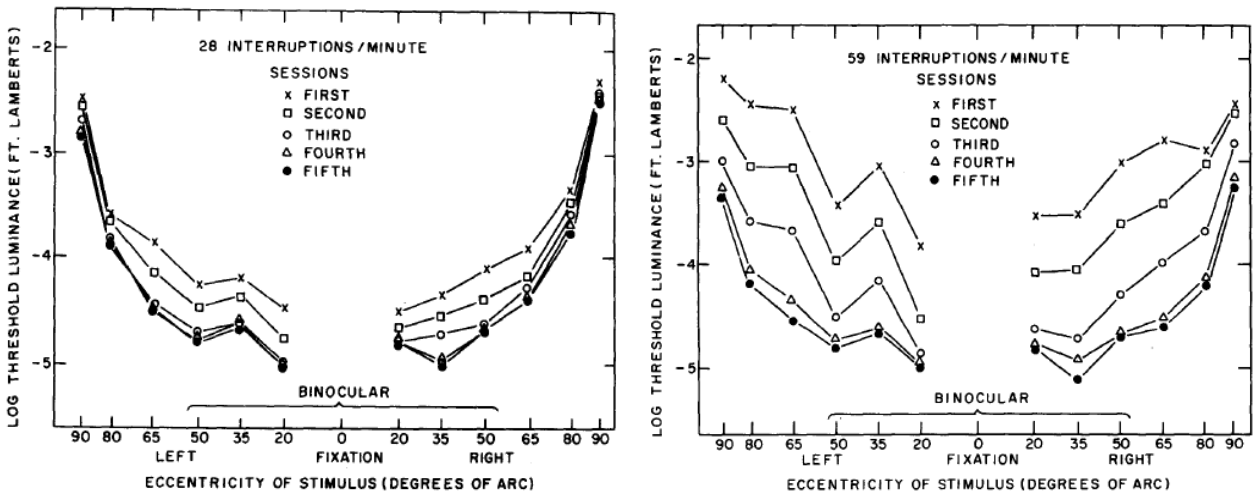

(a) Experiment with 28 interruptions

(b) Experiment with 58 interruptions

Figure 4.5: Relation between detection threshold and stimulus eccentricity in the presence of a foveal load task with two levels of interruptions [56].

4.3. Photobleaching and recovery

Visibility may be reduced due to a bright light source in the visual field [58]. This phenomenon can be linked to disability glare [58]. An example is the reduced visibility of road markers in the presence of oncoming headlights. Again, when the eye is in a dark-adapted condition, the presence of a bright light source can result in instantaneous bleaching, preventing it from seeing or distinguishing objects [47]. The phenomenon of bleaching and recovery is closely related to dark adaptation. The eye takes several minutes to recover from exposure to photopic illumination levels under dark-adapted conditions [47].

A study was made by Hecht *et al.* [52] to determine the eye's effect on dark and light adaptation. A subject was dark-adapted for 10 – 15 min and then exposed to an adapting light used for photobleaching. A violet light was used to secure the largest range of rod adaptation and red for the smallest. The stimulus was presented for 0.2 ms. The threshold intensity required by the observer was plotted against time after the subject was bleached in five different intensity levels. It was observed that the total recovery period lasted for 30 mins.

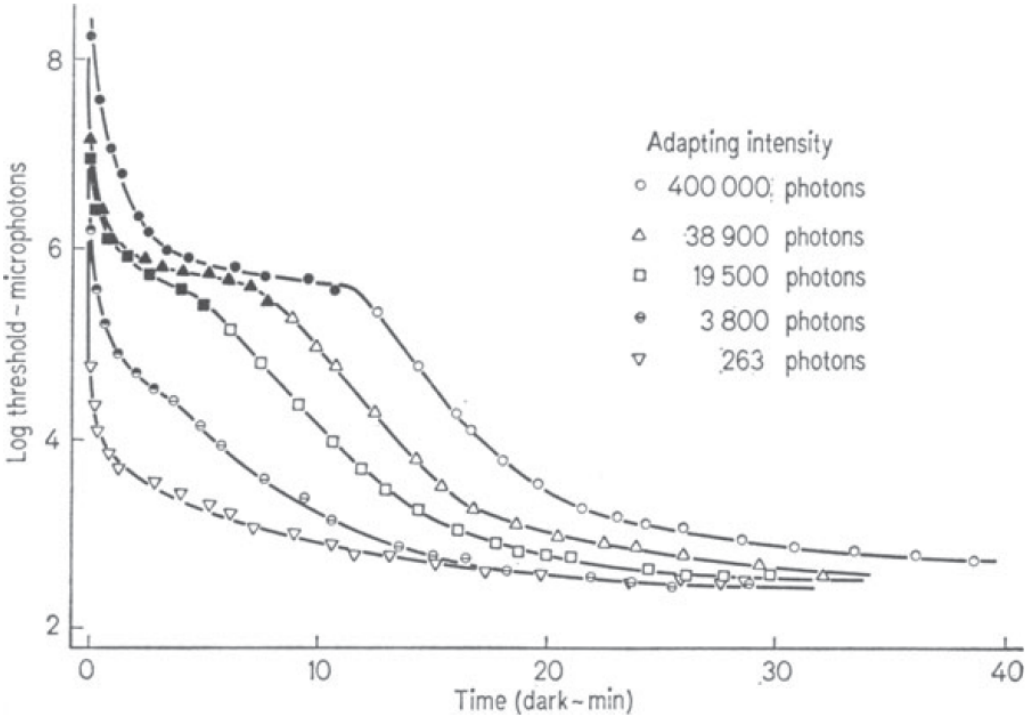

Figure 4.6: Detection Threshold recovery curve with 5 different levels of bleaching [52].

As shown in fig. 4.6, five bleaching intensities were used, and their recovery time was measured. The initial recovery after immediate exposure was rapid, covering 3 log units that were attributed to the recovery of the cone photoreceptor system. After approximately 11 mins, the threshold starts dropping again as the rod system recovers. Still, the drop is less rapid while being steady than the initial one before the plateau. It takes 40 mins for full recovery of the dark-adapted sensitivity post bleaching [52]. eq. (4.1) represents the percentage of photoreceptors bleached for a certain luminance over a period of time [48]. r is the percentage of photoreceptors bleached, I is the luminance of the light source in trolands, and t is the exposure time in seconds.

$$\log_{10}(1 - r) = -\frac{It}{2 \times 10^7} \tag{4.1}$$

Recovery time can also be related to the fraction of photoreceptors bleached. fig. 4.7 shows a linear relationship between the fraction bleached and the time taken for recovery for two stimulus sizes. It was found that the fit is linear over time, with the time rising to 12 mins for 100 % bleached. For bleaches above 20 %, the recovery line is primarily linear, as fitted by the dotted straight line. For bleaches below that, a logarithmic trend is followed with $\Delta T = \tau \log(x)$ where ΔT is the time for recovery, τ being the decay constant and x is the change in bleaching [59].

4.4. Effect on reaction time

When the stimulus detection threshold is increased following dark adaptation and photobleaching, detecting a stimulus below that threshold level will become problematic as more stimuli will go undetected. This can lead to a higher reaction time, and a search can also be performed. Babur [60] established a relation between reaction time and latency of stimulus detection under photobleached

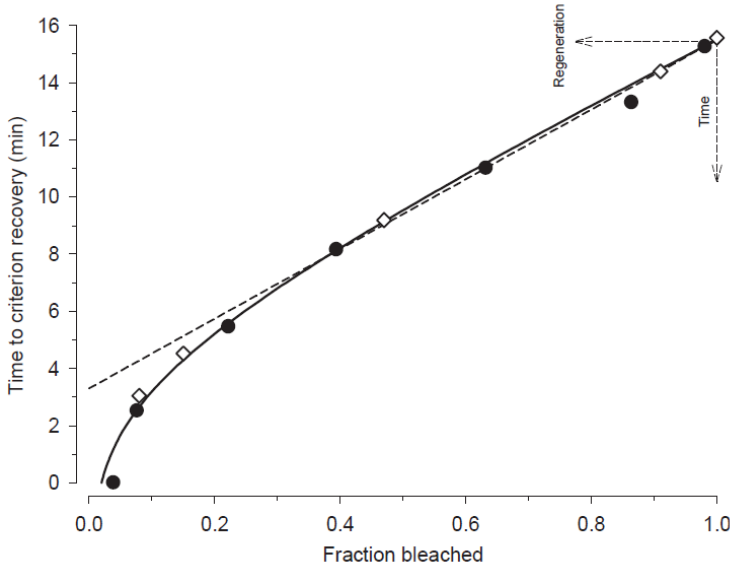

Figure 4.7: Relationship between recovery time and a fraction of photopigments bleached [45].

conditions. The experiment consisted of three sub experiments; a) estimating reaction time; b) latency due to apparent motion; and c) latency due to real motion [60].

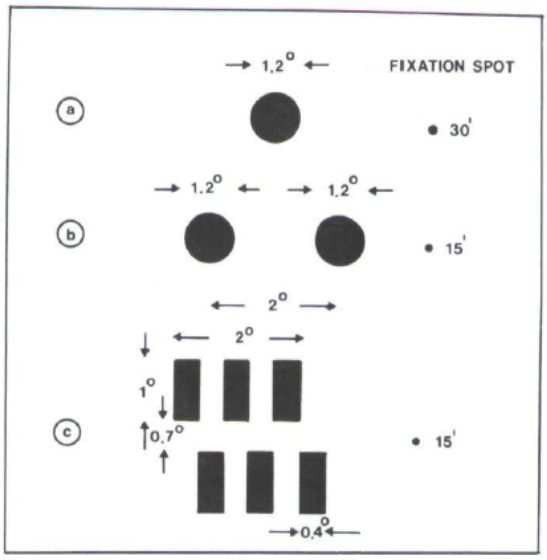

Figure 4.8: Stimulus type : a) Reaction time; b) Apparent motion; c) Real motion [60].

For the experiment, three variations were used; a circular 1.2° stimulus was used with the center of fixation for the reaction time task, and the luminance was set 0.5 log units above the minimum detection threshold of the dark-adapted subject. The test stimulus was red or blue stimulating cones and rods, respectively. Two stimuli with a separation of 2 ° were used for apparent motion. For this task, the subject had to detect the relative or simultaneous movement of the stimuli. The last task included real motion, where the subject tracked stimuli until they aligned to reference stimuli. The stimuli consisted of two rectangles separated vertically by 0.7 ° with three vertical bars. The lower bars were displaced by 0.4 log units from the upper reference bars. The subject was asked to track the

lower bars until they align with the upper bars [60]. The stimuli used are shown in fig. 4.8. It can be observed in fig. 4.9a that the reaction time for the rods (filled circles) is higher than the cones (empty circles) specific stimuli as a function of eccentricity. Also, the difference can be noticed in the latency for the two motions. However, the initial value was the same. Latency for the real motion was less by 20 ms than the apparent motion task as shown in fig. 4.9b. However, latencies in both tasks increased with the increase of eccentricity. The author concluded that the velocity of signal transmission along visual pathways and the motor loop gets reduced for non-foveal stimulus [60].

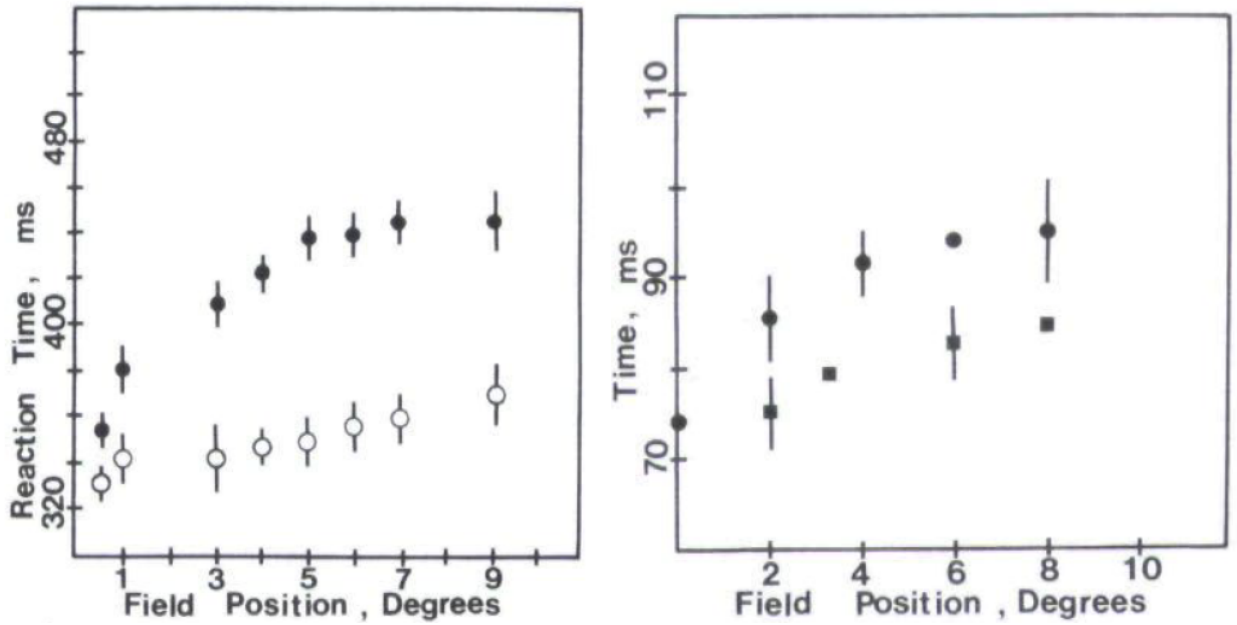

(a) Reaction time of rods (filled) and cones (empty) with respect to eccentricity

(b) Relations between Apparent motion(circle) and Real motion(box) latency and eccentricity.

Figure 4.9: Reaction time, Latency due to real and apparent motion variation with respect to stimuli location [60].

4.4.1. Reaction time & search time based on stimulus contrast

Walkey *et. al.* [61] found that reaction time and search time can vary as a function of the background luminance. Search performance was unaffected by contrast change, but the range of reaction time variation for the same changes was more significant at mesopic levels [61]. For the study, filters were used to reduce the luminance of the stimulus from the photopic to the mesopic level while keeping the luminance of the used CRT constant. The luminance level range has already been shown in fig. 4.1 in section 4.1. For the reaction time experiment, a Landolt-C ring was used with a diameter of 2 ° presented 10 ° from the center of fixation art 6 random spots. To increase the randomness the pre-stimulus duration was set to 600 ms and 1000 ms, with the stimulus duration of 500 ms. The search test included multiple targets of Landolt-C rings placed within eccentricity of 11 ° from the center of fixation. The maximum duration is 8 sec. The subject had to indicate the target's unique orientation among the multiple distractors. fig. A.6 shows the stimulus used for both tests. For the search experiment, the unique stimulus is the one in pink with a gap on the top left. Both experiments had 4 sets with 5 , 8.5 , 13 and 20 min duration for 10 , 1 , 0.05 and 0.01 cdm^{-2} level of background, respectively.

The test compared results from 46 trials for each stimulus condition. fig. 4.11a shows a trend for a

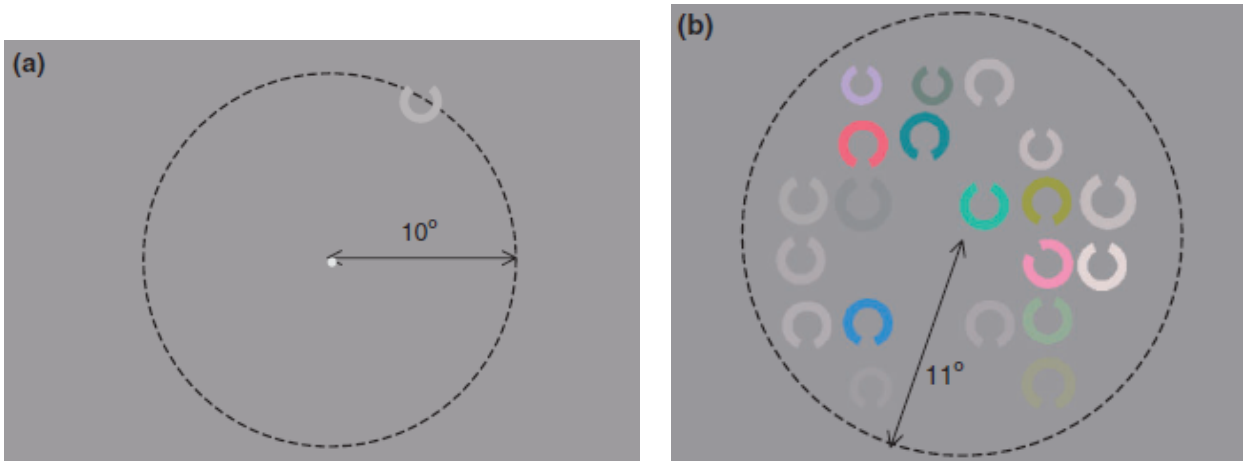

(a) Stimuli used for reaction time experiment

(b) Stimuli used for search time experiments

Figure 4.10: (A) Reaction time stimuli with a Landolt-C place within 10 ° of CoF. (B) A cluster of distractors along with an unique stimuli for search time experiments [61].

specific background luminance. The reaction time decreases with increased stimulus contrast. Also, If the background luminance increases, the reaction time decreases for the same contrast level. The search time trend in fig. 4.11b shows the same decreasing trend with increasing stimulus contrast. It can be observed in both experiments that the minimum detection stimulus contrast increased with the decrease in background luminance. However, the reaction time curve displayed an upward shift with decreasing brightness, and the search time plots remained stationary. eq. (4.2) and eq. (4.3) were fitted for the reaction time and search time curves to visualize the general trend [61]. In eq. (4.2), R is the reaction time, R_{min} is the minimum reaction time, C is the contrast, C_0 is the contrast threshold and k is a constant. For eq. (4.3), S is the reaction time, S_{min} is the minimum reaction time, C is the contrast, k is a constant, and β is the power.

$$R = R_{min} + \frac{k}{C - C_0} \tag{4.2}$$

$$S = S_{min} + k.C^{\beta} \tag{4.3}$$

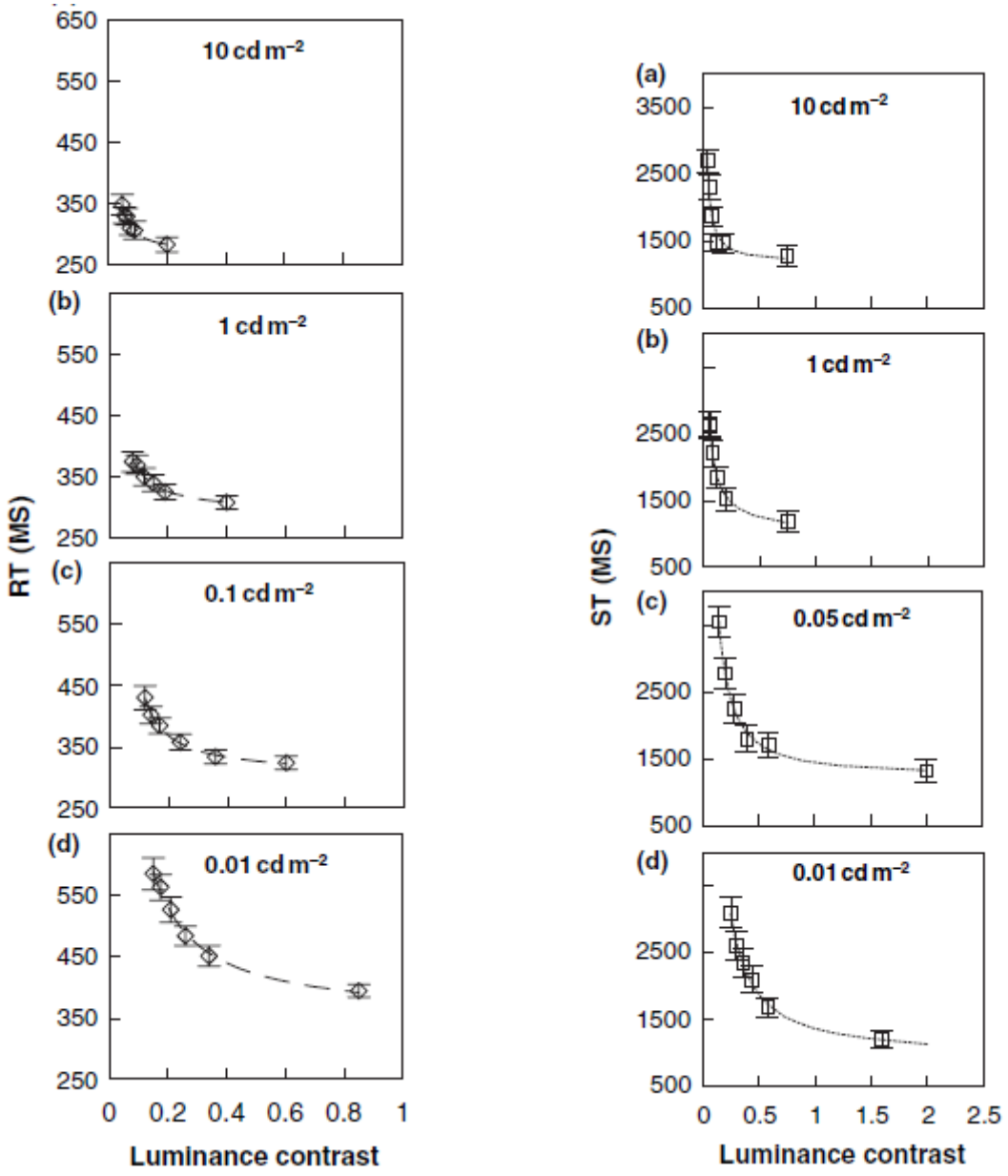

(a) Reaction Time **(b)** Search Time

Figure 4.11: Reaction time and search time variations with respect to the varying stimuli contrast at various background luminance level [61].

4.4.2. Rod and cones reaction time based on weber constrast

Given the findings that reaction time increases or decreases with decreasing or increasing luminance contrast, it is possible to predict the behavior of a dark-adapted subject at different luminance levels. Initial parameter estimation to detect the specific luminance range to stimulate different cells can be helpful. Cao *et al.* [62] studied the reaction time of rod and cone cells for different luminance levels and Weber contrast and pointed out the active luminance level for each cell type. The experiment was based on iterations of decremental and incremental stimuli based on retinal luminance. Reaction times for rods and cones were expressed as a function of stimulus contrast.

The range of the retinal luminance was from 0.002 Td ($\approx 10^{-6}$cdm^{-2}) to 200 Td (0.1cdm^{-2}). Based on

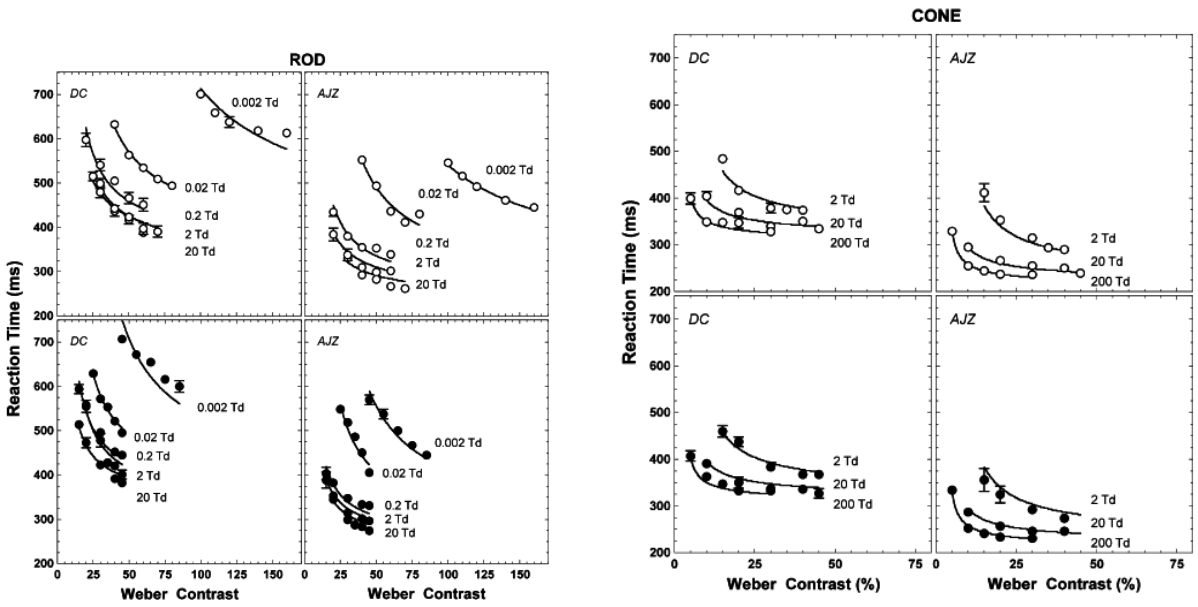

(a) Reaction time of rod cells

(b) Reaction time of cone cells

Figure 4.12: Reation time of rods and cones vs. Stimuli contrast at various levels on retinal luminance [62].

the incremental and decremental stimuli, the rod cells remained remained active between 0.002 Td - 0.2 Td (10^{-6}cdm^{-2} - 10^{-5}cdm^{-2}), rods and cones in 2 Td - 20 Td(10^{-4}cdm^{-2} - 10^{-2}cdm^{-2}) and cones at 200 Td. fig. 4.12 shows that an increase in retinal luminance level or contrast reaction time decreased. Reaction time to rod decrements was shorter than for rod increments at low retinal luminance levels. However, for the same conditions, the difference between the rod and cone reaction time became larger at higher levels of illuminance [62].

4.5. Conclusion

The chapter tries to answer the question, "How will the visual changes found in glaucoma be induced in a healthy individual without affecting the wellbeing?" by exploring the effects of photobleaching and dark-adaptation on the human visual system. It was found that photobleaching of the retinal cells can successfully elevate the stimulus detection threshold. The reaction time of a photobleached The findings are summarised as follows:

- Visual sensitivity under dark-adapted and photobleached conditions can be altered either by manipulating the stimuli contrast or changing the background luminance, both methods affecting the visual threshold of detection similarly.

- The effect of dark adaptation and photobleaching is predominant in the first 10 mins till the rod recovery begins. Each trial should be limited to 10 mins to maximize the effect of the dark-adapted and photobleached conditions. The percentage of bleached photoreceptors can be a controlled parameter and adjusted following eq. (4.1).

- Inducing tunnel vision by increasing foveal load is impractical. The increased foveal load has undesirable side effects. Additionally, subjects may (rapidly) adapt to increased foveal load. As a result, SRTs are not consistently affected by this manipulation.

5

Project Setup and Planning

This section briefly overviews the experiment setup and the research timeline. For the thesis, the experiments will be performed in a lab setup at **Erasmus MC**. The experimental design will have three main sub-parts described below. The first part is the platform for performing stimuli-based visual experiments. **Psychtoolbox** will be used as the platform. With the help of the toolbox, the experiment will be programmed as designed in MATLAB. From an experimenter's perspective, the experimenter programs the stimuli dimensions, presentation durations, and frames of presentations, along with the background of the display and all the timings associated with the program to run. The output from the toolbox will be displayed on the monitors viewed by the participants. The system used for the experiment where the participant sits is called **Haplo**. Haplo consists of one eye tracker, two monitors, and two pairs of mirrors. The participant does not look at the monitors directly. The visual output from the monitors is projected to the first pair of mirrors, then the image is projected to the second set of mirrors, and the participant looks at the second set of mirrors. The eye tracking unit is placed below the second set of mirrors which tracks the eye movement of the participant.
The second step is to select a proper eye tracker and program it. There are two options available , one is **Tobii X2-60** and the other is **Tobii X3-120**. The latter is chosen because it gives more control and tracks more accurately. Tobii provides a development studio that can be coupled with MATLAB. For properly using the eye tracker, it has to be calibrated according to the user. A calibration script is prepared by modifying the inbuilt calibration program of the eye tracked. The modified calibration script couples with the psychtoolbox and gives out the calibration information for a 9-point calibration of the participant's eye. To make it a bit interactive, the script shows the participant a map of his eye movement during the calibration and displays the error or mean deviation from the target.
The last step will be to enable all three different systems, the experimenter system, Haplo, and Tobii eye tracker, to communicate with each other. This will be done through a MATLAB script where the experimenter can communicate with the eye tracker and Haplo/PsychWindow and get the data back. The loop can be summarised by: the central computer to Haplo/PsychWindow, Haplo/PsychWindow to the subject, the subject to the eye tracker, and the eye tracker to the main computer. Once the data from the experiment is obtained, the data will be analyzed per participant to look for reaction times, variability in eye movement, etc.
The developed framework will have photobleaching input parameters followed by discrete semi-randomized stimuli. The output will be eye-tracking data displaying parameters like reaction time, accuracy, and eye movement variability. The results will also be compared with data from glaucoma patients for validation. The effects of bleaching according to various parameters will also affect eye movements. The different types of eye movement patterns obtained, if matched with glaucoma patients, can be used to model a predictive behavior of eye patterns in different stages of glaucoma. Since any data used in the medical field needs to be accurate, the outcome of the thesis will be to

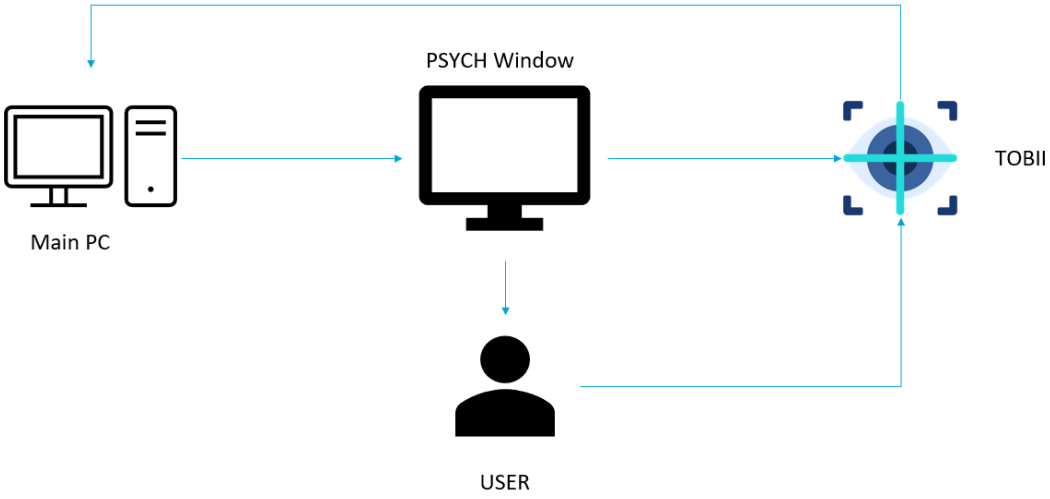

Figure 5.1: Simplified diagram of experiment module

draw up a framework that can produce glaucoma-like eye movements in healthy individuals, which can later be used to evaluate new diagnostic methods or do medical research related to glaucoma.

Project planning and gantt Chart
The project planning for the thesis is divided into six main phases. The plan is depicted as a Gantt chart in **??** of Appendix D. The project started with the literature review phase just after kick-off. The literature phase is divided into smaller sub-phases. The time taken is more than the recommended time due to one examination. Also, since the topic differs from aerospace engineering, it took considerable time to understand the concept at the beginning. Also, some small tasks related to the project, like fixing timing issues, were carried out during the literature phase. After the literature phase, a break of 1 month was taken, after which work was resumed again. During the time of submission of this report, tasks related to experiment setup are being performed. Looking into the future, it is estimated that by the first week of September, the experimental design will be completed. The month of September will be allocated to the experimentation part of the thesis. The initial stage will be to get approval from the ethics committee and recruit participants for the project. The month's latter half will be allotted to experimentation and data collection. Once the data collection is done, the focus will be on the data analysis. The data analysis phase will be further divided into subphases, aiming to get the results by November 2022. The entire of December 2022 will be dedicated to writing the final master thesis report. January of 2023 will be for the final preparations, which include implementing feedback on information from supervisors, the green light meeting, and preparation for the final graduation. It is estimated that the total duration of the thesis will be 11 months.

6 Conclusion

The report attempts to search for relevant information to support and construct a roadmap for the thesis project. This project's main challenge is successfully reproducing glaucoma's effects in a healthy individual. The research question from chapter 1 is further modified into:

How to create a framework that can reversibly induce glaucoma-like reaction time in healthy individuals by photobleaching?

To approach this question, a step-wise procedure is followed. In chapter 2, various diagnostic algorithms were studied to find the best fit for the project. EMP methodology suits the purpose because of its simplicity, fewer false results, and low test duration. In chapter 4, conclusions about the experiment parameters were reached. It was found that the duration of photobleaching can last. Also, the percentage of photoreceptors bleached can be a controlled parameter based on the light source.

Furthermore, induced tunnel vision based on foveal load was discarded as unforeseen cognitive changes can be an uncontrollable parameter inducing variability in the experiment. Since the entire study is based on eye movements in glaucoma, chapter 3 focused on the eye movements exhibited by glaucoma patients and eye movement in general. The chapter concluded that various discrete tracking and smooth pursuit tasks could be used to evaluate the eye movements of glaucoma-induced individuals. The dynamics of different kinds of eye movements provided can also be used for validation purposes. This chapter primarily focuses on the task design for the experiment. In short, chapter 2 focuses on algorithms, chapter 4 on mechanisms to induce glaucoma, and chapter 3 on eye movement patterns and devising the experiment tasks. In the end, chapter 5 gives some overview of the short-term aim and some debugging work and its output. Apart from answering the formulated research question, the objective of the thesis project is :

"To create a human model of glaucoma by successfully desensitizing a healthy retina by photobleaching and estimating the photobleaching parameters required to induce visual deficiencies caused by glaucoma in terms of saccadic reaction time."

If successful, the project will help to understand glaucoma's dynamics and the variability in vision. The project will serve as a base framework to recreate diseases related to visual deficiencies. This is to study the diseases and evaluate the effects on the visual field without involving an original patient. The idea is very novel and, if successful, can be extended to recreate other diseases non-invasively without affecting the well-being of any individual. Alongside this, the project will

contribute to developing a model predicting the outcome of vision-based experiments depending on input parameters and indicating the progression curve of visual impairment diseases. Also, it will immensely contribute to the research and development of new diagnosis techniques by reducing the required time and eliminating the heavy dependency on patient data, as data can be readily recreated from any individual willing to contribute.

References

[1] N.W. Daw. "Visual development: Second edition". In: *Visual Development: Second Edition* (Jan. 2006), pp. 7–24. DOI: 10.1007/0-387-30484-3.

[2] Robert J. Casson et al. "Definition of glaucoma: Clinical and experimental concepts". In: 40.4 (May 2012), pp. 341–349. ISSN: 14426404. DOI: 10.1111/j.1442-9071.2012.02773.x.

[3] Helga Kolb, Eduardo Fernandez, and Ralph Nelson. "Webvision: the organization of the retina and visual system [Internet]". In: (1995).

[4] James K Bowmaker and HJk Dartnall. "Visual pigments of rods and cones in a human retina." In: *The Journal of physiology* 298.1 (1980), pp. 501–511.

[5] Helga Kolb, Eduardo Fernandez, and Ralph Nelson. "Webvision: the organization of the retina and visual system [Internet]". In: (1995).

[6] GA Osterberg. "Topography of the layer of the rods and cones in the human retima". In: *Acta ophthalmol* 13.6 (1935), pp. 1–102.

[7] Robert N Weinreb, Tin Aung, and Felipe A Medeiros. "The pathophysiology and treatment of glaucoma: a review". In: *Jama* 311.18 (2014), pp. 1901–1911.

[8] Karen Allison, Deepkumar Patel, and Omobolanle Alabi. "Epidemiology of Glaucoma: The Past, Present, and Predictions for the Future". In: *Cureus* (Nov. 2020). ISSN: 2168-8184. DOI: 10.7759/cureus.11686.

[9] Cindy X Hu et al. "What do patients with glaucoma see? Visual symptoms reported by patients with glaucoma". In: *The American journal of the medical sciences* 348.5 (2014), pp. 403–409.

[10] Elaine C. Johnson et al. "Neurotrophin roles in retinal ganglion cell survival: Lessons from rat glaucoma models". In: *Experimental Eye Research*. Vol. 88. 4. Apr. 2009, pp. 808–815. DOI: 10.1016/j.exer.2009.02.004.

[11] Yasemin Budak and Muberra Akdog. "Retinal Ganglion Cell Death". In: *Glaucoma - Basic and Clinical Concepts*. InTech, Nov. 2011. DOI: 10.5772/19003.

[12] Alfred Sommer. "Intraocular pressure and glaucoma". In: *American Journal of Ophthalmology*. Vol. 107. 2. Feb. 1989, pp. 186–188. DOI: 10.1016/0002-9394(89)90221-3.

[13] Deepmala Mazumdar. "Visual Field Responsiveness in Glaucoma: An eye tracking approach". In: (2021).

[14] Ronnie George, Ramesh S. Ve, and Lingam Vijaya. "Glaucoma in India: Estimated burden of disease". In: *Journal of Glaucoma* 19.6 (Aug. 2010), pp. 391–397. ISSN: 10570829. DOI: 10.1097/IJG.0b013e3181c4ac5b.

[15] Mihaela L Popescu et al. "Explaining the relationship between three eye diseases and depressive symptoms in older adults". In: *Investigative ophthalmology & visual science* 53.4 (2012), pp. 2308–2313.

[16] Chris A Johnson, Michael Wall, and H Stanley Thompson. *A History of Perimetry and Visual Field Testing*. Tech. rep. 2011. URL: www.optvissci.com..

[17] Anders Heijl. "The Effect of Perimetric Experience in Normal Subjects". In: *Archives of Ophthalmology* 107.1 (Jan. 1989), p. 81. ISSN: 0003-9950. DOI: 10.1001/archopht.1989.01070010083032.

[18] John Landers et al. "Comparison of visual field sensitivities between the Medmont automated perimeter and the Humphrey field analyser". In: *Clinical and Experimental Ophthalmology* 38.3 (Apr. 2010), pp. 273–276. ISSN: 14426404. DOI: 10.1111/j.1442-9071.2010.02246.x.

[19] Ryo Asaoka. "Mapping glaucoma patients' 30-2 and 10-2 visual fields reveals clusters of test points damaged in the 10-2 grid that are not sampled in the sparse 30-2 grid". In: *PLoS ONE* 9.6 (June 2014). ISSN: 19326203. DOI: 10.1371/journal.pone.0098525.

[20] Brad Bowling. *Kanski's Clinical Ophthalmology, Eighth Edition (2016)*. Tech. rep. 2016. DOI: 10.1016/B978-0-7020-5572-0.00025-8.

[21] Armin Toepfer et al. "Perimetry while moving the eyes: implications for the variability of visual field defects". In: *Journal of Neuro-Ophthalmology* 28.4 (2008), pp. 308–319.

[22] Andrew J Anderson and Chris A Johnson. "Frequency-doubling technology perimetry." In: *Ophthalmology Clinics of North America* 16.2 (2003), pp. 213–225.

[23] Shu Liu et al. "Frequency-Doubling Technology Perimetry for Detection of the Development of Visual Field Defects in Glaucoma Suspect Eyes". In: *JAMA Ophthalmology* 132.1 (Jan. 2014), p. 77. ISSN: 2168-6165. DOI: 10.1001/jamaophthalmol.2013.5511.

[24] Kouros Nouri-Mahdavi. "Selecting visual field tests and assessing visual field deterioration in glaucoma". In: *Canadian Journal of Ophthalmology* 49.6 (Dec. 2014), pp. 497–505. ISSN: 17153360. DOI: 10.1016/j.jcjo.2014.10.002.

[25] Boel Bengtsson' et al. " A new generation of algorithms for computerized threshold perimetry, SITA". In: *ACTA OPHTHALMOLOGICA SCANDINAVICA Scientific Section* 75 (1997), pp. 368–375.

[26] Anders Heijl et al. "A New SITA Perimetric Threshold Testing Algorithm: Construction and a Multicenter Clinical Study". In: *American Journal of Ophthalmology* 198 (Feb. 2019), pp. 154–165. ISSN: 18791891. DOI: 10.1016/j.ajo.2018.10.010.

[27] Gabriella Szatmáry, Valérie Biousse, and Nancy J. Newman. *Can Swedish Interactive Thresholding Algorithm Fast Perimetry Be Used as an Alternative to Goldmann Perimetry in Neuro-ophthalmic*

Practice? Tech. rep. 9. Sept. 2002, pp. 1162–1173. DOI: 10.1001/archopht.120.9.1162. eprint: https://jamanetwork.com/journals/jamaophthalmology/articlepdf/271828/ecs10216.pdf. URL: https://doi.org/10.1001/archopht.120.9.1162.

[28] Johan J. M. Pel et al. "Validity and Repeatability of Saccadic Response Times Across the Visual Field in Eye Movement Perimetry". In: *Translational Vision Science & Technology* 2.7 (Nov. 2013), p. 3. DOI: 10.1167/tvst.2.7.3.

[29] Boel Bengtsson and Anders Heijl. "A Visual Field Index for Calculation of Glaucoma Rate of Progression". In: *American Journal of Ophthalmology* 145.2 (Feb. 2008), pp. 343–353. ISSN: 00029394. DOI: 10.1016/j.ajo.2007.09.038.

[30] Michael R. MacAskill and Tim J. Anderson. "Eye movements in neurodegenerative diseases". In: 29.1 (2016), pp. 61–68. ISSN: 14736551. DOI: 10.1097/WCO.0000000000000274.

[31] Martin Gorges, Elmar H. Pinkhardt, and Jan Kassubek. *Alterations of eye movement control in neurodegenerative movement disorders*. 2014. DOI: 10.1155/2014/658243.

[32] David P. Crabb, Nicholas D. Smith, and Haogang Zhu. "What's on TV? Detecting age-related neurodegenerative eye disease using eye movement scanpaths". In: *Frontiers in Aging Neuroscience* 6.NOV (2014). ISSN: 16634365. DOI: 10.3389/fnagi.2014.00312.

[33] Alfred L. Yarbus. *Eye Movements and Vision*. Springer US, 1967, pp. 129–170. DOI: 10.1007/978-1-4899-5379-7.

[34] Ronald B. Weber and Robert B. Daroff. "The metrics of horizontal saccadic eye movements in normal humans". In: *Vision Research* 11.9 (Sept. 1971), 921–IN2. ISSN: 00426989. DOI: 10.1016/0042-6989(71)90212-4.

[35] DA Robinson. "The mechanics of human saccadic eye movement". In: *The Journal of physiology* 174.2 (1964), p. 245.

[36] M. M. (Rene) van Paasen, J. C. (Hans) van der Vaart, and J. A. (Bob) Mulder. "Model of the Neuromuscular Dynamics of the Human Pilot's Arm". In: *Journal of Aircraft* 41.6 (Nov. 2004), pp. 1482–1490. ISSN: 0021-8669. DOI: 10.2514/1.14434.

[37] Alfred L. Yarbus. *Eye Movements and Vision*. Springer US, 1967, pp. 147–158. DOI: 10.1007/978-1-4899-5379-7.

[38] Casper J. Erkelens. "Coordination of smooth pursuit and saccades". In: *Vision Research* 46.1-2 (Jan. 2006), pp. 163–170. ISSN: 00426989. DOI: 10.1016/j.visres.2005.06.027.

[39] Robyn Burton, Nicholas D. Smith, and David P. Crabb. "Eye movements and reading in glaucoma: observations on patients with advanced visual field loss". In: *Graefe's Archive for Clinical and Experimental Ophthalmology* 252.10 (Oct. 2014), pp. 1621–1630. ISSN: 1435702X. DOI: 10.1007/s00417-014-2752-x.

[40] Mark A Bullimore and Ian L Bailey. "Reading and eye movements in age-related maculopathy." In: *Optometry and vision science: official publication of the American Academy of Optometry* 72.2 (1995), pp. 125–138.

[41] Angelica Cerulli et al. "Evaluation of eye movements pattern during reading process in patients with glaucoma: A microperimeter study". In: *European Journal of Ophthalmology* 24.3 (2014), pp. 358–363. ISSN: 11206721. DOI: 10.5301/ejo.5000397.

[42] John Stein and Joel Talcott. "Impaired Neuronal Timing in Developmental Dyslexia-The Magnocellular Hypothesis". In: 5 (1999), pp. 59–77.

[43] Deepmala Mazumdar et al. "Comparison of saccadic reaction time between normal and glaucoma using an eye movement perimeter". In: *Indian Journal of Ophthalmology*. Vol. 62. 1. Jan. 2014, pp. 55–59. DOI: 10.4103/0301-4738.126182.

[44] Felipe A Medeiros et al. "Driving simulation as a performance-based test of visual impairment in glaucoma". In: *Journal of glaucoma* 21.4 (2012), p. 221.

[45] T. D. Lamb and E. N. Pugh. *Dark adaptation and the retinoid cycle of vision*. May 2004. DOI: 10.1016/j.preteyeres.2004.03.001.

[46] Malgorzata Perz. "Flicker perception in the periphery". In: (Sept. 2022).

[47] Guo Qing Yang et al. "Recent advances in the dark adaptation investigations". In: *International Journal of Ophthalmology* 8.6 (Dec. 2015), pp. 1245–1252. ISSN: 22274898. DOI: 10.3980/j.issn.2222-3959.2015.06.31.

[48] Horace B. Barlow. "Dark and Light Adaptation: Psychophysics". In: *Visual Psychophysics*. Ed. by Dorothea Jameson and Leo M. Hurvich. Berlin, Heidelberg: Springer Berlin Heidelberg, 1972, pp. 1–28. ISBN: 978-3-642-88658-4. DOI: 10.1007/978-3-642-88658-4_1. URL: https://doi.org/10.1007/978-3-642-88658-4_1.

[49] M. Aguilar and W. S. Stiles. "Saturation of the rod mechanism of the retina at high levels of stimulation". In: *Optica Acta: International Journal of Optics* 1.1 (Jan. 1954), pp. 59–65. ISSN: 00303909. DOI: 10.1080/713818657.

[50] C Quentin Davis, Olga Kraszewska, and Colette Manning. "Constant luminance (cd· s/m2) versus constant retinal illuminance (Td· s) stimulation in flicker ERGs". In: *Documenta Ophthalmologica* 134.2 (2017), pp. 75–87.

[51] BH Crawford and WS Stiles. "Equivalent adaptation levels in localized retinal areas." In: (1932).

[52] Selig Hecht, Charles Haig, and Aurin M Chase. "The influence of light adaptation on subsequent dark adaptation of the eye". In: *The Journal of general physiology* 20.6 (1937), pp. 831–850.

[53] C B Blakemore and W A Rushton. "Dark adaptation and increment threshold in a rod monochromat." In: *The Journal of Physiology* 181.3 (Dec. 1965), pp. 612–628. ISSN: 00223751. DOI: 10.1113/jphysiol.1965.sp007786.

[54] HB Barlow. "Intrinsic noise of cones". In: *Visual problems of colour* 2 (1958), pp. 617–630.

[55] L Sloan. *How we see: A summary of basic principles : Human factors in undersea warfar*. Panel on Psychology and Physiology, Committee on Undersea Warfare, National . . ., 1949.

[56] Charles N Abernethy and Herschel W Leibowitz. "The effect of feedback on luminance thresholds for peripherally presented stimuli". In: *Perception & Psychophysics* 10.3 (1971), pp. 172–174.

[57] Robert G. Webster and George M. Haslerud. "Influence on extreme peripheral vision of attention to a visual or auditory task." In: *Journal of Experimental Psychology* 68.3 (Sept. 1964), pp. 269–272. ISSN: 0022-1015. DOI: 10.1037/h0043256.

[58] Gary S. Rubin. "Contrast Sensitivity and Glare Testing in the Evaluation of Anterior Segment Disease". In: *American Academy of Ophthalmology* 97.9 (1990), pp. 1233–1237. ISSN: 01616420. DOI: 10.1016/S0161-6420(90)32431-4.

[59] T.D. Lamb. "The involvement of rod photoreceptors in dark adaptation". In: *Vision Research* 21.12 (Jan. 1981), pp. 1773–1782. ISSN: 00426989. DOI: 10.1016/0042-6989(81)90211-X.

[60] John L Barbur. "Reaction-time determination of the latency between visual signals generated by rods and cones". In: *Ophthalmic and Physiological Optics* 2.3 (1982), pp. 179–185.

[61] H. C. Walkey, J. A. Harlow, and J. L. Barbur. "Changes in reaction time and search time with background luminance in the mesopic range". In: *Ophthalmic and Physiological Optics* 26.3 (2006), pp. 288–299. DOI: https://doi.org/10.1111/j.1475-1313.2006.00412.x. eprint: https://onlinelibrary.wiley.com/doi/pdf/10.1111/j.1475-1313.2006.00412.x. URL: https://onlinelibrary.wiley.com/doi/abs/10.1111/j.1475-1313.2006.00412.x.

[62] Dingcai Cao, Andrew J. Zele, and Joel Pokorny. "Linking impulse response functions to reaction time: Rod and cone reaction time data and a computational model". In: *Vision Research* 47.8 (Apr. 2007), pp. 1060–1074. ISSN: 00426989. DOI: 10.1016/j.visres.2006.11.027.

[63] Tobii. "obii Analytics SDK Developer's Guide". In: *Tobii Analytics SDK Developer's Guide* 3 (2013), pp. 54–65.

[64] Flaviu Cristian. "Probabilistic clock synchronization". In: *Distributed computing* 3.3 (1989), pp. 146–158.

[65] LJ Fleishman and JA Endler. "Some comments on visual perception and the use of video playback in animal behavior studies". In: *Acta ethologica* 3.1 (2000), pp. 15–27.

[66] Dario D Salvucci and Joseph H Goldberg. "Identifying fixations and saccades in eye-tracking protocols". In: *Proceedings of the 2000 symposium on Eye tracking research & applications*. 2000, pp. 71–78.

[67] Ralf Engbert and Reinhold Kliegl. "Microsaccades uncover the orientation of covert attention". In: *Vision research* 43.9 (2003), pp. 1035–1045.

Part III

Paper Appendices

A

Eye Tracking

A significant portion of the study included managing and developing the eye-tracking environment for the experimentation. The eye tracker used here is a Tobii X3-120 screen-based eye tracker. The eye tracker uses a pupil-tracking mechanism where the eye tracker samples the movement of the pupil at 120 Hz. The tracker uses a (0,1) cartesian coordinate system, which needs to be converted to pixels for a coordinate system for analysis. All the development done on the project was based on the Tobii developer kit environment [63]. This section focuses on various aspects of the eye-tracking methods used during the study and the saccade detections performed. The section is divided into three subsections: calibration, gaze estimation, and saccade detection.

A.1. Eye tracker calibration

The eye tracker software has to adapt according to the subject to get the correct estimation of the gaze points and direction with accuracy and precision. This adaptation and adjustment of the tracker are made through the calibration process when the user tracks a set of points on the active display area. In this case, the active display area is the screen display where the user looks. For the experiment, a 9-point calibration process, the location of which is shown in table A.1.

Loc	1	2	3	4	5	6	7	8	9
X [-]	0.9	0.9	0.9	0.5	0.5	0.5	0.1	0.1	0.1
Y [-]	0.9	0.5	0.1	0.9	0.5	0.1	0.9	0.5	0.1

Table A.1: Calibration coordinates used for the 9-point calibration during the experiments.

The calibration pattern for the experiment was randomized, and the subjects were asked to track moving white dots that moved from one calibration point to another. The calibration ends by providing an output result from the eye movement data gathered during the process as shown in fig. A.1. Figure A.1 shows the deviation of the gaze samples and the calibration points based on the closest fit to the eye model of the collected data by the eye tracker.The closed environment of the Tobii allowed no changes to the calibration process. Thus, the original application was used throughout the study. No information on the backend calibration algorithm was found for documentation.

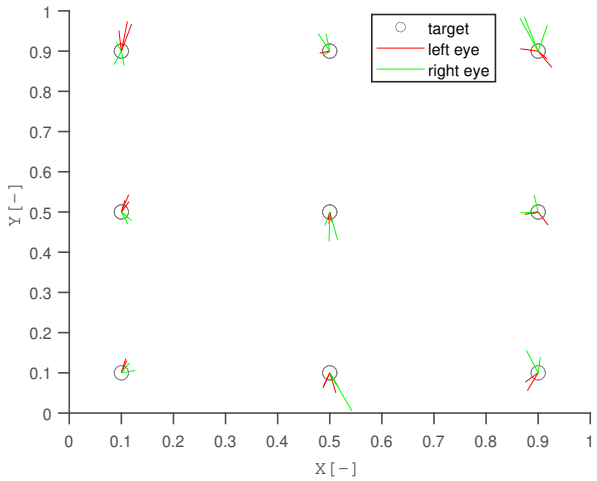

Figure A.1: Example calibration result from a single subject. The circle(○) is a target, the red lines(—) are the relative endpoint position left eye, and the green lines(—) are the relative endpoint position of the right eye. Multiple endpoints for each location are the pupil location recorded at different time stamps.

A.2. Gaze estimation

The eye tracker acquires the gaze or eye movements during the experimentation phase at a frequency of 120 Hz. Again the gaze is obtained on a (0,1) cartesian coordinate system and needs to be converted to a visual field perspective in a polar coordinate system.

A.2.1. Timing Synchorization

The eye tracker considers two timing conditions for a successful data collection run. The first one is the timing of the eye tracker clock, and the second one is the timing of the client's computer. To correctly correlate the stimulus presentation events with the acquired gaze data, the clock of the eye tracker needs to be synced with the clock of the client computer on which the experimentation is being run. The offset is calculated based on the deviation of the tick rate of both clocks. However, since the two clocks are based on the client computer clocks, they will most likely drift from each other. The drift can also be due to changes in luminance condition, temperature, or imperfection in processors. The synchronization process includes two steps: a stabilization process that compensates for the offset of the clocks but not the overtime drift and a sync process that corrects for the drift.

An example of the offset between two clocks is shown in fig. A.2. To correct for the offset, the eye tracker considers the time and offset for both the clocks performed in the synchronization procedure at regular intervals. The synchronization is based on Cristian's algorithm, which considers a RTT to sync both the clocks [64]. The process accounts for two local timestamps(L_1, L_2) and one remote timestamp(R) as shown in fig. A.3.
The synchronization process aims to align point L of the SDK clock with R of the eye tracker clock as shown in fig. A.3. L is the average of L_1 and L_2. The round trip time is between L_1 and L_2. If two synchronization points of the eye tracker are used, it is feasible to account for the drift. Equation (A.1) takes into account two average RTT l_1 and l_2 and two eye tracker clock timestamps to l_1 and l_2 calculate the drift. Offset is calculated in eq. (A.2) by only considering one eye tracker timestamp and one average RTT. Finally, either clock can be corrected for drifts and offset using eq. (A.3).

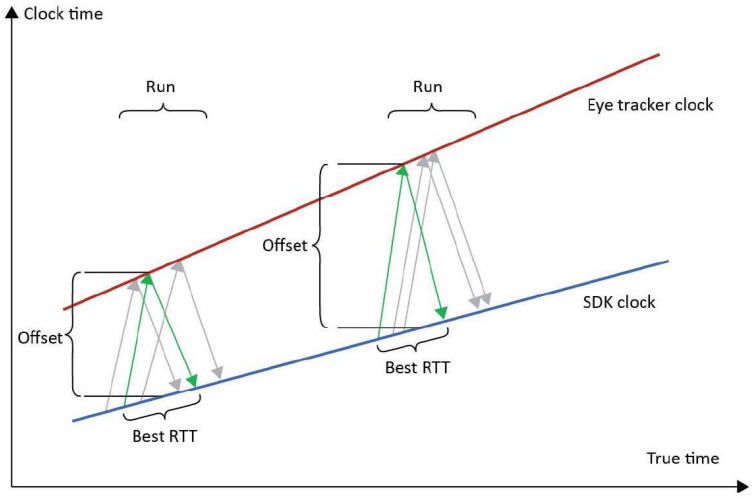

Figure A.2: Example of the drift and offset of two clocks during a run [63].

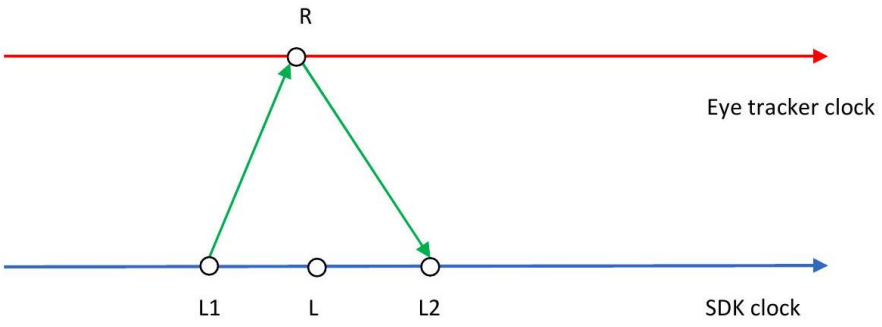

Figure A.3: Synchrohisation procedure for eye tracker [63].

$$\text{drift} = \frac{r_2 - r_1}{l_2 - l_1} \tag{A.1}$$

$$\text{offset} = r_1 - l_1 \tag{A.2}$$

$$\begin{aligned} t_{\text{eyetracker}} &= \text{drift} \times t_{\text{sdk}} + \text{offset} \\ t_{\text{sdk}} &= \frac{t_{\text{eyetracker}} - \text{offset}}{drift} \end{aligned} \tag{A.3}$$

During the initial setup phase, issues were discovered related to the timing of the eye tracker. For the initial set of 5 experimental runs, it was found that the drift was almost 13.5 ° elevation from the baseline as shown in fig. A.4a. A drift correction was made to the original set of data by running the synchronization process in the loop for each trial with a set or run, and the results with no drift were obtained, depicted in fig. A.4b.

A.2.2. Gaze coordinate

As the eye tracker uses a (0,1) coordinate system, it needs to be converted into viewing angles according to the field of vision. The conversion process followed is similar to the techniques used by Fleishman *et al.* [65]. The relationship between pixel spacing (p), viewing distance(D), width of the screen(e) and minimum resolvable angle($\Delta\phi$) can be derived using fig. A.5. The angular distance of

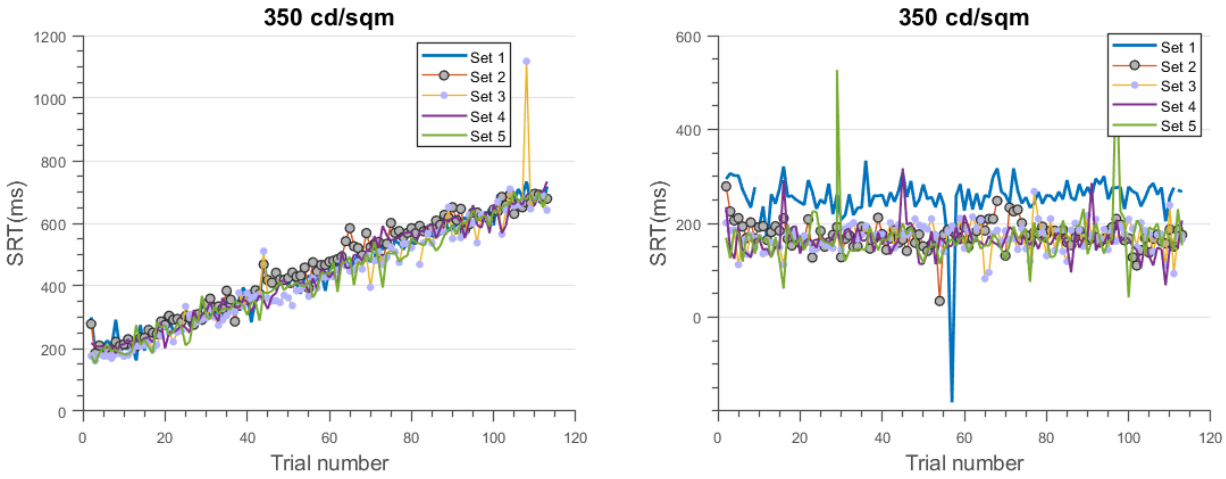

(a) Observed time drift experiment trials for five sets

(b) Corrected time drift and offset for 5 experiment trials.

Figure A.4: (A) Observed time drift and offset in SRT over 5 runs each run, including 120 trials. (B) SRT results for corrected values for time drift and offset. During all runs, the luminance of the display was set to 350 cdm^{-2}.

a pixel from the center can be derived using eq. (A.4). In eq. (A.4) θ_{deg} and ψ_{deg} are the respective angles of X_{pix} and Y_{pix} from the center of the screen.

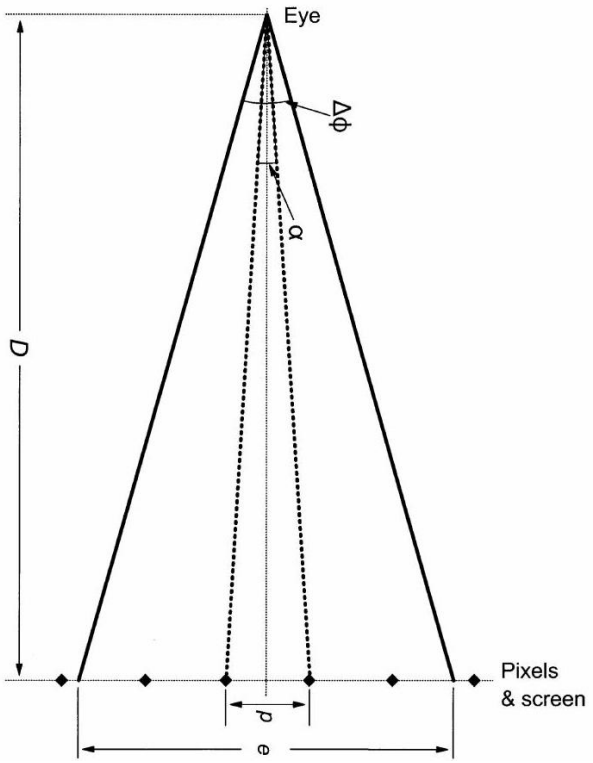

Figure A.5: Schematic demonstrating the relationship between subtended angle(α), pixel spacing (p), viewing distance(D), width of the screen(e) and minimum resolvable angle($\Delta\phi$). The total viewing angle vertically and horizontally is expressed as ϕ and θ respectively in eq. (A.4). [65]

$$\begin{aligned}
\theta = \alpha + 2\Delta\Phi &= 2\arctan\left(\frac{e}{2D}\right) \\
\text{pix2degX} &= \frac{\theta}{\text{Res(x)}} \\
\psi &= \theta.\frac{\text{Res(y)}}{\text{Res(x)}} \\
\text{pix2degY} &= \frac{\psi}{\text{Res(y)}} \\
\theta_{\text{deg}} &= \text{X}_{\text{pix}}.\text{pix2degX} \\
\psi_{\text{deg}} &= \text{Y}_{\text{pix}}.\text{pix2degY}
\end{aligned} \tag{A.4}$$

A.3. Saccade detection

Saccades are high-velocity eye movements measured in hundredths of a second performed by directing the sensitive region of the retina towards a point of interest in the visual field. Salvucci *et al.* provides a brief layout of the several saccade detection algorithms based on different criteria [66]. Velocity-based detections are more suitable for this study as more focus is given to reaction times. In the velocity-based method, Velocity-Threshold Identification (VTI) is preferred because of the simplicity of the task performed during experimentation. I-VT takes only one input parameter, i.e., the minimum detectable velocity. It differentiates points based on their velocity; the algorithm calculates the distance between two points and the time to determine the velocity. A simplified form of VTI can be described by eq. (A.5) is implemented in the thesis. Another method of velocity-based detection is centered on the algorithm proposed by Engbert *et al.* [67]. The algorithm focuses on moving averages, which facilitates the detection of microsaccades, and only focuses on primary saccades. Equation (A.6) represents an equation to determine the velocity vector using the windowing algorithm [67].

$$v = \frac{\sqrt{(x_i - x_{i-1})^2 + (y_i - y_{i-1})^2}}{\Delta t} \tag{A.5}$$

$$\vec{v}_n = \frac{\vec{x}_{n+2} + \vec{x}_{n+1} - \vec{x}_{n-1} - \vec{x}_{n-2}}{6\Delta t} \tag{A.6}$$

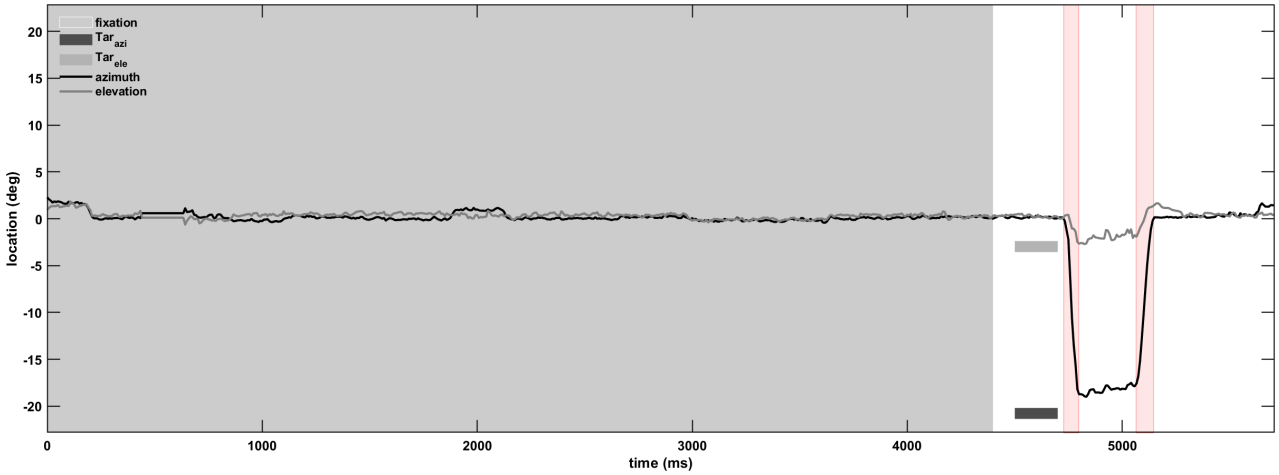

(a) Example of a saccade performed in response to a certain target by a subject during experimentation.

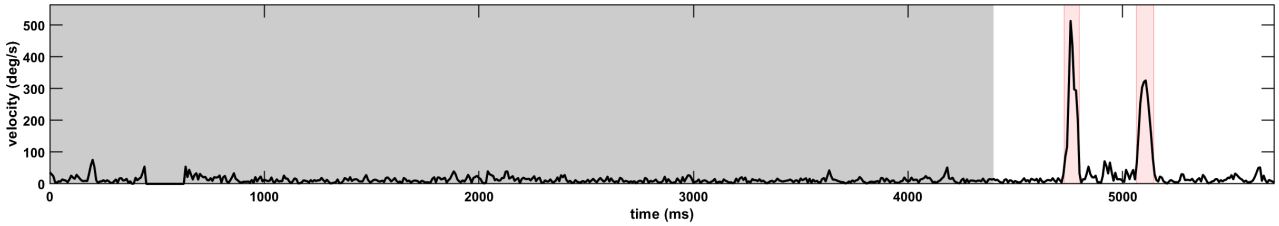

(b) Two velocity peaks detected by the algorithm corresponding to the saccades shown above.

Figure A.6: An example of a saccade detected using the velocity threshold algorithm. The area of interest marked by a red patch is determined if the saccade velocity is above $100\,^{\circ}s^{-1}$. Then for the detected saccade, a lower threshold of $50\,^{\circ}s^{-1}$ is implemented to detect the start and end of the saccade further accurately. The gray patch represents the fixation duration. The azimuth and elevation of the targets are represented by the two small black and gray boxes, respectively.

B

Results

B.1. Lower Hemifield Bleaching results

B.1.1. Subject 2 SRTs

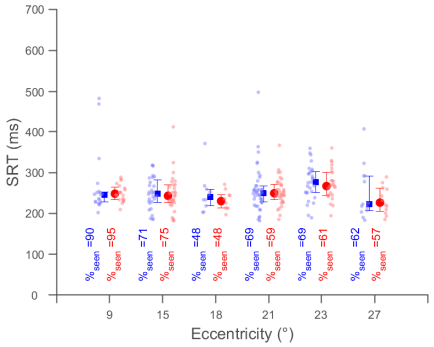

(a) SRT distribution upper hemifield

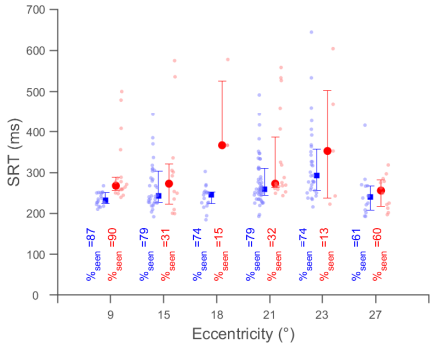

(b) SRT distribution lower hemifield

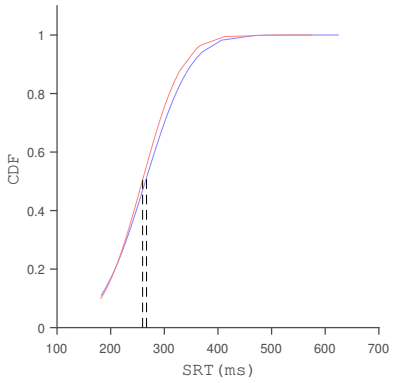

(c) SRT CDF upper hemifield

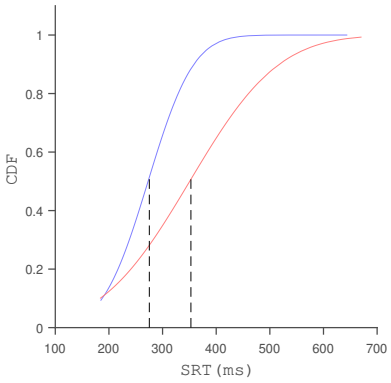

(d) SRT CDF lower hemifield

Figure B.1: SRT distribution of non-bleaching and bleaching conditions for upper and lower hemifield, for subject 2. In fig. B.1a and fig. B.1b, the small light blue dots (●) and light red dots (●) are the SRTs for non-bleaching and bleaching conditions. The blue square (■) and red circle (●) represent the median values of SRTs in both hemifields' non-bleaching and bleaching conditions. The 25th and 75th percentile of SRTs are given by the blue (–) and red (–) error bars for each condition in each hemifield. $\%_{seen}$ signifies the percentage of detections at each eccentricity for each condition. In fig. B.1cand fig. B.1d, the blue (–) and red (–) lines show the cdf of non-bleaching and bleaching conditions in each hemifield.

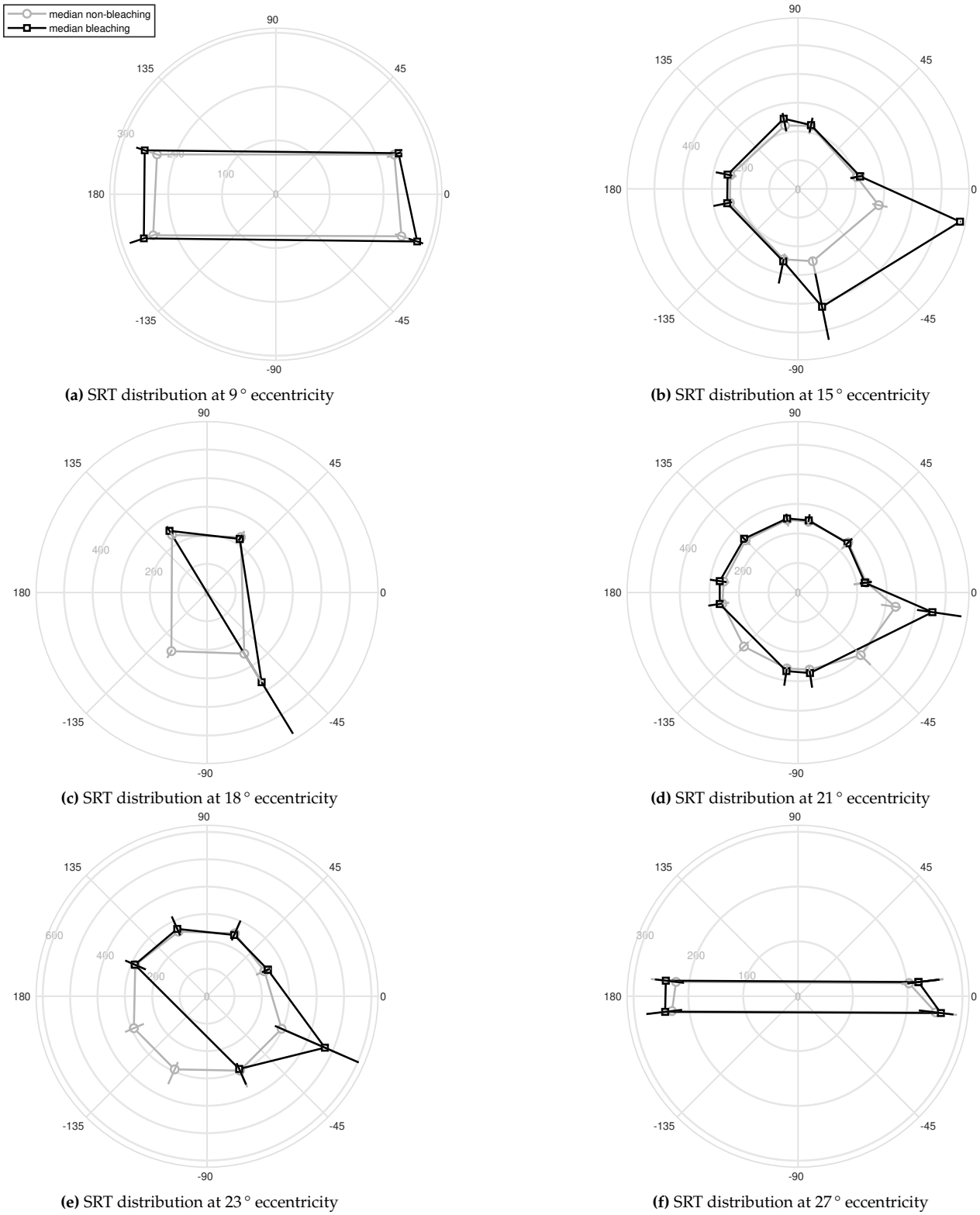

(a) SRT distribution at 9 ° eccentricity

(b) SRT distribution at 15 ° eccentricity

(c) SRT distribution at 18 ° eccentricity

(d) SRT distribution at 21 ° eccentricity

(e) SRT distribution at 23 ° eccentricity

(f) SRT distribution at 27 ° eccentricity

Figure B.2: SRT distributions from subject 2 at each eccentricity. The gray boxes (□) indicate the median SRTs from non-bleaching trials. The black open boxes show the SRTs from the bleaching trials(□). The 25^{th} and 75^{th} percentile of SRTs are given by the gray (−) and black (−) error bars for each condition in each hemifield.

B.1.2. Subject 3 SRTs

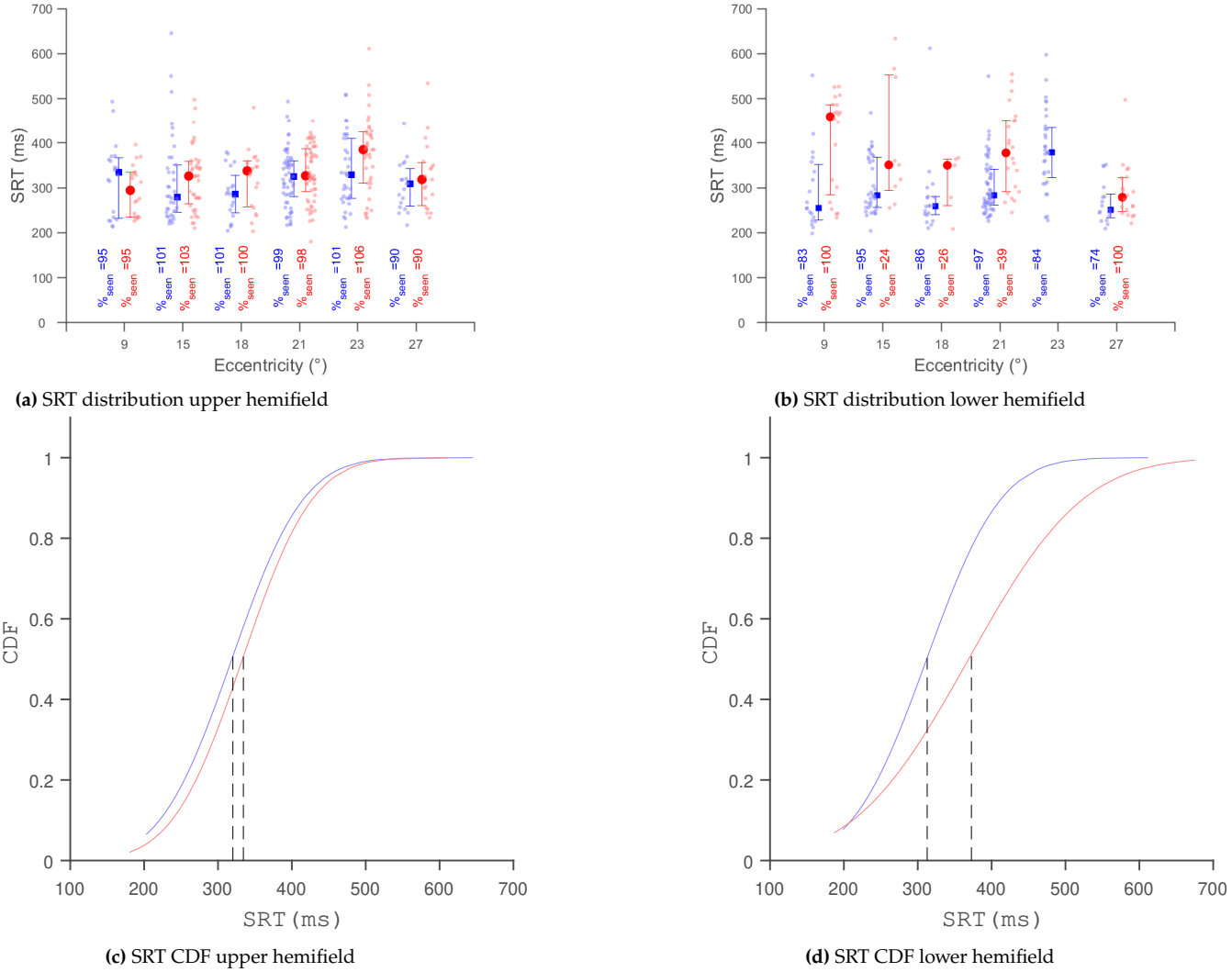

(a) SRT distribution upper hemifield

(b) SRT distribution lower hemifield

(c) SRT CDF upper hemifield

(d) SRT CDF lower hemifield

Figure B.3: SRT distribution of non-bleaching and bleaching conditions for upper and lower hemifield, for subject 3. In fig. B.3a and fig. B.3b, the small light blue dots (●) and light red dots (●) are the SRTs for non-bleaching and bleaching conditions. The blue square (■) and red circle (●) represent the median values of SRTs in both hemifields' non-bleaching and bleaching conditions. The 25^{th} and 75^{th} percentile of SRTs are given by the blue (–) and red (–) error bars for each condition in each hemifield. $\%_{seen}$ signifies the percentage of detections at each eccentricity for each condition. In fig. B.3cand fig. B.3d, the blue (–) and red (–) lines show the cdf of non-bleaching and bleaching conditions in each hemifield.

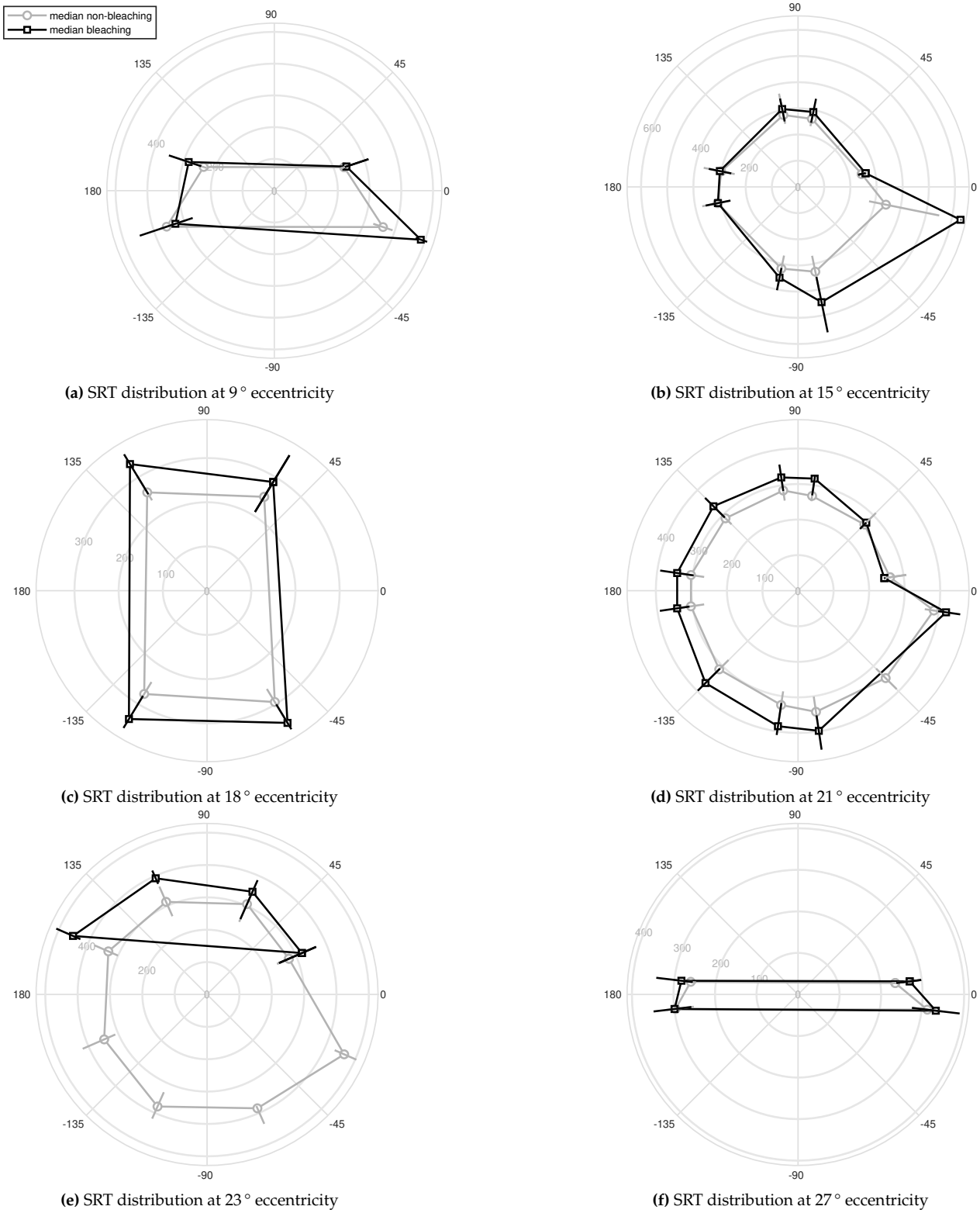

(a) SRT distribution at 9 ° eccentricity

(b) SRT distribution at 15 ° eccentricity

(c) SRT distribution at 18 ° eccentricity

(d) SRT distribution at 21 ° eccentricity

(e) SRT distribution at 23 ° eccentricity

(f) SRT distribution at 27 ° eccentricity

Figure B.4: SRT distributions from subject 3 at each eccentricity. The gray boxes (□) indicate the median SRTs from non-bleaching trials. The black open boxes show the SRTs from the bleaching trials(□). The 25^{th} and 75^{th} percentile of SRTs are given by the gray (−) and black (−) error bars for each condition in each hemifield.

B.1.3. Subject 4 SRTs

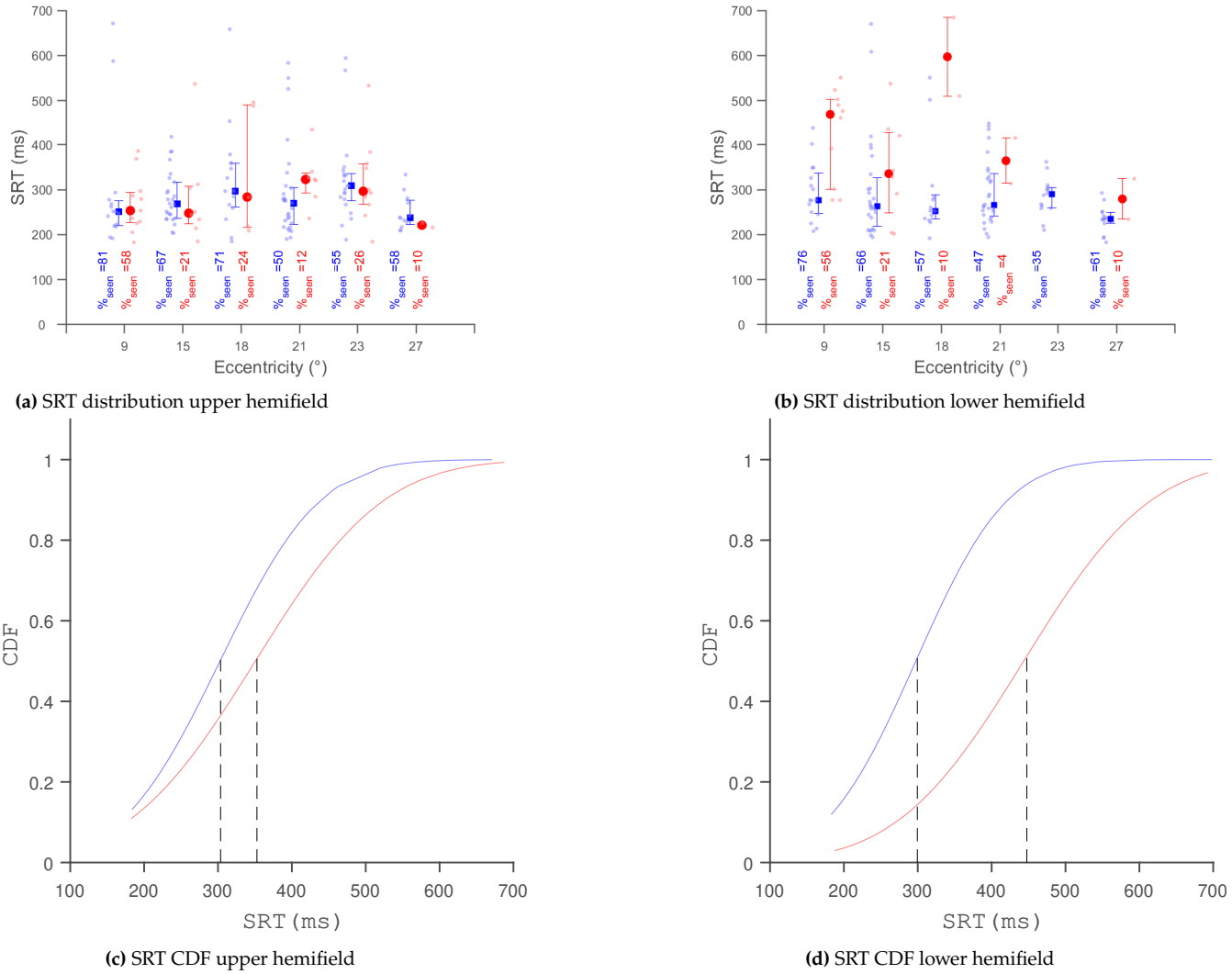

(a) SRT distribution upper hemifield

(b) SRT distribution lower hemifield

(c) SRT CDF upper hemifield

(d) SRT CDF lower hemifield

Figure B.5: SRT distribution of non-bleaching and bleaching conditions for upper and lower hemifield, for subject 4. In fig. B.5a and fig. B.5b, the small light blue dots (●) and light red dots (●) are the SRTs for non-bleaching and bleaching conditions. The blue square (■) and red circle (●) represent the median values of SRTs in both hemifields' non-bleaching and bleaching conditions. The 25^{th} and 75^{th} percentile of SRTs are given by the blue (–) and red (–) error bars for each condition in each hemifield. $\%_{seen}$ signifies the percentage of detections at each eccentricity for each condition. In fig. B.5cand fig. B.5d, the blue (–) and red (–) lines show the cdf of non-bleaching and bleaching conditions in each hemifield.

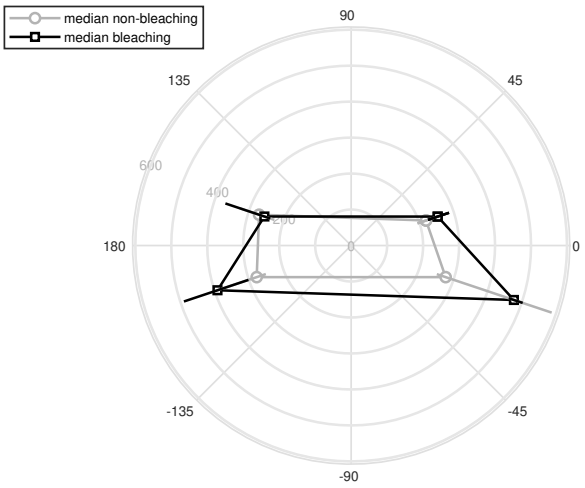

(a) SRT distribution at 9 ° eccentricity

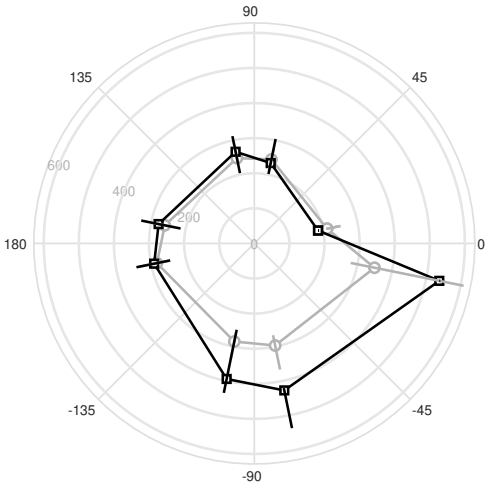

(b) SRT distribution at 15 ° eccentricity

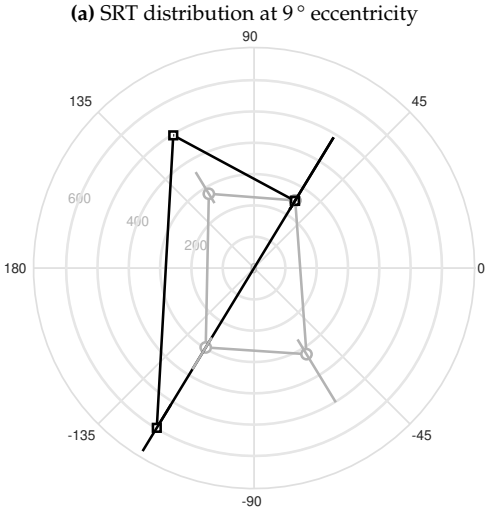

(c) SRT distribution at 18 ° eccentricity

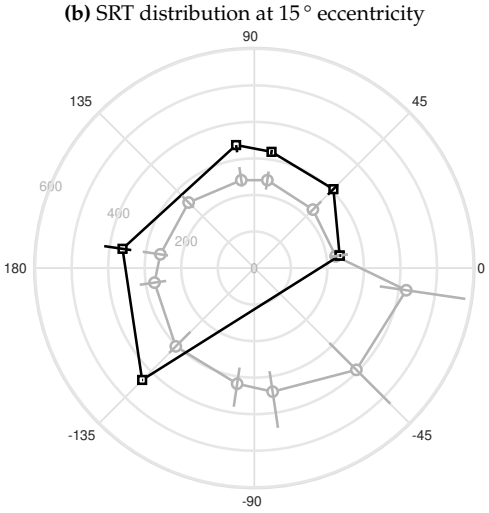

(d) SRT distribution at 21 ° eccentricity

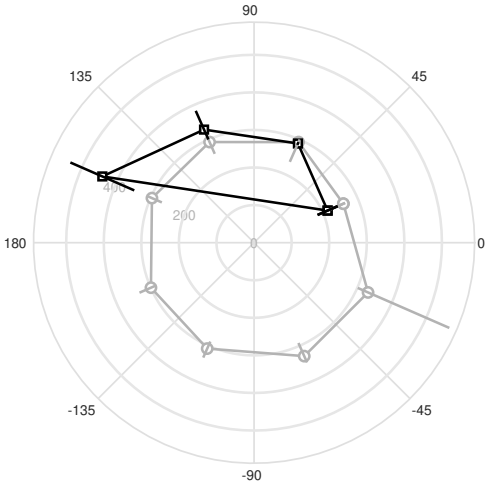

(e) SRT distribution at 23 ° eccentricity

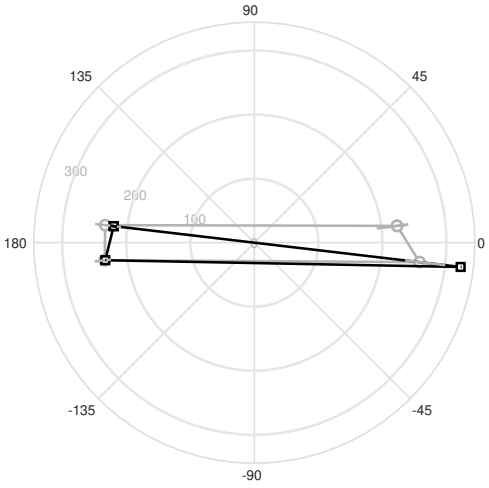

(f) SRT distribution at 27 ° eccentricity

Figure B.6: SRT distributions from subject 4 at each eccentricity. The gray boxes (□) indicate the median SRTs from non-bleaching trials. The black open boxes show the SRTs from the bleaching trials(□). The 25^{th} and 75^{th} percentile of SRTs are given by the gray (−) and black (−) error bars for each condition in each hemifield.

B.1.4. Subject 5 SRTs

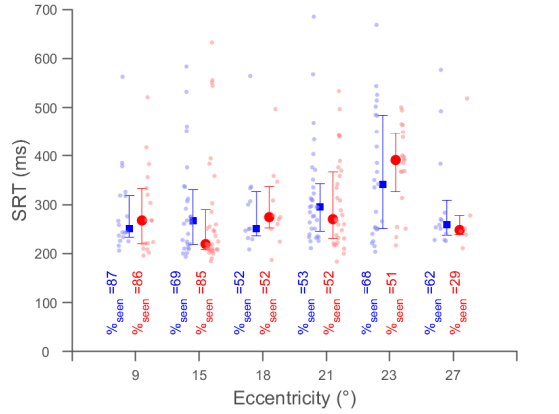

(a) SRT distribution upper hemifield

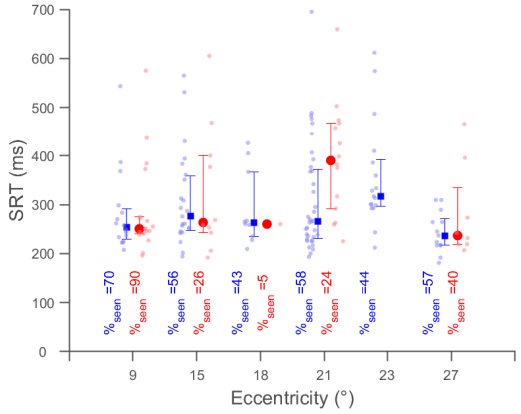

(b) SRT distribution lower hemifield

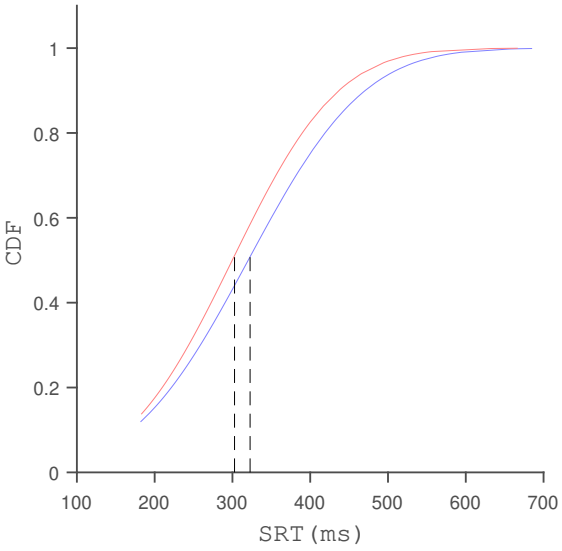

(c) SRT CDF upper hemifield

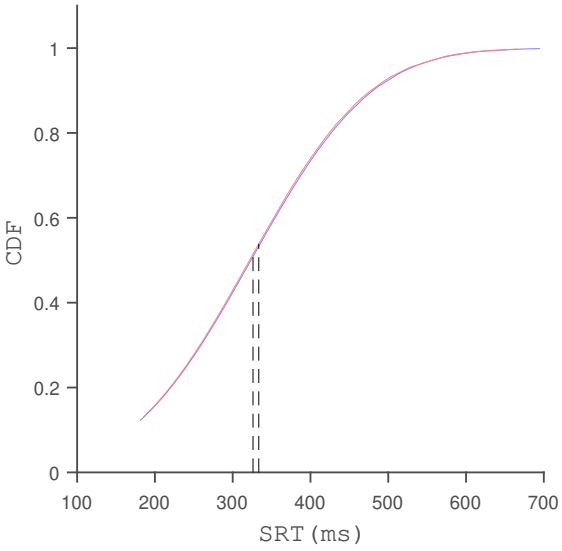

(d) SRT CDF lower hemifield

Figure B.7: SRT distribution of non-bleaching and bleaching conditions for upper and lower hemifield, for subject 5. In fig. B.7a and fig. B.7b, the small light blue dots (●) and light red dots (●) are the SRTs for non-bleaching and bleaching conditions. The blue square (■) and red circle (●) represent the median values of SRTs in both hemifields' non-bleaching and bleaching conditions. The 25th and 75th percentile of SRTs are given by the blue (—) and red (—) error bars for each condition in each hemifield. $\%_{seen}$ signifies the percentage of detections at each eccentricity for each condition. In fig. B.7cand fig. B.7d, the blue (—) and red (—) lines show the cdf of non-bleaching and bleaching conditions in each hemifield.

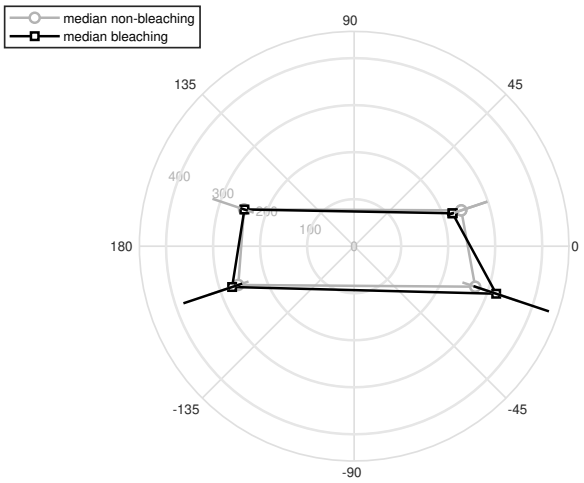

(a) SRT distribution at 9 ° eccentricity

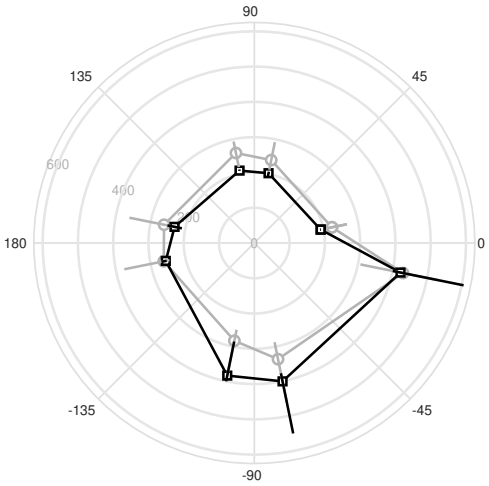

(b) SRT distribution at 15 ° eccentricity

(c) SRT distribution at 18 ° eccentricity

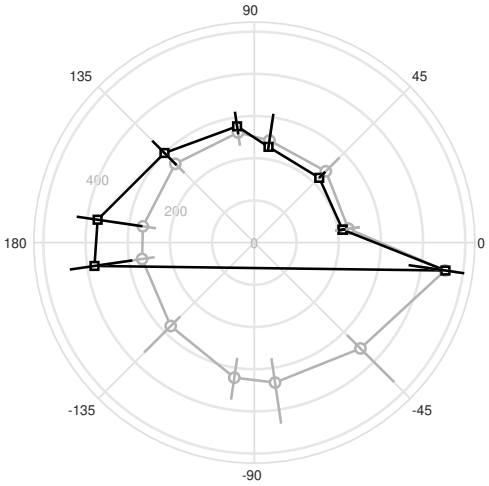

(d) SRT distribution at 21 ° eccentricity

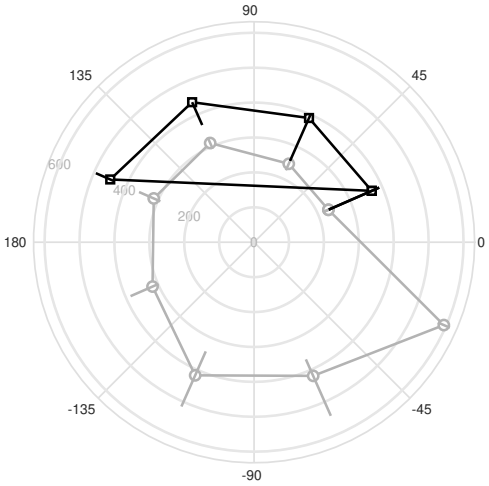

(e) SRT distribution at 23 ° eccentricity

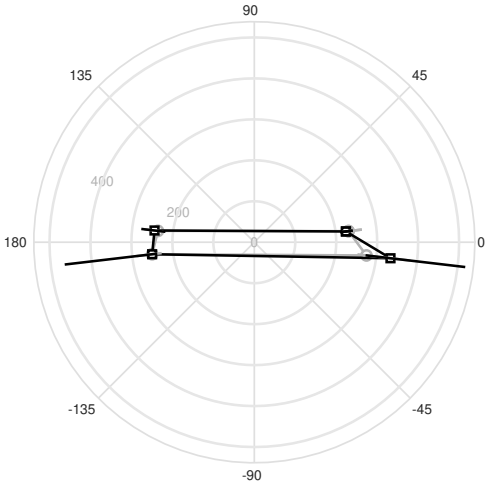

(f) SRT distribution at 27 ° eccentricity

Figure B.8: SRT distributions from subject 5 at each eccentricity. The gray boxes (□) indicate the median SRTs from non-bleaching trials. The black open boxes show the SRTs from the bleaching trials(□). The 25^{th} and 75^{th} percentile of SRTs are given by the gray (−) and black (−) error bars for each condition in each hemifield.

B.1.5. Subject 6 SRTs

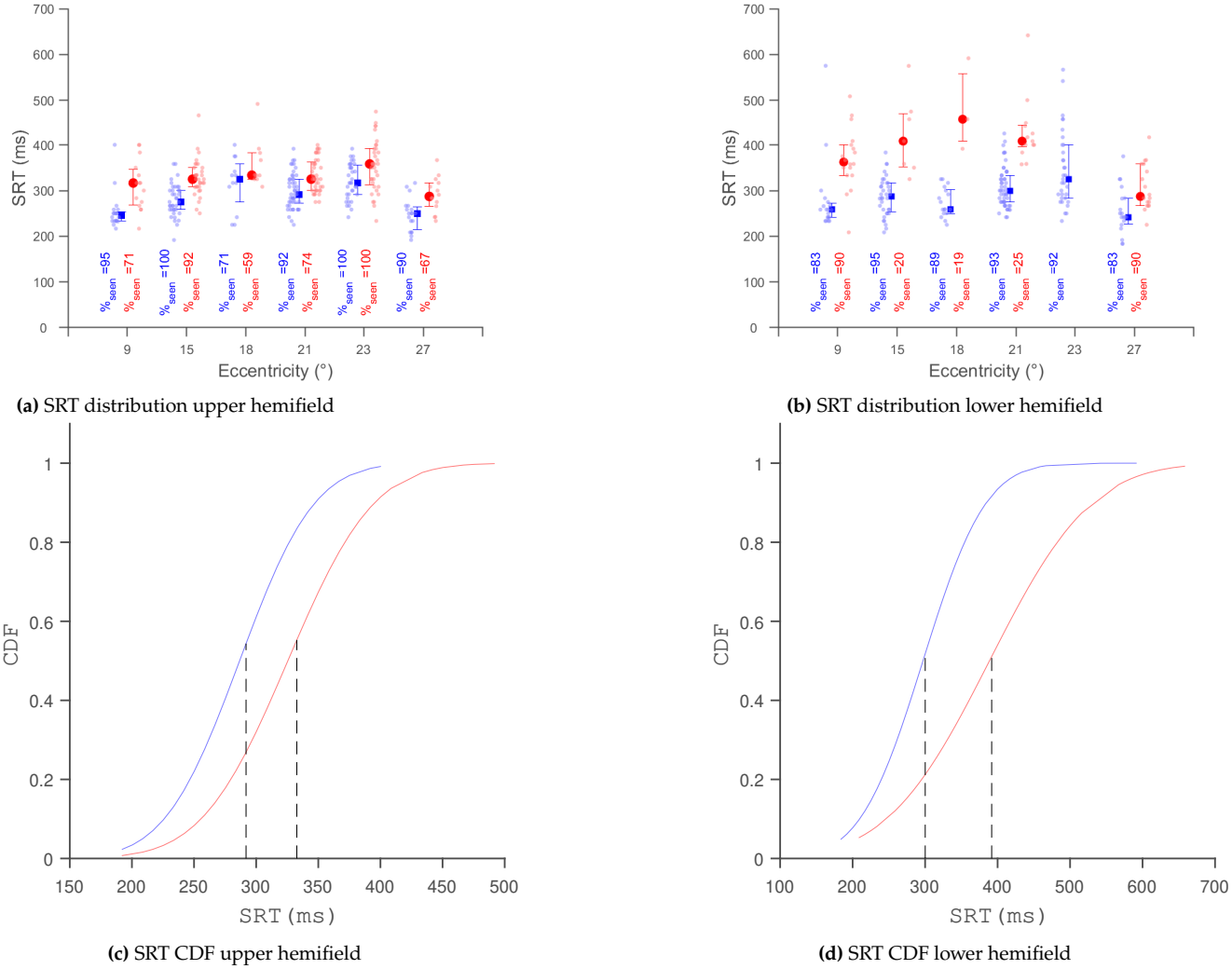

(a) SRT distribution upper hemifield

(b) SRT distribution lower hemifield

(c) SRT CDF upper hemifield

(d) SRT CDF lower hemifield

Figure B.9: SRT distribution of non-bleaching and bleaching conditions for upper and lower hemifield, for subject 6. In fig. B.9a and fig. B.9b, the small light blue dots (●) and light red dots (●) are the SRTs for non-bleaching and bleaching conditions. The blue square (■) and red circle (●) represent the median values of SRTs in both hemifields' non-bleaching and bleaching conditions. The 25th and 75th percentile of SRTs are given by the blue (—) and red (—) error bars for each condition in each hemifield. $\%_{seen}$ signifies the percentage of detections at each eccentricity for each condition. In fig. B.9cand fig. B.9d, the blue (—) and red (—) lines show the cdf of non-bleaching and bleaching conditions in each hemifield.

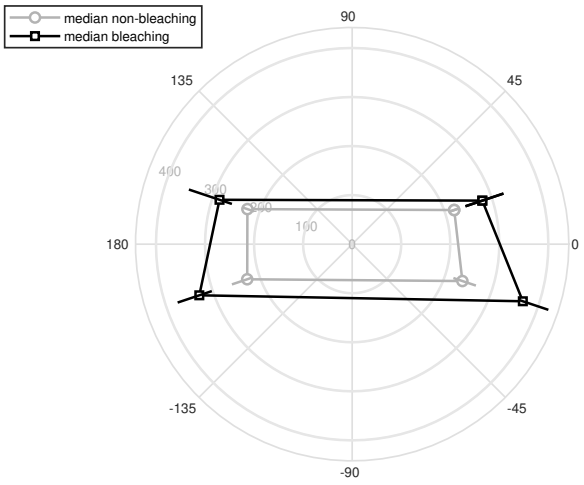

(a) SRT distribution at 9 ° eccentricity

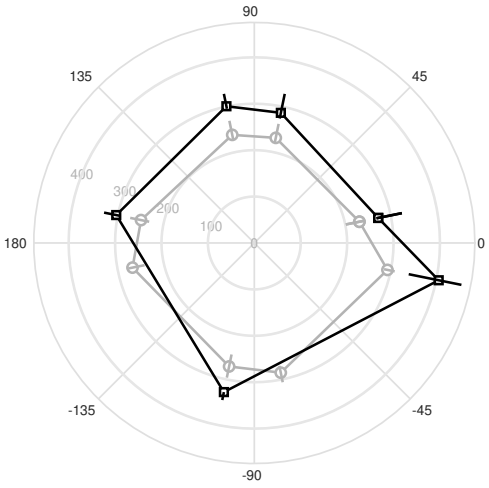

(b) SRT distribution at 15 ° eccentricity

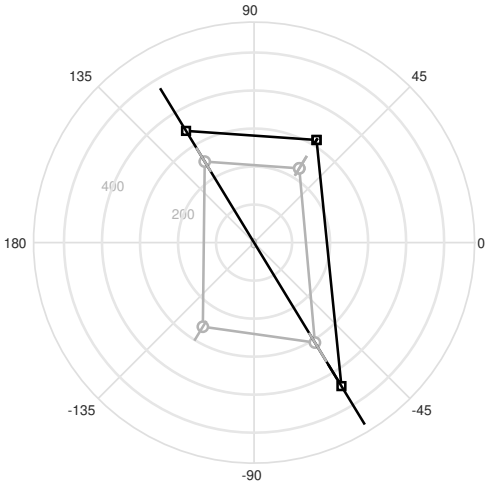

(c) SRT distribution at 18 ° eccentricity

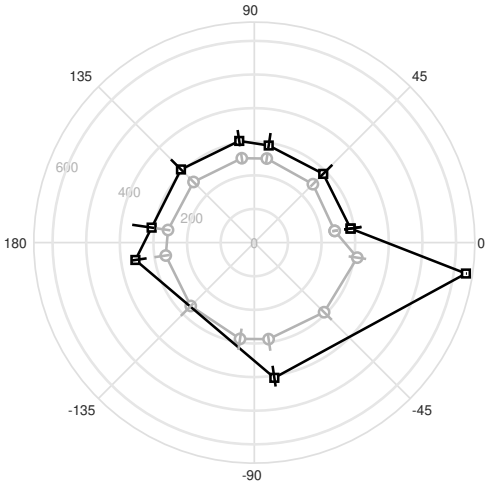

(d) SRT distribution at 21 ° eccentricity

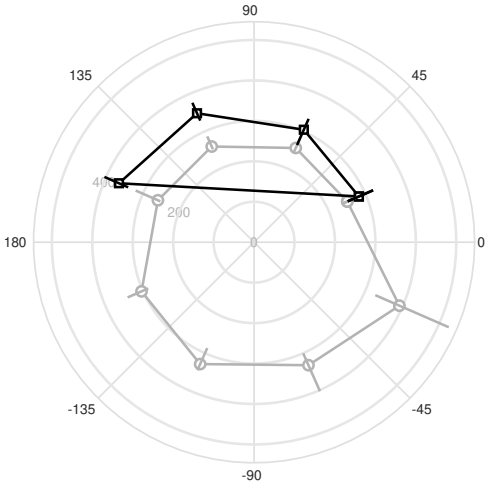

(e) SRT distribution at 23 ° eccentricity

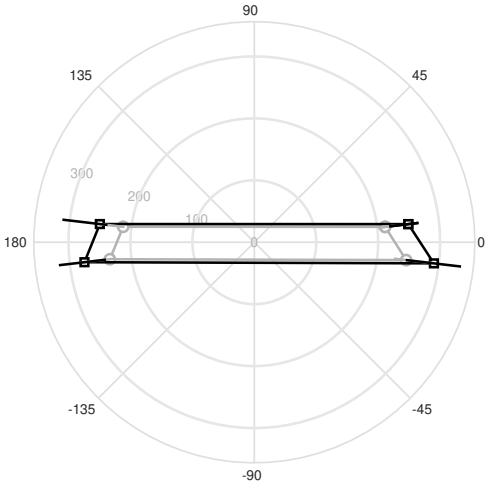

(f) SRT distribution at 27 ° eccentricity

Figure B.10: SRT distributions from subject 6 at each eccentricity. The gray boxes (□) indicate the median SRTs from non-bleaching trials. The black open boxes show the SRTs from the bleaching trials(□). The 25^{th} and 75^{th} percentile of SRTs are given by the gray (−) and black (−) error bars for each condition in each hemifield.

B.1.6. Subject 7 SRTs

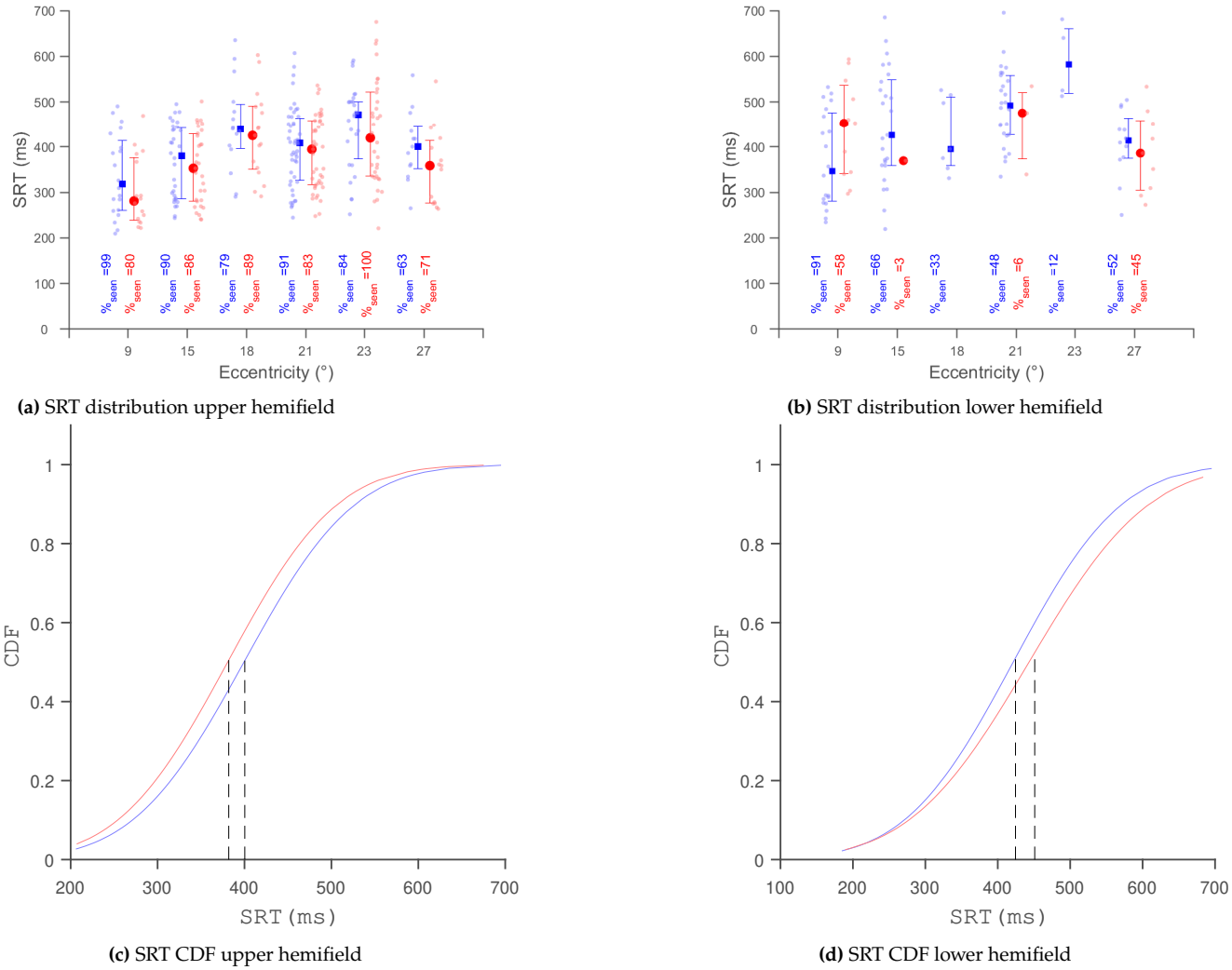

(a) SRT distribution upper hemifield

(b) SRT distribution lower hemifield

(c) SRT CDF upper hemifield

(d) SRT CDF lower hemifield

Figure B.11: SRT distribution of non-bleaching and bleaching conditions for upper and lower hemifield, for subject 7. In fig. B.11a and fig. B.11b, the small light blue dots (●) and light red dots (●) are the SRTs for non-bleaching and bleaching conditions. The blue square (■) and red circle (●) represent the median values of SRTs in both hemifields' non-bleaching and bleaching conditions. The 25th and 75th percentile of SRTs are given by the blue (—) and red (—) error bars for each condition in each hemifield. $\%_{seen}$ signifies the percentage of detections at each eccentricity for each condition. In fig. B.11cand fig. B.11d, the blue (—) and red (—) lines show the cdf of non-bleaching and bleaching conditions in each hemifield.

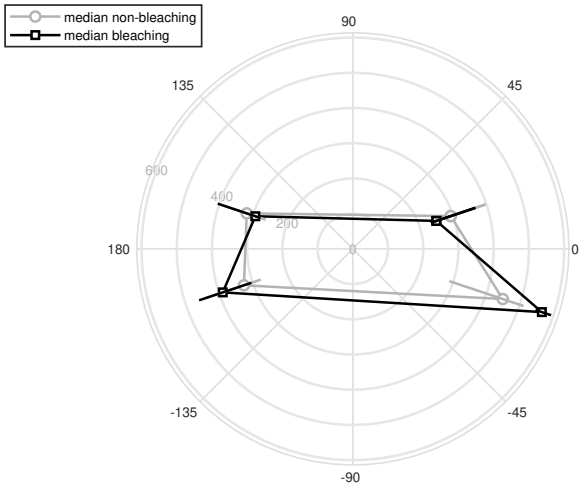

(a) SRT distribution at 9 ° eccentricity

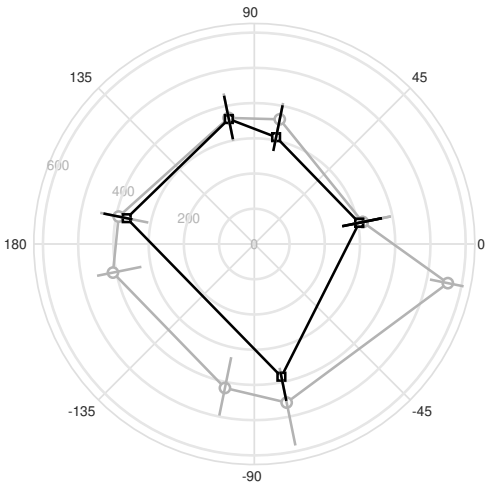

(b) SRT distribution at 15 ° eccentricity

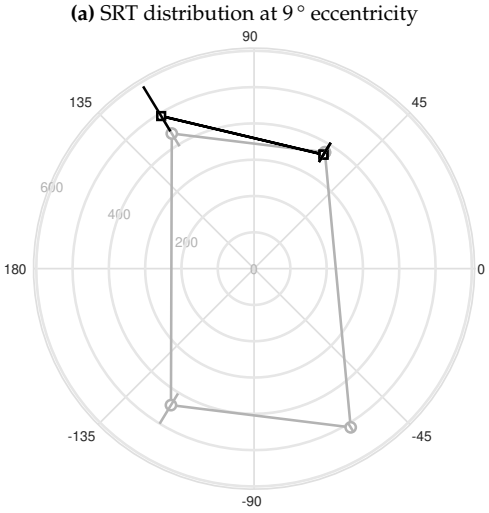

(c) SRT distribution at 18 ° eccentricity

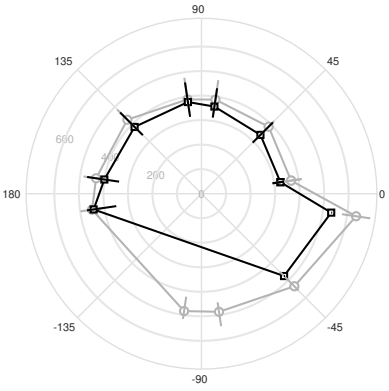

(d) SRT distribution at 21 ° eccentricity

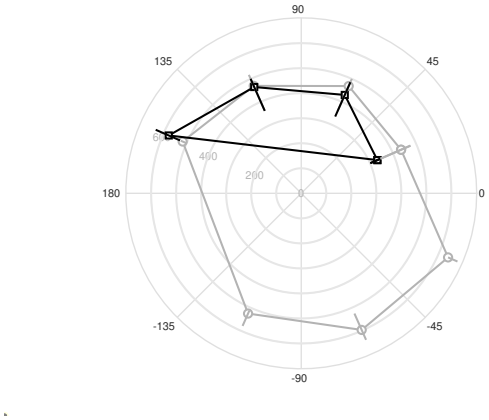

(e) SRT distribution at 23 ° eccentricity

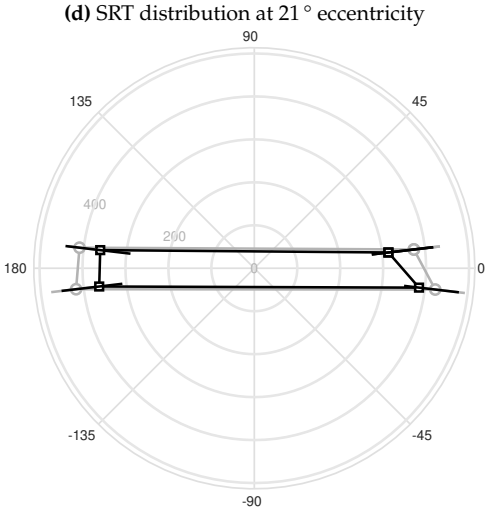

(f) SRT distribution at 27 ° eccentricity

Figure B.12: SRT distributions from subject 7 at each eccentricity. The gray boxes (□) indicate the median SRTs from non-bleaching trials. The black open boxes show the SRTs from the bleaching trials(□). The 25^{th} and 75^{th} percentile of SRTs are given by the gray (−) and black (−) error bars for each condition in each hemifield.

B.1.7. Subject 8 SRTs

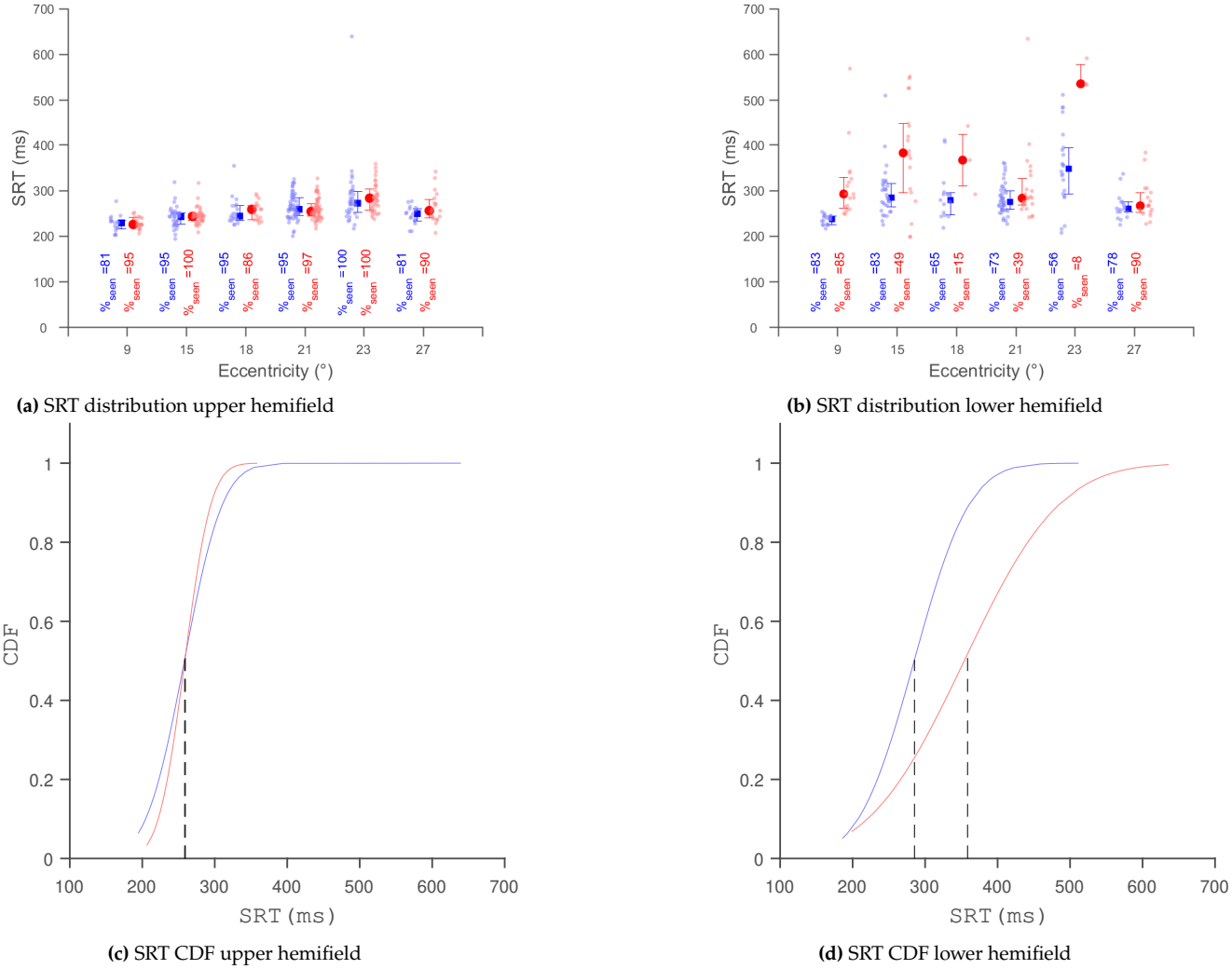

(a) SRT distribution upper hemifield

(b) SRT distribution lower hemifield

(c) SRT CDF upper hemifield

(d) SRT CDF lower hemifield

Figure B.13: SRT distribution of non-bleaching and bleaching conditions for upper and lower hemifield, for subject 8. In fig. B.13a and fig. B.13b, the small light blue dots (●) and light red dots (●) are the SRTs for non-bleaching and bleaching conditions. The blue square (■) and red circle (●) represent the median values of SRTs in both hemifields' non-bleaching and bleaching conditions. The 25^{th} and 75^{th} percentile of SRTs are given by the blue (—) and red (—) error bars for each condition in each hemifield. $\%_{seen}$ signifies the percentage of detections at each eccentricity for each condition. In fig. B.13cand fig. B.13d, the blue (—) and red (—) lines show the cdf of non-bleaching and bleaching conditions in each hemifield.

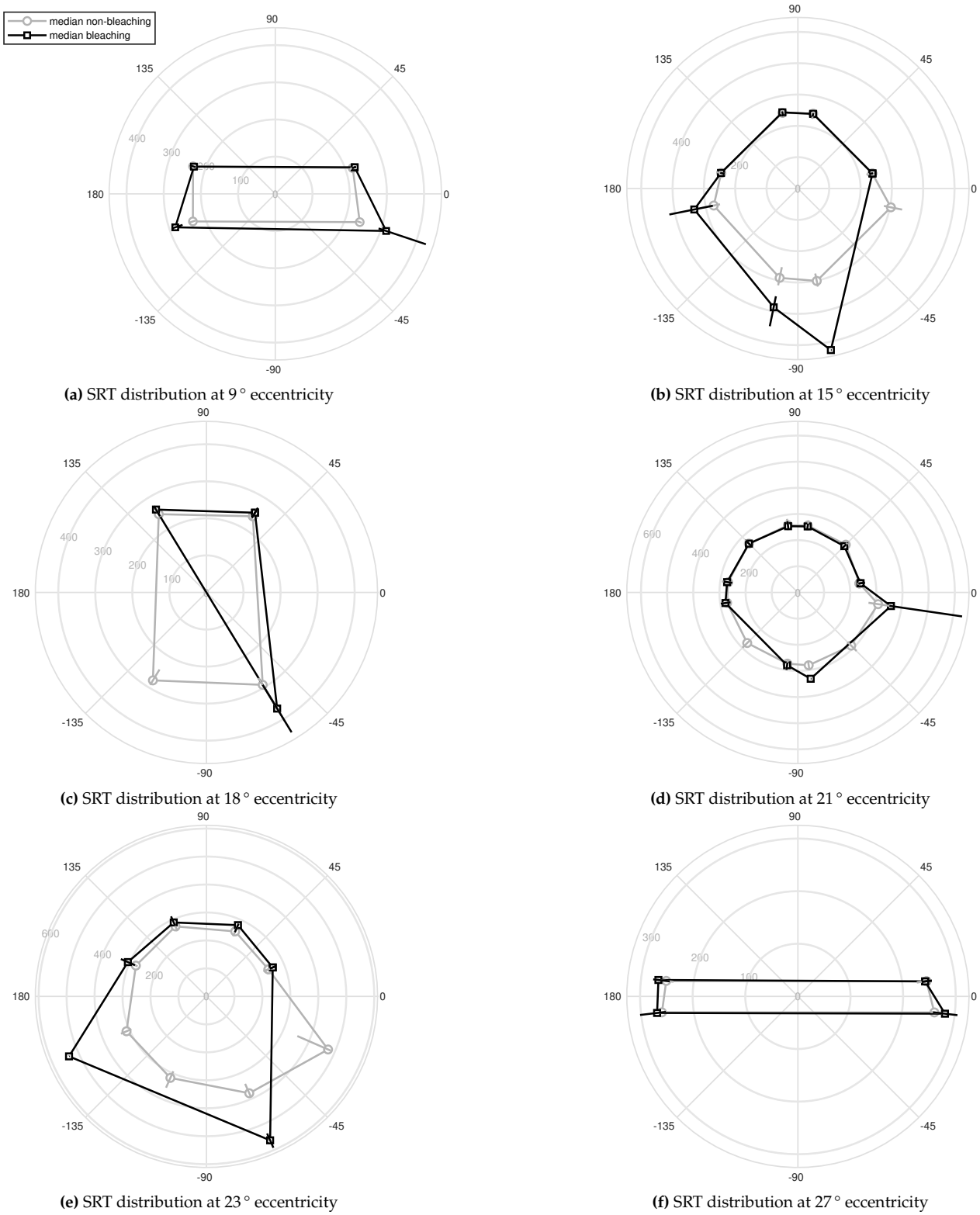

(a) SRT distribution at 9 ° eccentricity

(b) SRT distribution at 15 ° eccentricity

(c) SRT distribution at 18 ° eccentricity

(d) SRT distribution at 21 ° eccentricity

(e) SRT distribution at 23 ° eccentricity

(f) SRT distribution at 27 ° eccentricity

Figure B.14: SRT distributions from subject 8 at each eccentricity. The gray boxes (□) indicate the median SRTs from non-bleaching trials. The black open boxes show the SRTs from the bleaching trials(□). The 25^{th} and 75^{th} percentile of SRTs are given by the gray (−) and black (−) error bars for each condition in each hemifield.

B.1.8. Subject 9 SRTs

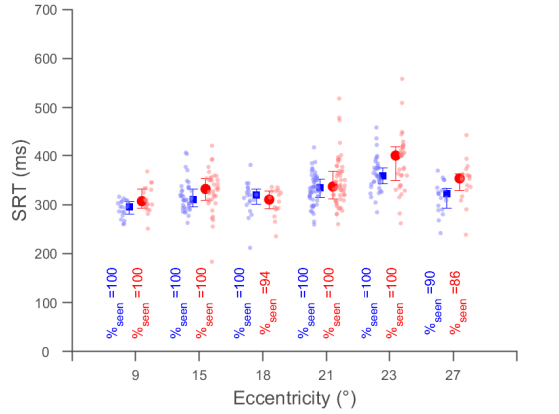

(a) SRT distribution upper hemifield

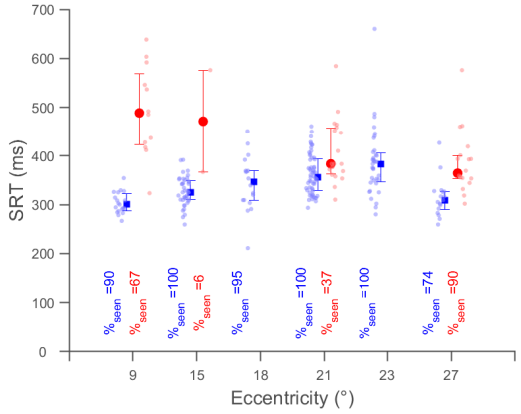

(b) SRT distribution lower hemifield

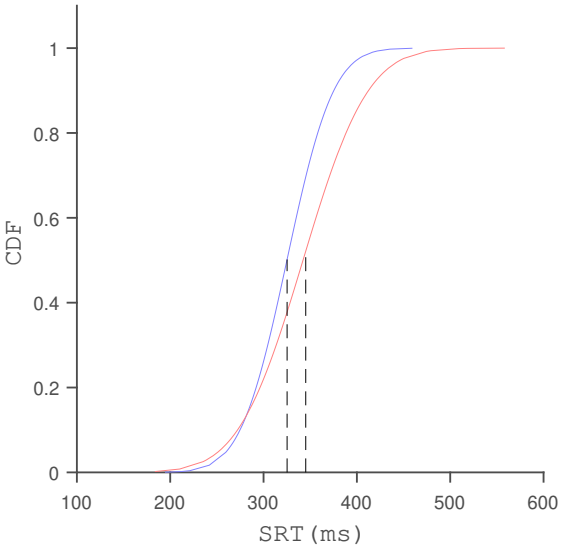

(c) SRT CDF upper hemifield

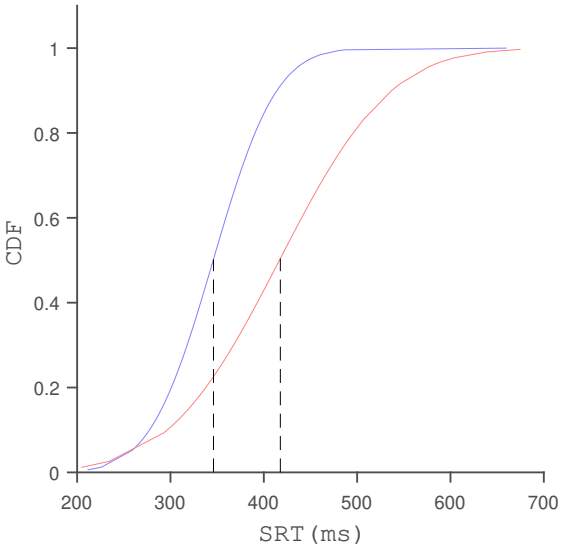

(d) SRT CDF lower hemifield

Figure B.15: SRT distribution of non-bleaching and bleaching conditions for upper and lower hemifield, for subject 9. In fig. B.15a and fig. B.15b, the small light blue dots (●) and light red dots (●) are the SRTs for non-bleaching and bleaching conditions. The blue square (■) and red circle (●) represent the median values of SRTs in both hemifields' non-bleaching and bleaching conditions. The 25th and 75th percentile of SRTs are given by the blue (—) and red (—) error bars for each condition in each hemifield. $\%_{seen}$ signifies the percentage of detections at each eccentricity for each condition. In fig. B.15cand fig. B.15d, the blue (—) and red (—) lines show the cdf of non-bleaching and bleaching conditions in each hemifield.

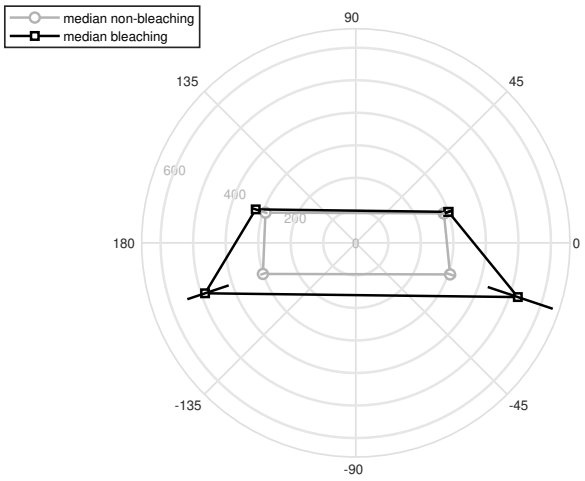

(a) SRT distribution at 9 ° eccentricity

(b) SRT distribution at 15 ° eccentricity

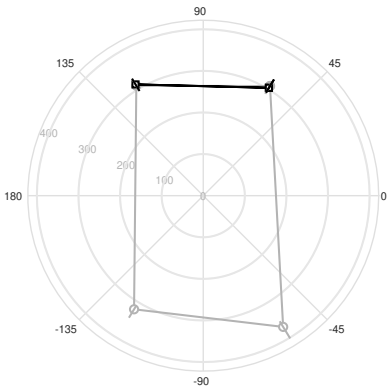

(c) SRT distribution at 18 ° eccentricity

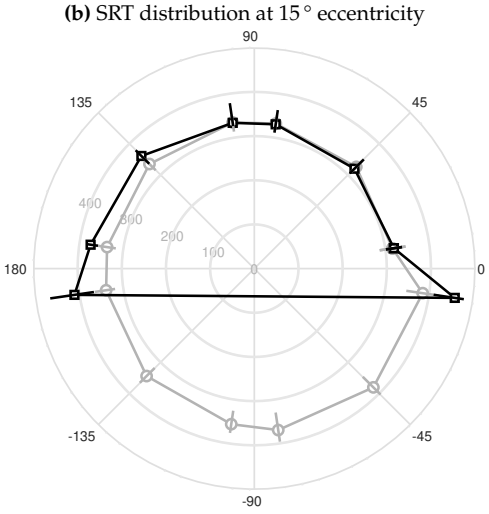

(d) SRT distribution at 21 ° eccentricity

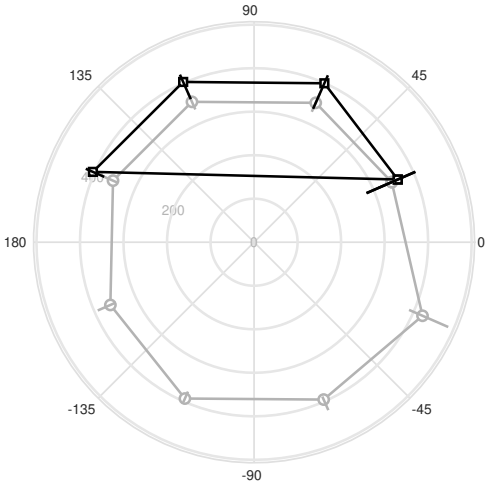

(e) SRT distribution at 23 ° eccentricity

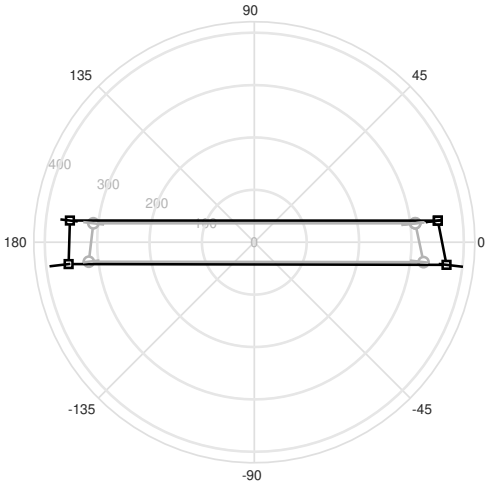

(f) SRT distribution at 27 ° eccentricity

Figure B.16: SRT distributions from subject 9 at each eccentricity. The gray boxes (□) indicate the median SRTs from non-bleaching trials. The black open boxes show the SRTs from the bleaching trials(□). The 25^{th} and 75^{th} percentile of SRTs are given by the gray (−) and black (−) error bars for each condition in each hemifield.

B.1.9. Subject 2 SRTs: LHBV_2 results

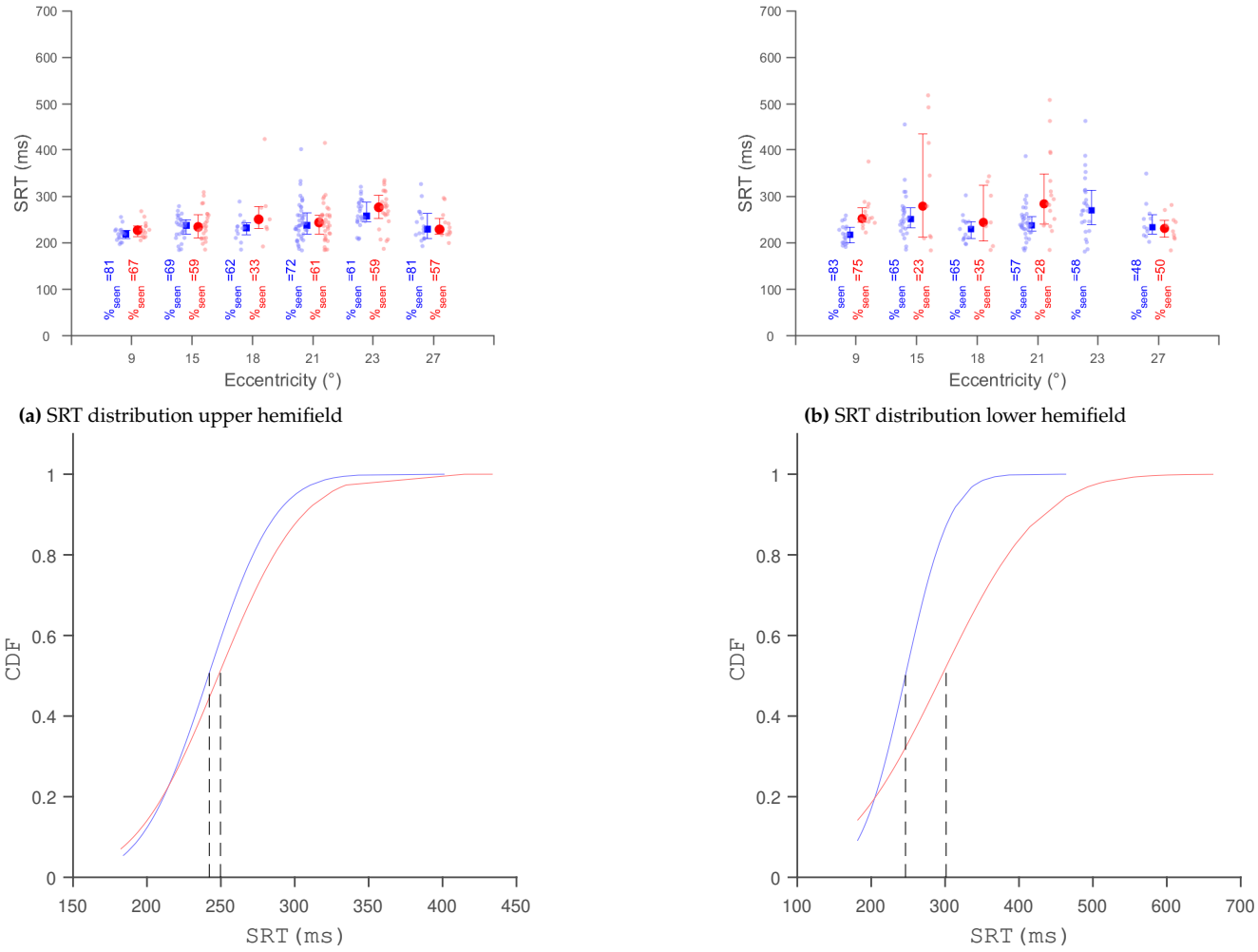

(a) SRT distribution upper hemifield

(b) SRT distribution lower hemifield

(c) SRT CDF upper hemifield

(d) SRT CDF lower hemifield

Figure B.17: SRT distribution of non-bleaching and bleaching conditions for upper and lower hemifield, for subject 2 from LHB_V_2. In fig. B.17a and fig. B.17b, the small light blue dots (●) and light red dots (●) are the SRTs for non-bleaching and bleaching conditions. The blue square (■) and red circle (●) represent the median values of SRTs in both hemifields' non-bleaching and bleaching conditions. The 25^{th} and 75^{th} percentile of SRTs are given by the blue (—) and red (—) error bars for each condition in each hemifield. $\%_{seen}$ signifies the percentage of detections at each eccentricity for each condition. In fig. B.19cand fig. B.17d, the blue (—) and red (—) lines show the cdf of non-bleaching and bleaching conditions in each hemifield.

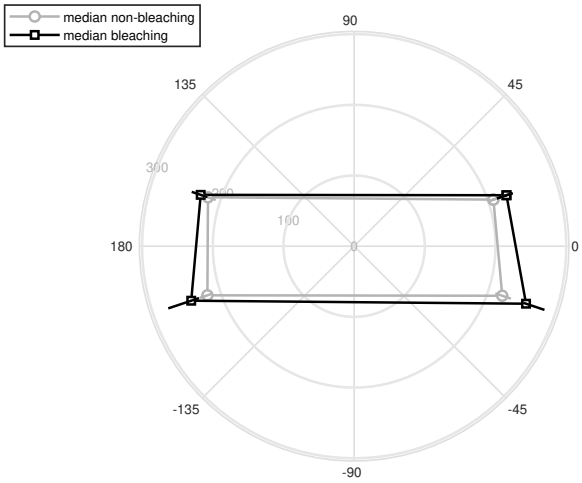

(a) SRT distribution at 9 ° eccentricity

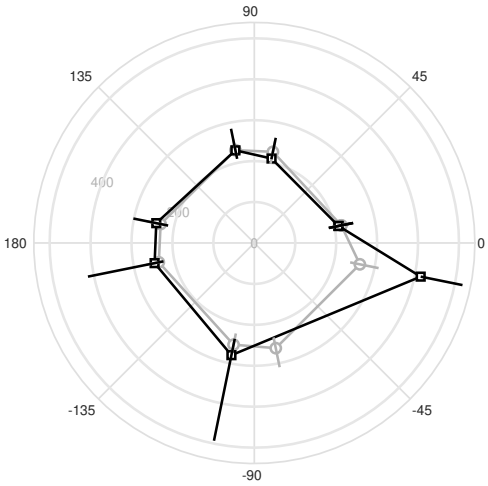

(b) SRT distribution at 15 ° eccentricity

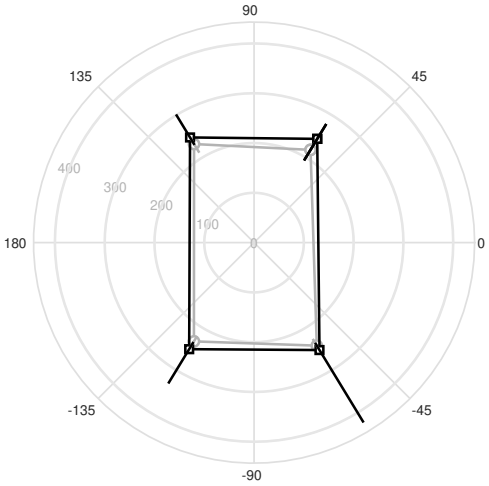

(c) SRT distribution at 18 ° eccentricity

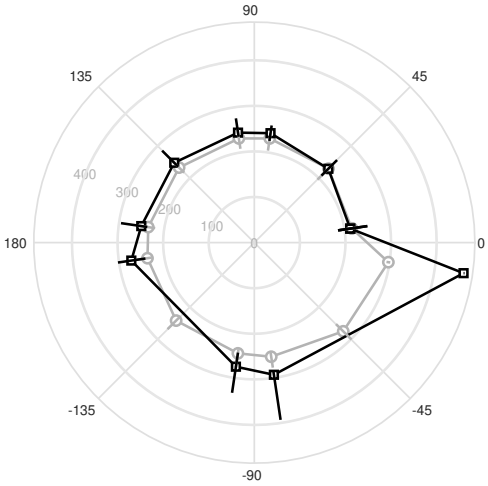

(d) SRT distribution at 21 ° eccentricity

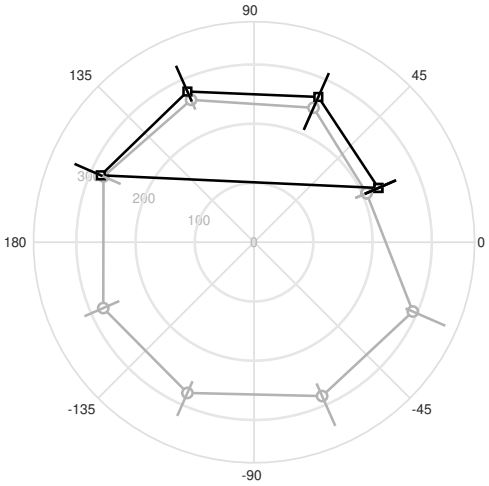

(e) SRT distribution at 23 ° eccentricity

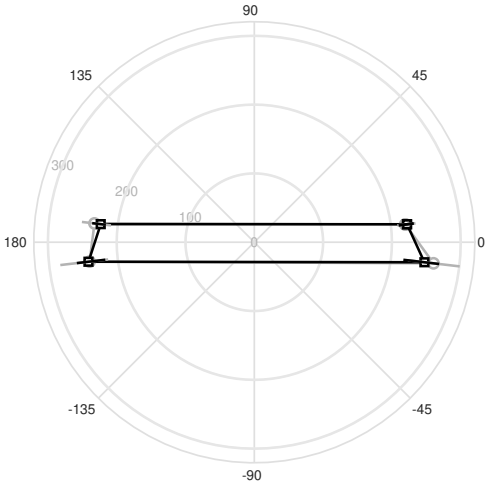

(f) SRT distribution at 27 ° eccentricity

Figure B.18: SRT distributions from subject 2 at each eccentricity from LHB_V_2. The gray boxes (□) indicate the median SRTs from non-bleaching trials. The black open boxes show the SRTs from the bleaching trials(□). The 25^{th} and 75^{th} percentile of SRTs are given by the gray (−) and black (−) error bars for each condition in each hemifield.

B.1.10. Subject 9 SRTs: LHB_V_2 results

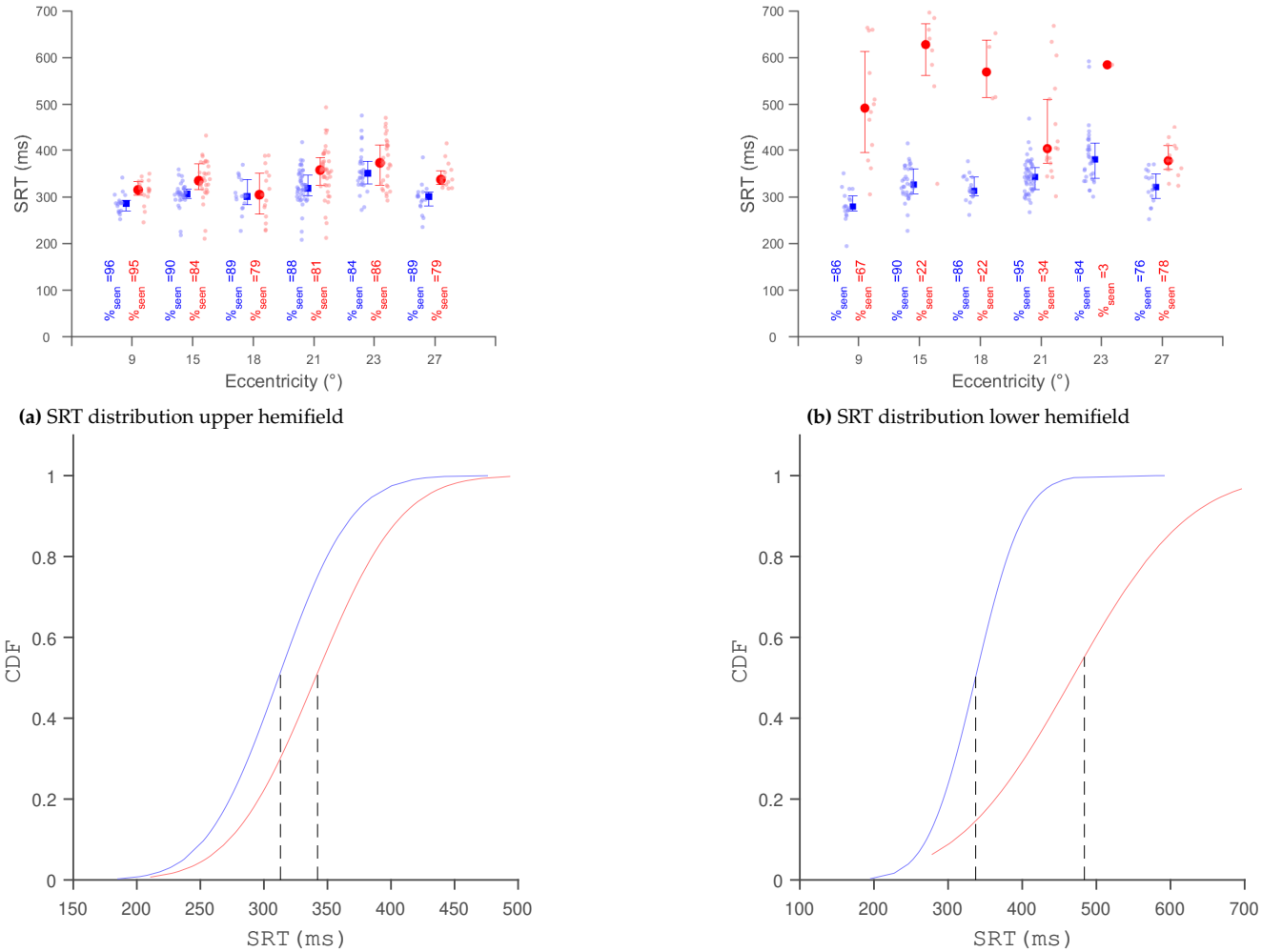

(a) SRT distribution upper hemifield

(b) SRT distribution lower hemifield

(c) SRT CDF upper hemifield

(d) SRT CDF lower hemifield

Figure B.19: SRT distribution of non-bleaching and bleaching conditions for upper and lower hemifield, for subject 2 from LHB_V_2. In fig. B.19a and fig. B.19b, the small light blue dots (●) and light red dots (●) are the SRTs for non-bleaching and bleaching conditions. The blue square (■) and red circle (●) represent the median values of SRTs in both hemifields' non-bleaching and bleaching conditions. The 25^{th} and 75^{th} percentile of SRTs are given by the blue (—) and red (—) error bars for each condition in each hemifield. $\%_{seen}$ signifies the percentage of detections at each eccentricity for each condition. In fig. B.19cand fig. B.19d, the blue (—) and red (—) lines show the cdf of non-bleaching and bleaching conditions in each hemifield.

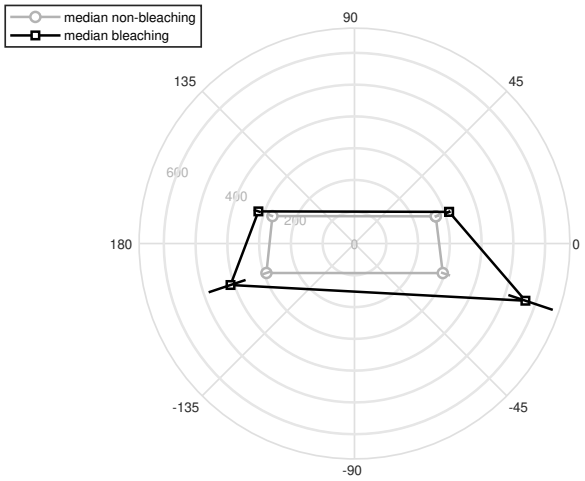

(a) SRT distribution at 9 ° eccentricity

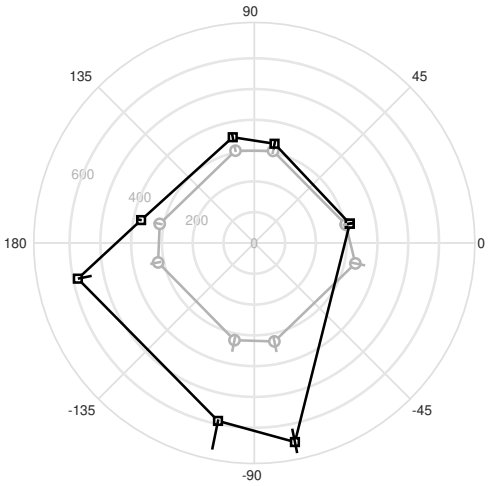

(b) SRT distribution at 15 ° eccentricity

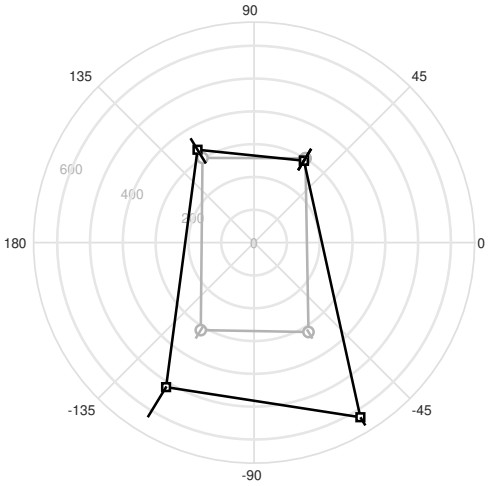

(c) SRT distribution at 18 ° eccentricity

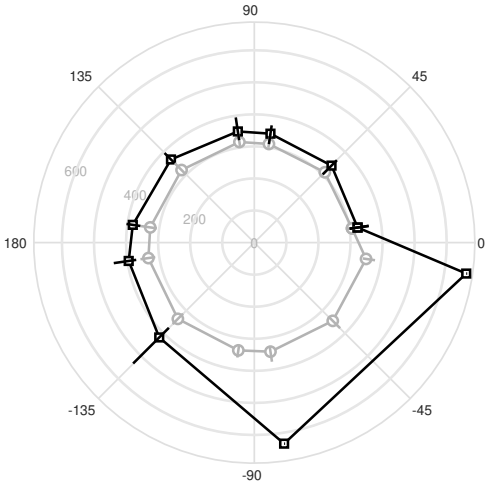

(d) SRT distribution at 21 ° eccentricity

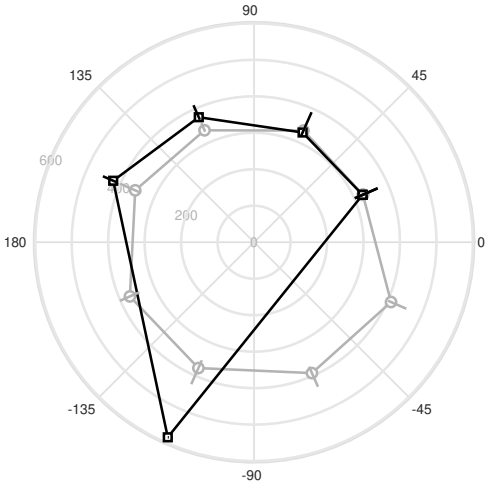

(e) SRT distribution at 23 ° eccentricity

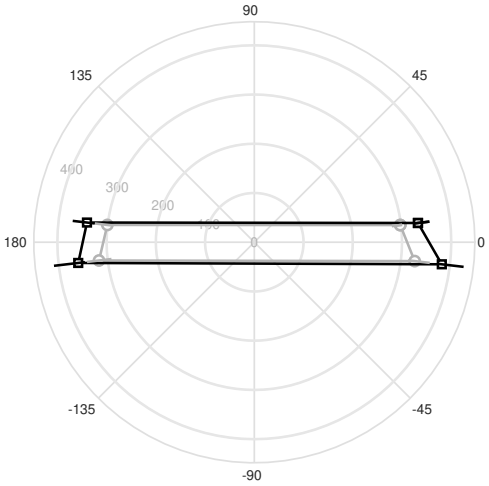

(f) SRT distribution at 27 ° eccentricity

Figure B.20: SRT distributions from subject 9 at each eccentricity from LHB_V_2. The gray boxes (□) indicate the median SRTs from non-bleaching trials. The black open boxes show the SRTs from the bleaching trials(□). The 25^{th} and 75^{th} percentile of SRTs are given by the gray (−) and black (−) error bars for each condition in each hemifield.

B.2. LHB and LHB_V_2 pooled cdfs

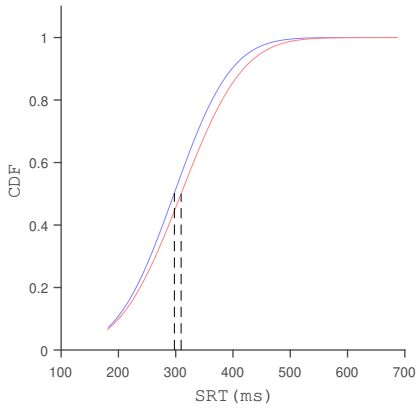

(a) SRT CDF upper hemifield

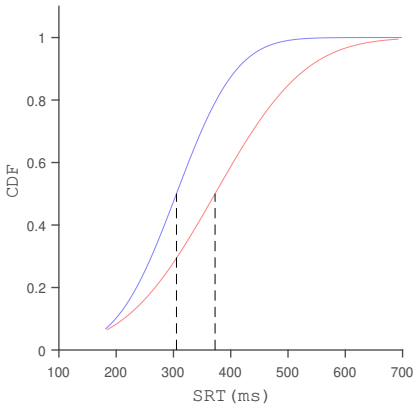

(b) [SRT CDF lower hemifield

Figure B.21: Comparision between the cdfs of SRTs in both the hemifields obtained from non-bleaching and bleaching trials pooled across all subjects. The blue (–) and red (–) lines indicate the cdfs of the non-bleaching and bleaching trials .

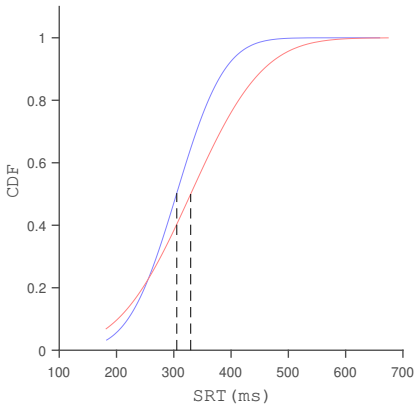

(a) LHB SRT CDF

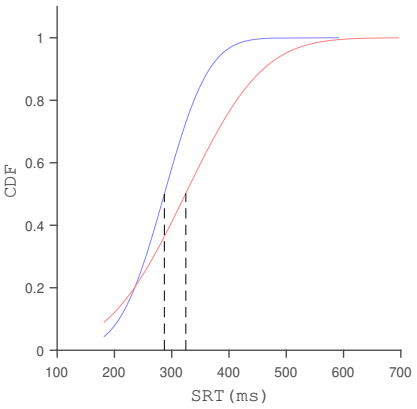

(b) LHB_V_2 SRT CDF

Figure B.22: Comparision between the SRT cdfs LHB and LHB_V_2 respectively pooled from subject 2 and 9. The blue (–) and red (–) lines indicate the cdfs of the non-bleaching and bleaching trials.

B.3. BO

B.3.1. Subject 2 SRTs

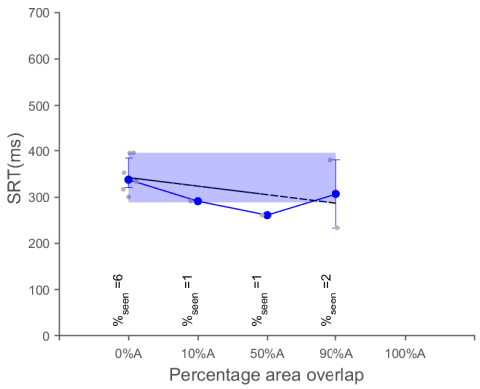

(a) SRTs at for +12.2 ° $R^2 = 0.43$

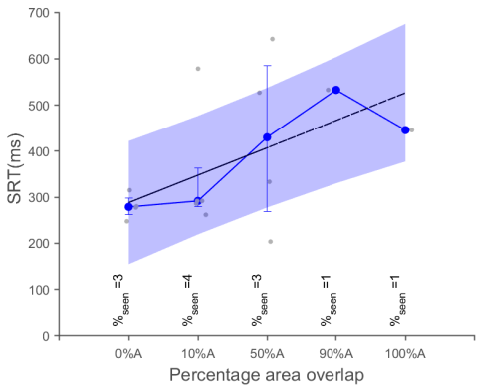

(b) SRTs at for -12.2 ° $R^2 = 0.50$

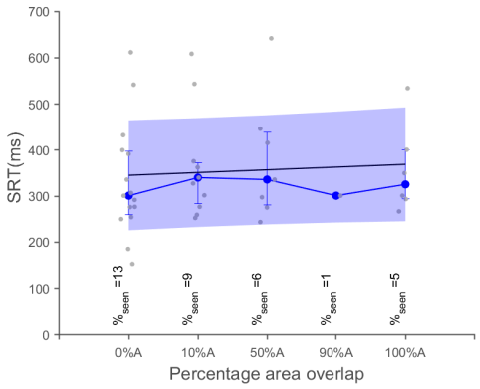

(c) SRTs at +6.4 ° $R^2 = 0.07$

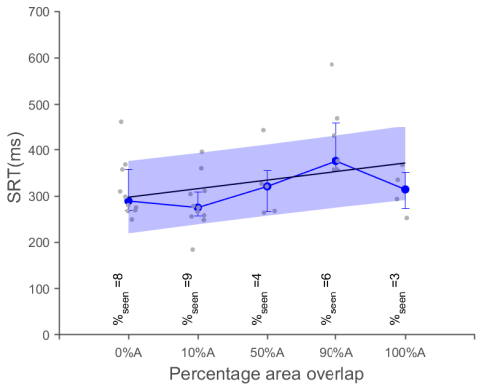

(d) SRTs at for -6.4 ° $R^2 = 0.32$

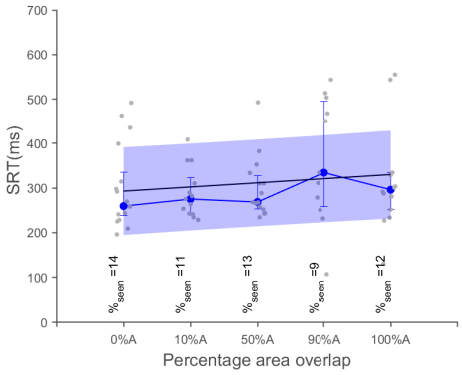

(e) SRTs at +2.8 ° $R^2 = 0.14$

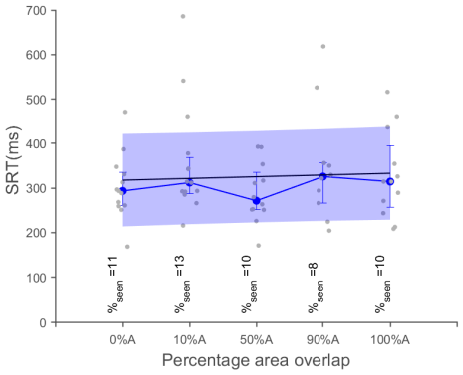

(f) SRTs at for -2.8 ° $R^2 = 0.054$

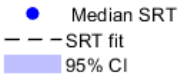

(g) Figure Legend

Figure B.23: A linear equation fit to SRT distributions across 6 elevations from experiment BO from subject 2. The dark blue(●) circle indicates the median values of the SRTs. Gray dots show individual SRTs (◉). The blue error bars represent the 25th and 75th percentile of SRTs. The black shows a linear fit dashed lines (−). Linearity and high correlation are proved in fig. B.29c to fig. B.29f. N represents the percentage of targets detected at a specific elevation. Each elevation had a total of 100 targets. Each overlap has 20 targets

B.3.2. Subject 3 SRTs

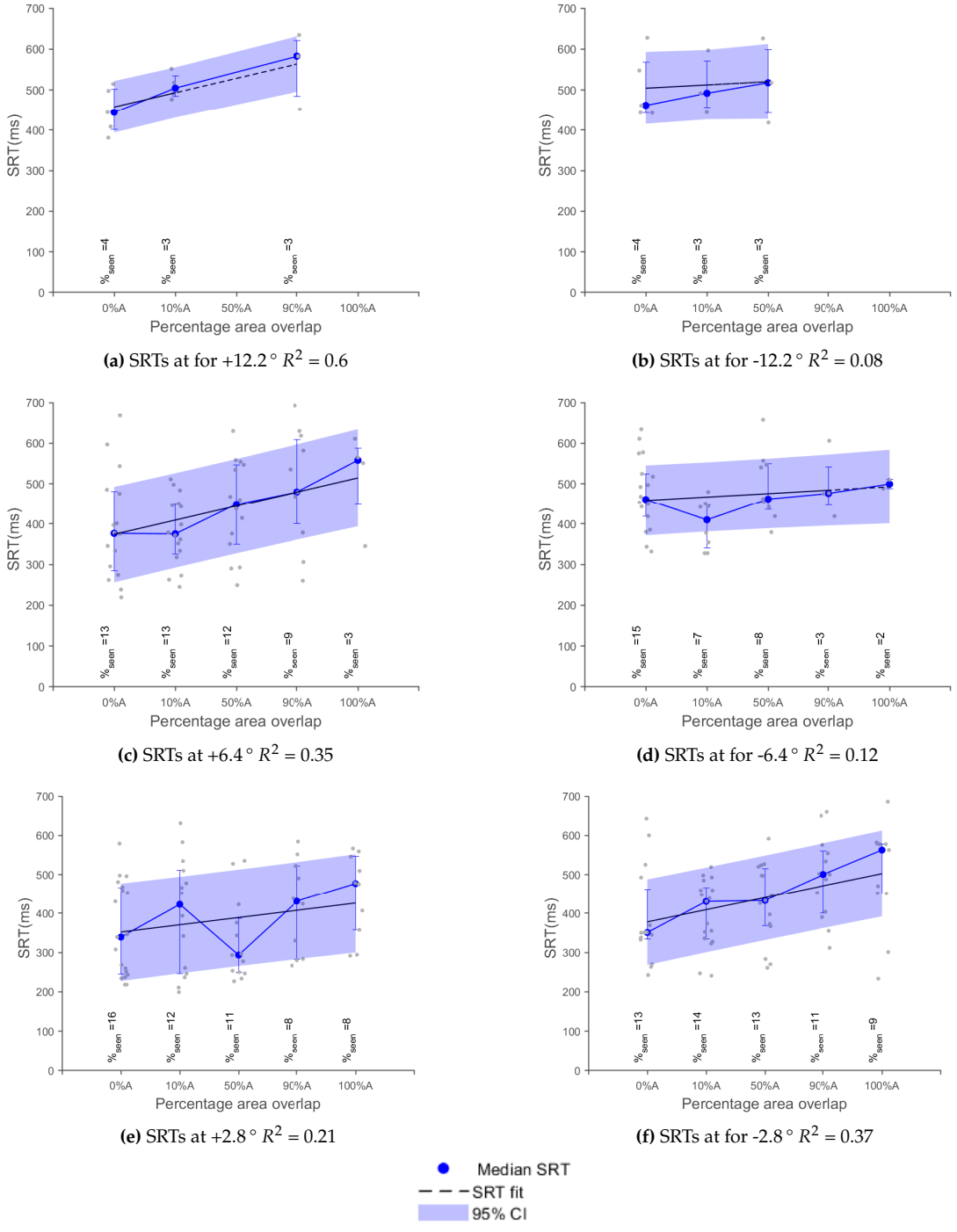

(a) SRTs at for +12.2 ° $R^2 = 0.6$

(b) SRTs at for -12.2 ° $R^2 = 0.08$

(c) SRTs at +6.4 ° $R^2 = 0.35$

(d) SRTs at for -6.4 ° $R^2 = 0.12$

(e) SRTs at +2.8 ° $R^2 = 0.21$

(f) SRTs at for -2.8 ° $R^2 = 0.37$

(g) Figure Legend

Figure B.24: A linear equation fit to SRT distributions across 6 elevations from experiment BO from subject 3. The dark blue(●) circle indicates the median values of the SRTs. Gray dots show individual SRTs (●). The blue error bars represent the 25th and 75th percentile of SRTs. The black shows a linear fit dashed lines (−). N represents the percentage of targets detected at a specific elevation. Each elevation had a total of 100 targets. Each overlap has 20 targets

B.3.3. Subject 4 SRTs

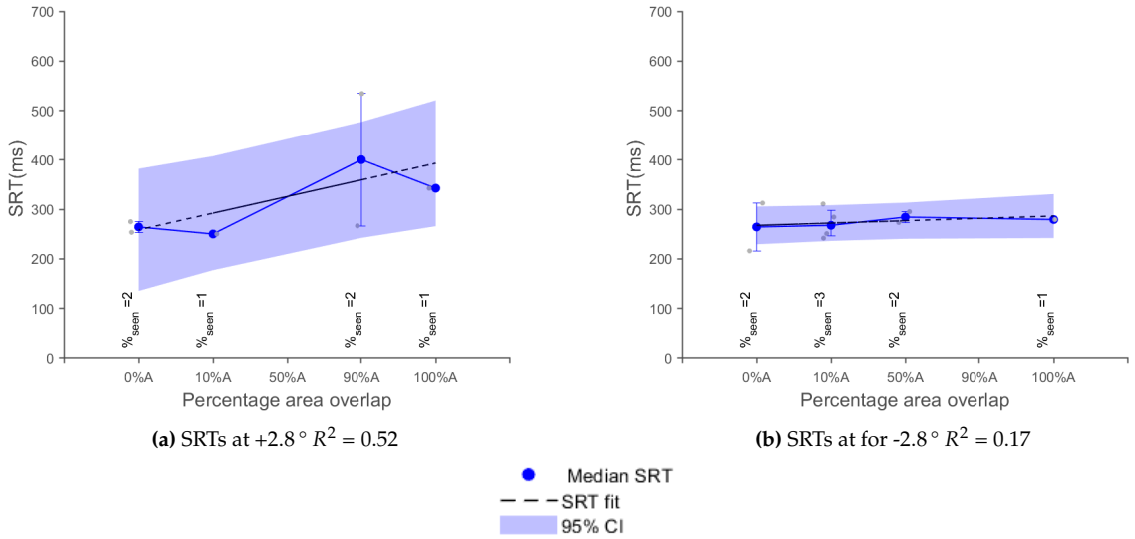

(a) SRTs at +2.8 ° R^2 = 0.52

(b) SRTs at for -2.8 ° R^2 = 0.17

(c) Figure Legend

Figure B.25: A linear equation fit to SRT distributions across 2 elevations from experiment BO from subject 4. The dark blue(●) circle indicates the median values of the SRTs. Gray dots show individual SRTs (◉). The blue error bars represent the 25th and 75th percentile of SRTs. The black shows a linear fit dashed lines (−). N represents the percentage of targets detected at a specific elevation. Each elevation had a total of 100 targets. Each overlap has 20 targets

B.3.4. Subject 5 SRTs

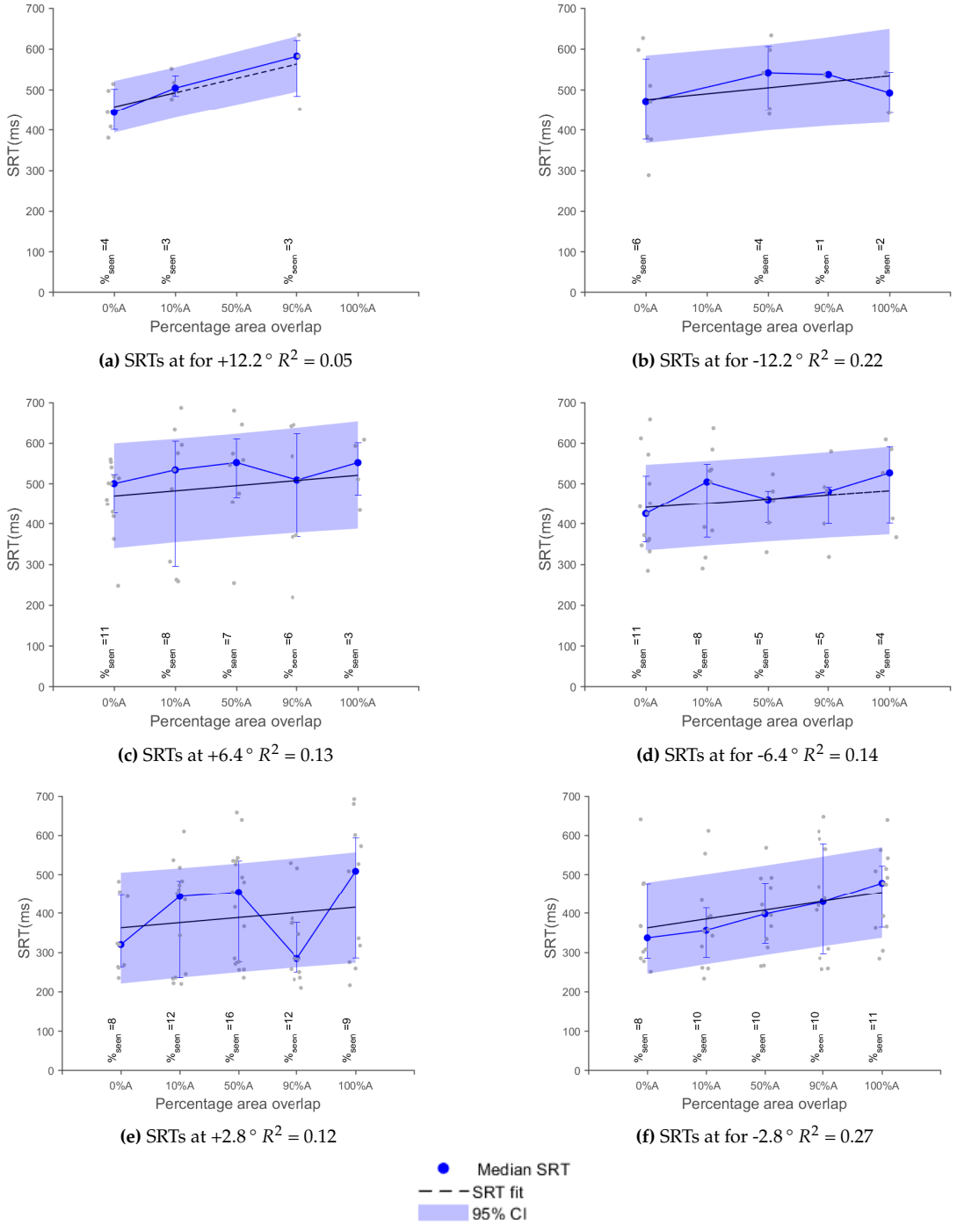

(a) SRTs at for +12.2 ° $R^2 = 0.05$

(b) SRTs at for -12.2 ° $R^2 = 0.22$

(c) SRTs at +6.4 ° $R^2 = 0.13$

(d) SRTs at for -6.4 ° $R^2 = 0.14$

(e) SRTs at +2.8 ° $R^2 = 0.12$

(f) SRTs at for -2.8 ° $R^2 = 0.27$

(g) Figure Legend

Figure B.26: A linear equation fit to SRT distributions across 6 elevations from experiment BO from subject 5. The dark blue(●) circle indicates the median values of the SRTs. Gray dots show individual SRTs (●). The blue error bars represent the 25th and 75th percentile of SRTs. The black shows a linear fit dashed lines (−). N represents the percentage of targets detected at a specific elevation. Each elevation had a total of 100 targets. Each overlap has 20 targets

B.3.5. Subject 6 SRTs

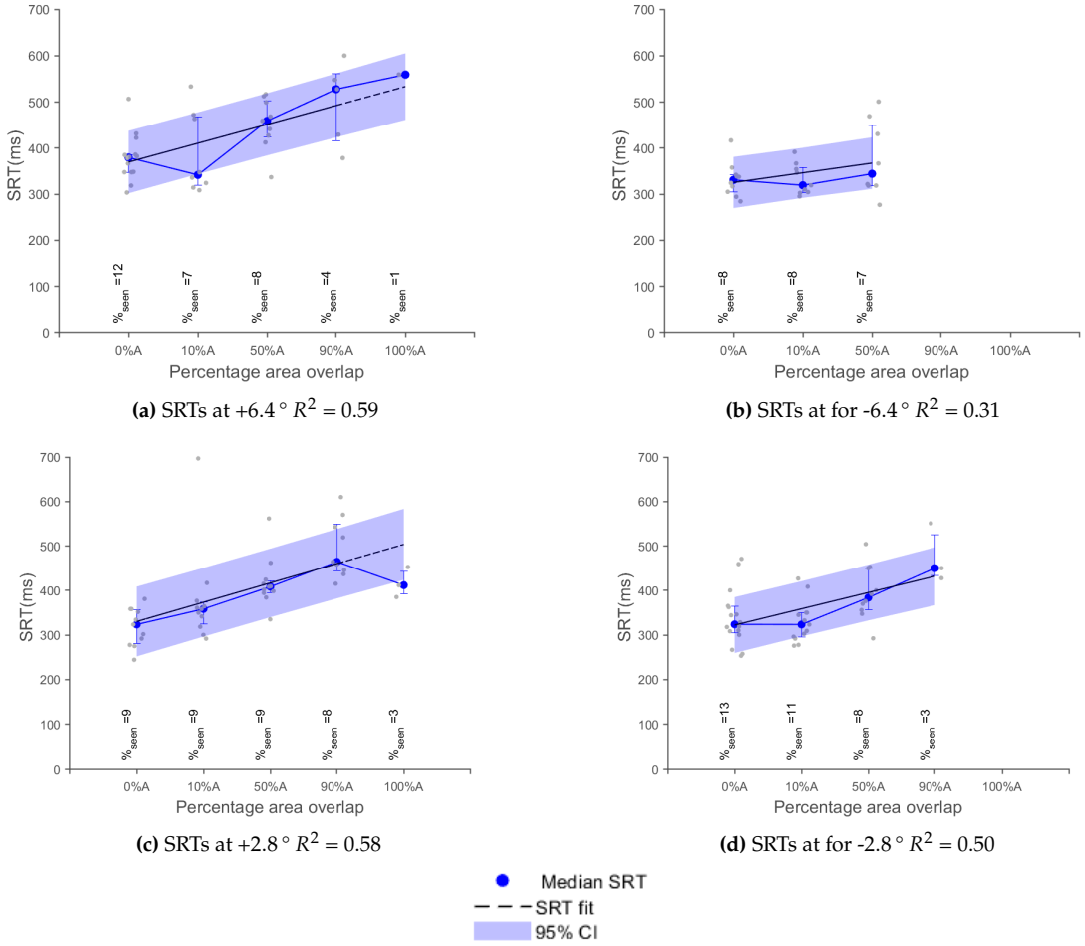

(a) SRTs at +6.4 ° $R^2 = 0.59$

(b) SRTs at for -6.4 ° $R^2 = 0.31$

(c) SRTs at +2.8 ° $R^2 = 0.58$

(d) SRTs at for -2.8 ° $R^2 = 0.50$

(e) Figure Legend

Figure B.27: A linear equation fit to SRT distributions across 6 elevations from experiment BO from subject 6. The dark blue(●) circle indicates the median values of the SRTs. Gray dots show individual SRTs (●). The blue error bars represent the 25th and 75th percentile of SRTs. The black shows a linear fit dashed lines (−). N represents the percentage of targets detected at a specific elevation. Each elevation had a total of 100 targets. Each overlap has 20 targets

B.3.6. Subject 7 SRTs

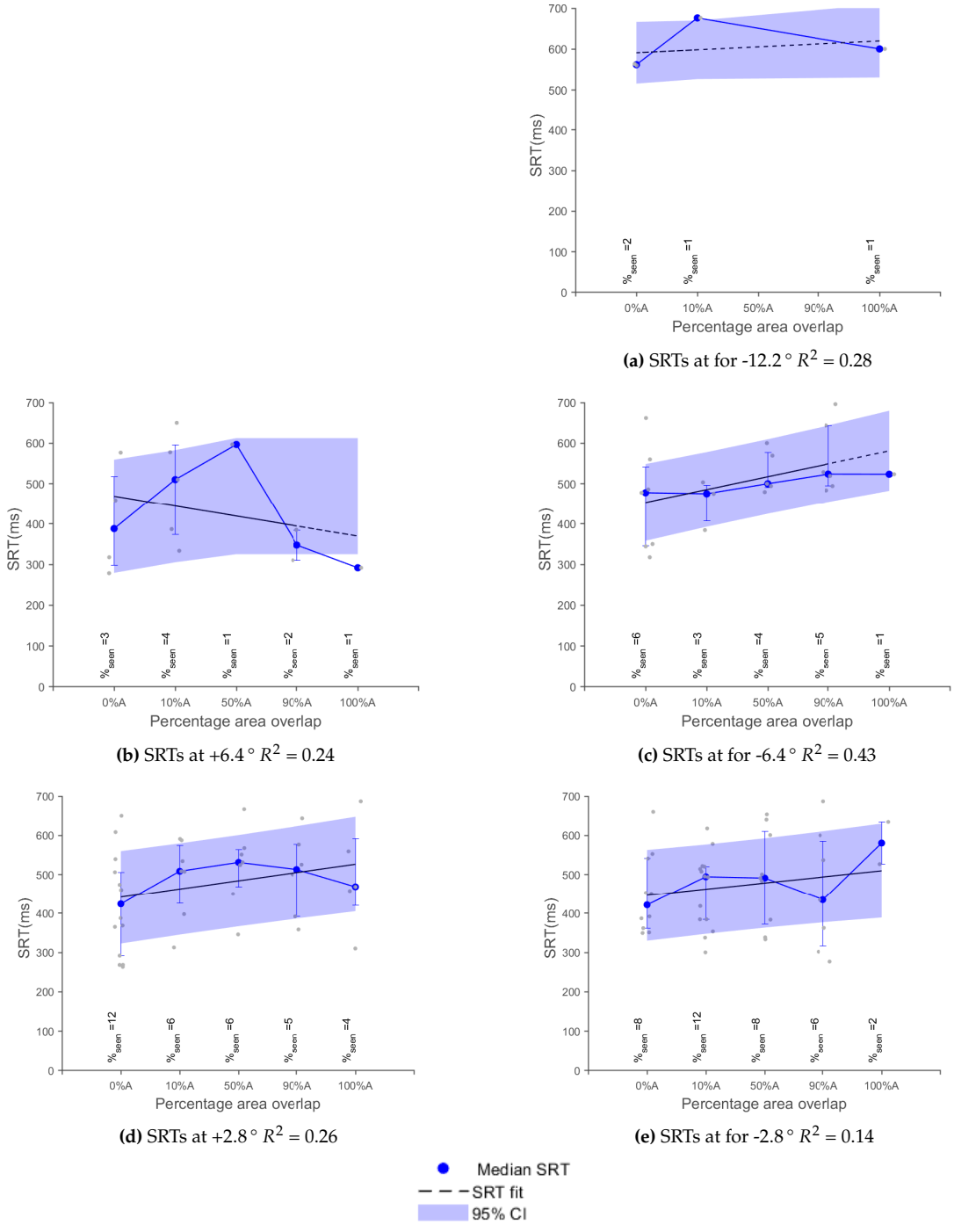

(a) SRTs at for -12.2 ° $R^2 = 0.28$

(b) SRTs at +6.4 ° $R^2 = 0.24$

(c) SRTs at for -6.4 ° $R^2 = 0.43$

(d) SRTs at +2.8 ° $R^2 = 0.26$

(e) SRTs at for -2.8 ° $R^2 = 0.14$

(f) Figure Legend

Figure B.28: A linear equation fit to SRT distributions across 5 elevations from experiment BO from subject 7. The dark blue(●) circle indicates the median values of the SRTs. Gray dots show individual SRTs (●). The blue error bars represent the 25th and 75th percentile of SRTs. The black shows a linear fit dashed lines (−). N represents the percentage of targets detected at a specific elevation. Each elevation had a total of 100 targets. Each overlap has 20 targets

B.3.7. Subject 8 SRTs

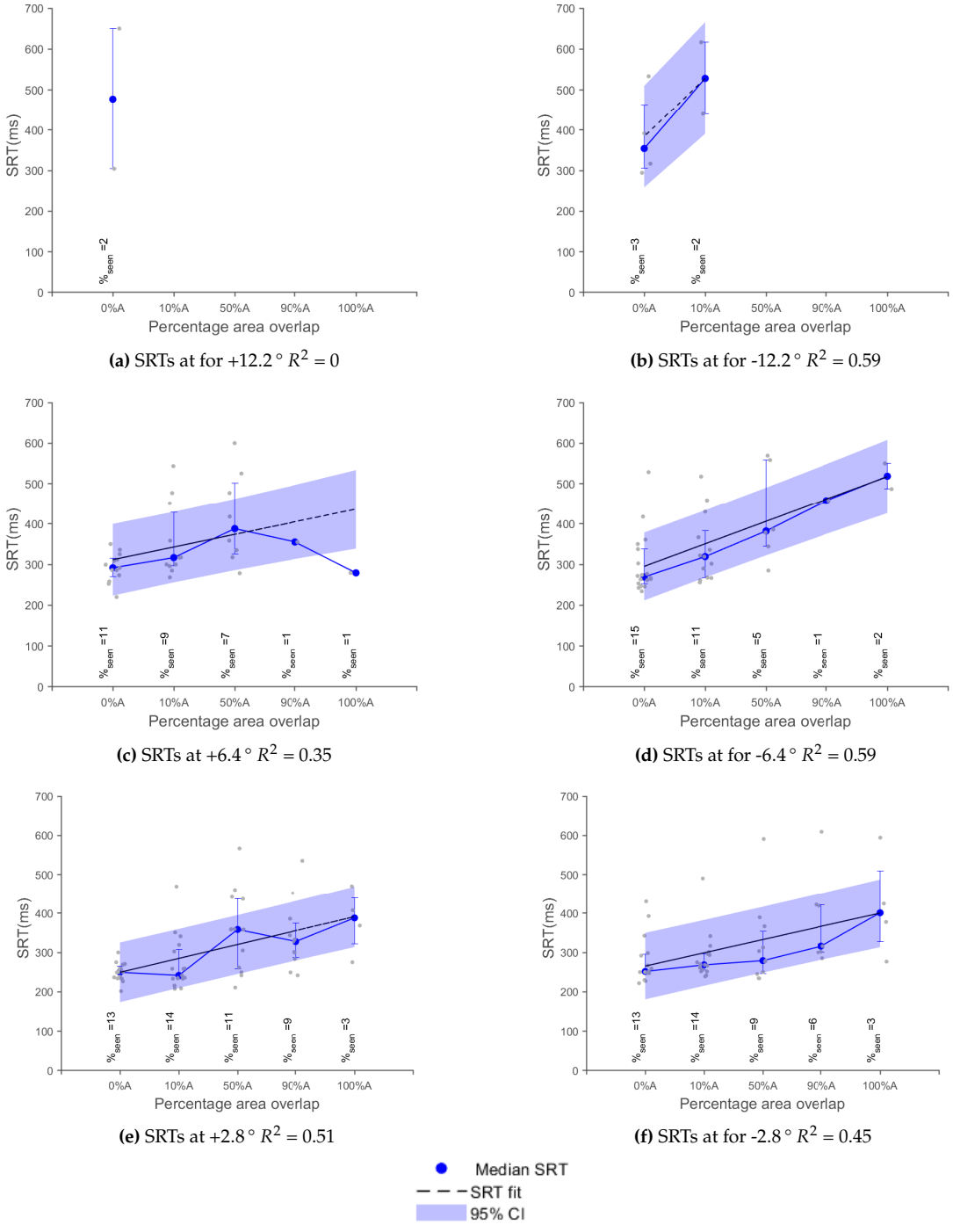

(a) SRTs at for +12.2 ° $R^2 = 0$

(b) SRTs at for -12.2 ° $R^2 = 0.59$

(c) SRTs at +6.4 ° $R^2 = 0.35$

(d) SRTs at for -6.4 ° $R^2 = 0.59$

(e) SRTs at +2.8 ° $R^2 = 0.51$

(f) SRTs at for -2.8 ° $R^2 = 0.45$

(g) Figure Legend

Figure B.29: A linear equation fit to SRT distributions across 6 elevations from experiment BO from subject 8. The dark blue(●) circle indicates the median values of the SRTs. Gray dots show individual SRTs (●). The blue error bars represent the 25th and 75th percentile of SRTs. The black shows a linear fit dashed lines (−). N represents the percentage of targets detected at a specific elevation. Each elevation had a total of 100 targets. Each overlap has 20 targets

C

Complemetary Results

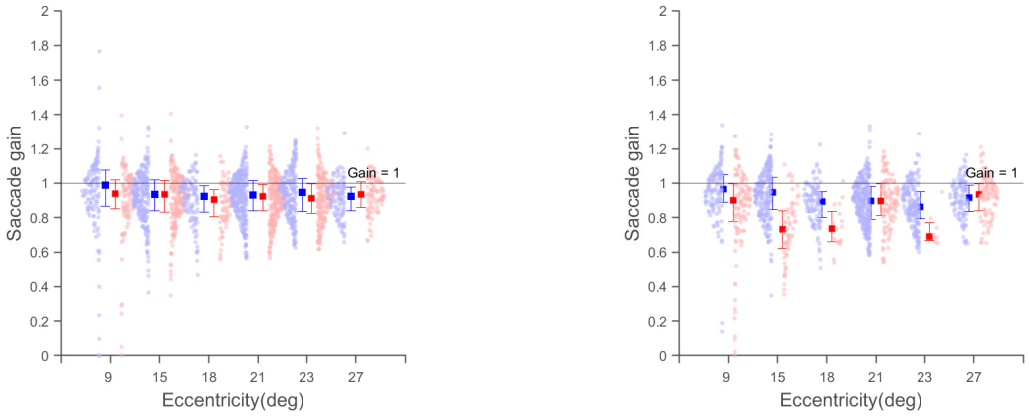

(a) Saccade gain in upper hemifield

(b) Saccade gain in lower hemifield

Figure C.1: distribution of saccade gain during both hemifields' non-bleaching and bleaching trials pooled across all subjects. The small blue dots (●) and red dots (●) are the gains for non-bleaching and bleaching conditions. The blue square (■) and red squares (■) represent the median values of gains in both hemifields' non-bleaching and bleaching conditions. The 25^{th} and 75^{th} percentile of saccade gains are given by the blue (—) and red (—) error bars for each condition in each hemifield.

The saccade gain results for both conditions are shown in fig. C.1. The gains shown in fig. C.1a for both conditions in the upper hemifield were similar. A t-test (H = 0, P = 0.18) accepts the null hypothesis. The null hypothesis is rejected by the t-test (H = 1, P = 0.004) for the gains in the lower hemifield, denoting a difference between the saccadic gains obtained during bleaching and non-bleaching trials. Again, this is primarily because of fewer stimuli detected during the bleaching trials. The higher undershoots (lower gain) are mainly observed in the eccentricities 15 °, 18 ° and 23 ° of the lower hemifield during the bleaching trials, shown in fig. C.1b.

Impact on motor functions

The saccade peak velocity and duration are also investigated to find conclusive differences between the non-bleaching and bleaching conditions. A one-to-one comparison using the main sequence analysis between the non-bleaching and bleaching conditions is shown in fig. C.2. No differences can be observed between the velocity profiles shown in fig. C.2a and fig. C.2b. A Mann-Whitney U test (H = 0 P = 0.52) confirms the similarity between the two data sets. The same can be observed for the saccade duration distributions in fig. C.2c and fig. C.2d. A Mann-Whitney U test (H = 0 P = 0.84)

Table C.1: Main sequence constant values for non-bleaching and bleaching conditions

Conditions	V_{max} (° / s)	c	D_1 (ms)	n
NBL	532.5	9.05	12.5	0.589
BL	545.8	10.1	5	0.9601

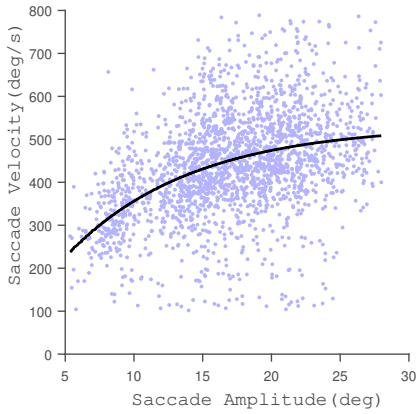

(a) Velocity fit for non bleaching condition $R^2 = 0.182$ $RMSE = 112.028$

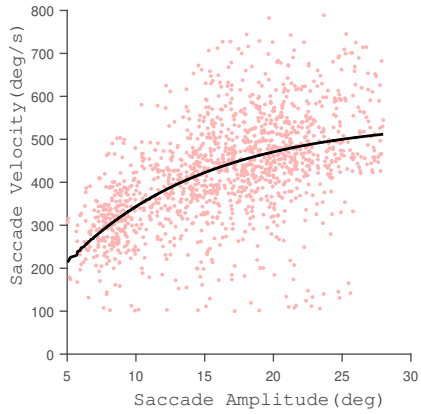

(b) Velocity fit for bleaching condition $R = 0.29$ $RMSE = 104.79$

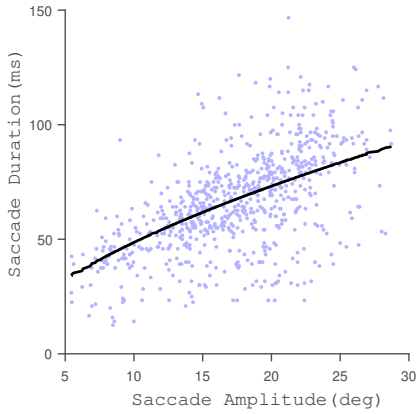

(c) Duration fit for non bleaching condition $R^2 = 0.3$ $RMSE = 18.83$

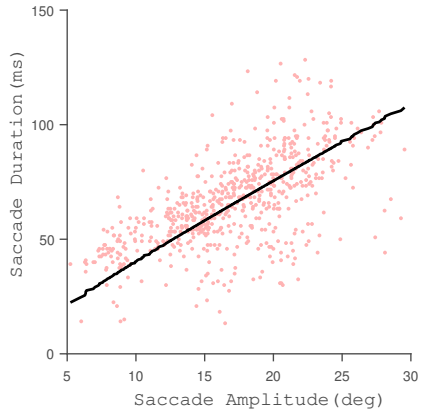

(d) Duration fit for bleaching condition $R^2 = 0.32$ $RMSE = 20.25$

Figure C.2: Fitting main sequence equation to the saccade velocity and duration profiles for non-bleaching and bleaching conditions pooled across all subjects. The blue dots(●) in fig. C.2a and fig. C.2c represents the saccade velocities and saccade durations for the non-bleaching condition, respectively. The red dots(●) in fig. C.2b and fig. C.2d represents the saccade velocities and saccade durations for the bleaching condition, respectively. The black fitted line represents the fit achieved by implementing the main sequence equation.

also accepts the similarity. A higher root means square values(RMSE) and lower R values obtained while evaluating the goodness of fit for all the main sequence fitted curves imply the low quality of fitted results. A larger spread in the data can also result in a lower fit quality. However, as expected, the saccades' motor properties remain uninfluenced by photobleaching and dark adaptation. The constants' values, duration, and velocity are given in table C.1.

D

Project Documentations

Informed Consent Form

The form below consists of a few questionaries that should be answered before taking part in the experimentation. Please read the form carefully and check the boxes accordingly. You have the right to ask questions any time and you also have the right to withdraw yourself from the experiment at any time. At the end, please put your name and signature with the date.

PLEASE TICK THE APPROPRIATE BOXES	Yes	No
A: GENERAL AGREEMENT – RESEARCH GOALS, PARTICPANT TASKS AND VOLUNTARY PARTICIPATION		
1. I have read and understood the study information dated at / / , or it has been read to me. I have been able to ask questions about the study and my questions have been answered to my satisfaction.		
2. I consent voluntarily to be a participant in this study and understand that I can refuse to answer questions and that I can withdraw from the study at any time, without having to give a reason.		
3. I declare that I have no symptoms of Covid-19 and I am willing to follow the Covid-19 guidelines of the institution if asked to.		
4. I understand that taking part in the study: [*see points below*]		
• involves a visual task where my eye movements are recorded with an eye tracker. • involves voluntary participation. • will take around 4 hours 20 minutes of my time. • all eye tracking data will be anonymized and stored for future use.		
5. I understand that I will be compensated for my participation by a coupon.		
B: GENERAL INFORMATION ABOUT PARTICIPANT		
6. I declare that my age is _____ on the day of experimentation and my gender is _____		
C: POTENTIAL RISKS OF PARTICIPATING		
7. I understand that taking part in the study in rare cases may involve the following risks, which I can always report to the experimenter so that experiment may be terminated: [*see points below*]		
• feeling dizzy and disoriented. • eye strain. • in severe cases seizures.		
8. I understand that the following steps will be taken to minimise the threat of a data breach and protect my identity as a participant: [*see points below*].		

PLEASE TICK THE APPROPRIATE BOXES	Yes	No
• All measured eye tracking data will be fully anonymized. • Scanned informed consent forms will be stored only on secure drives in the Erasmus MC/TU Delft.		
9. I understand that personal information collected about me that can identify me, such as name, signature and contact information, will not be shared beyond the study team.		
D: RESEARCH PUBLICATION, DISSEMINATION AND APPLICATION		
10. I understand that after the research study the findings in terms of eye tracking will be published as a master thesis report and scientific publications.		
E: (LONGTERM) DATA STORAGE, ACCESS AND REUSE		
11. I give permission for the de-identified eye tracking data that I provide to be archived in data repository of TU Delft and Erasmus MC so it can be used for future research and learning.		

Signatures

_____ _____ _____

Name of participant Signature Date

I, as legal representative, have witnessed the accurate reading of the consent form with the potential participant and the individual has had the opportunity to ask questions. I confirm that the individual has given consent freely.

_____ _____ _____

Name of witness Signature Date

I, as researcher, have accurately read out the information sheet to the potential participant and, to the best of my ability, ensured that the participant understands to what they are freely consenting.

_____ _____ _____

Researcher name Signature Date

Study contact details for further information: [*Name, phone number, email address*]

Experiment Briefing

Experiment: Measuring saccadic reaction times with a desensitized healthy retina
Researchers: Mayukh Sarkar (TU Delft), Dr. ir. Daan Pool (TU Delft), Dr. Johan Pel (Erasmus MC) and Dr. Peter Bremen (Erasmus MC)

Study Date -

Purpose:

Numerous, often age-related, diseases can affect the accuracy with which our visual system can process input from our eyes. An example is glaucoma, which is the world's leading cause of irreversible blindness caused by decreasing sensitivity of the retina. This experiment is part of a larger collaboration between TU Delft and Erasmus MC on the topic of glaucoma and aims to measure how saccadic reaction times (a measure of visual system performance) are affected by a desensitized retina. In this experiment, we aim to collect reference visual field test data from healthy participants, where retinal sensitivity will be varied using the natural and reversible adaptation mechanisms of the eyes in response to looking at dark or bright stimuli (photobleaching and dark adaptation). The experiment will contribute toward understanding the relationship between retinal sensitivity and saccadic reaction time data, which may contribute to the development of new diagnosis techniques. Participation in the experiment poses no (medical) risks and is completely voluntary.

Tasks to be performed:

As the participant, you will be seated on a chair, looking at a V shaped mirror placed within the haploscope. Stimuli for both calibration and trials will be projected to the V -shaped mirrors from two LED monitors through a pair of mirrors. The experiments will take place in a in a dark room to induce dark adaptation. The experimenter will instruct the participant to look at the display and try track the visual stimulus, white in colour shown as accurately as possible. The first set of task includes calibration where the participant will be asked to follow 9 points in the screen since the eye tracker needs to be calibrated. The start of the calibration process will be marked by the display of text “START OF CALIBRATION PROCESS, TRY TO FOLLOW THE POINTS” on the screen and the end will be marked as, “END OF CALIBRATION” on the screen visible to the participant. The beginning of the experiment will be marked as. “INITIATING EXPERIMENTATION, LOOK AT THE SCREEN AND TRACK POINTS”, the participant will be given a set of stimuli to track with or without a pre display of a white semi-circle on the screen. Once the experiment is over you will see the text on the display say, “END OF TRIAL”. Breaks will be taken between each trial. The entire experiment will consist of 20 trials and will take approximately 4 hours 20 minutes to complete, including the 3 minutes breaks in between trials.

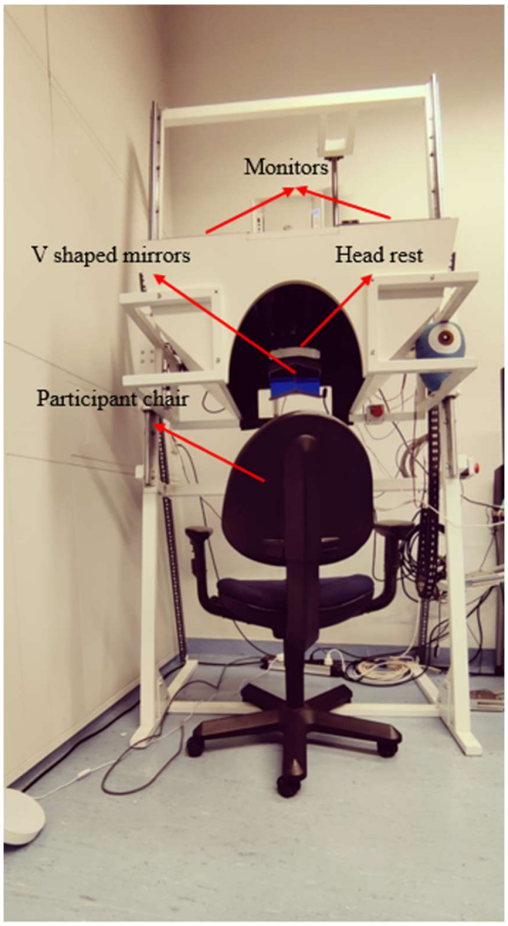

Figure 1 Depiction of the experiment setup where the participant will be seated

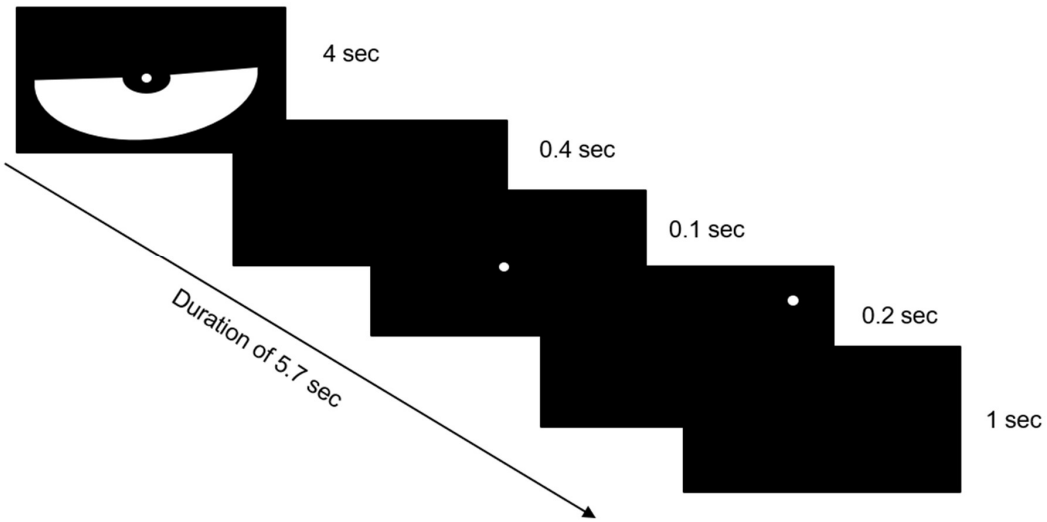

Figure 2 Frame by frame presentation of one trial

Benefits and risks of participating:

The participant will have the opportunity to contribute towards the development of a framework that will be able to solve the data problem in medical science. The participant must look at a monitor and track visual stimuli presented while remain seated on a chair. However, it cannot be excluded that some participants might feel dizzy, disoriented or experience anxiety, nausea, eye strain, or in severe cases seizures. **In case of having a history of seizures or epileptic**

episodes we ask you to avoid participation! All participants can follow Covid-19 precautions and it is their decision if they want to wear a facemask during their participation.

Personal data & research data:

We will record participants' age**, name and signature** in the consent form which will be stored on a protected storage drive that can only be accessed by authorized researchers (students) in this project, the supervisors. All the findings in terms of eye movement data will be anonymized. The age will only be collected for demographics purpose. This information from the experiments will be stored for 10 years and will only be used for the research. It is crucial to mention that only the eye movement is recorded, no picture or video material of your eyes will be collected. The name will only be indicated on the consent form, each subject will only be identified by an ID number. The consent forms and the tracking data will be stored in secure drives at Erasmus MC. The results of the research will be presented during a thesis presentation at TU Delft and Erasmus MC and will be a part of the thesis report and any following scientific publication. The subject can ask questions and to withdraw at any time from the research without consequences.

Mayukh Sarkar [redacted]

Signatures

Name of participant	Signature	Date

I, as legal representative, have witnessed the accurate reading of the consent form with the potential participant and the individual has had the opportunity to ask questions. I confirm that the individual has given consent freely.

Name of witness	Signature	Date

I, as researcher, have accurately read out the information sheet to the potential participant and, to the best of my ability, ensured that the participant understands to what they are freely consenting.

Researcher name	Signature	Date

Study contact details for further information: [*Name, phone number, email address*]